Regulation of heart development by the planar cell polarity pathway through the actomyosin complex and the mechanical forces

Inaugural-Dissertation
to obtain the academic degree
Doctor rerum naturalium (Dr. rer. nat.)

Submitted to the Department of Biology, Chemistry, Pharmacy
of Freie Universität Berlin

by
Kevin Manuel Méndez Acevedo

2022

I completed my doctorate studies from January 2018 to October 2022 under the supervision of Dr. Daniela Panáková at the Max Delbrück Center for Molecular Medicine in the Helmholtz Association, Berlin-Buch.

Primary Reviewer: Dr. Daniela Panáková

Secondary Reviewer: Prof. Dr. Helge Ewers

Date of defense: 20/01/2023

Acknowledgments

First of all, I would like to thank Dr. Daniela Panáková for giving me the opportunity to join her lab and work on this project with a lot of freedom and trust. For her supervision over these years, all the advices and support she has provided throughout my time as her student, helping me to become more critical and grow as a scientist.

I would like to thank Prof. Dr. Helge Ewers for his supervision at the Freie Universität Berlin, the discussions and for reviewing my doctoral thesis.

I want to thank my MDC committee members Dr. Mina Gouti and Prof. Dr. Holger Gerhardt for the discussion of my project and the insightful suggestions.

To all the members of the Panáková Lab for the time we overlap and spent there, Sara, Anne, Laura, Mikie, Luca. Alexander for the technical support.

Also, to my mentors over all my formative years, Dr. Brenda Valderrama, Dr. Luis Vaca, Dr. Julian Valdés, Dr. Jaime Mas-Oliva.
A special mention to my school teacher Adriana Pérez Sánchez, who introduce me for the first time to physics and chemistry.

To my family, especially my parents, Liliana and Isaac, thank you so much for everything! And my grandparents, Araceli, Zuly and Leonardo, Gracias por todo!

Last but not least, to all my friends from here and there, new and old ones. Thank you for being part of my life and enrich it in so many ways. Fer, David, Jacob, Jazzibe, Lorena, Arlette, Vicky, Rishab, Maike, Oscar, Megan, Alexis, Thilo, Nino, Alexandro, Maria, Alessia, Ernesto, Aikaterini, Leonie.

Dedicated to all the people who have been involved in my life, especially to the ones who know that./ Dedicado a todas las personas que han estado involucradas en mi vida, en especial a aquellas que lo saben.

Herewith I certify that I have prepared and written my thesis independently and that I have not used any sources and aids other than those indicated by me.

Table of Contents

I. Summary

The heart is the first functional organ to form during vertebrate development and it is evolutionarily conserved across species. It is crucial for the proper delivering of essential nutrients and oxygen throughout the embryo's body. Its development is complex and requires fine-tuning processes at levels involving growth, differentiation, and morphogenesis. First, a linear heart tube is formed, followed by cardiac looping, chamber formation, and maturation. As for many organs, the heart arises from a simple epithelium with planar polarity properties. The genetic and molecular programs involved in heart formation have been studied for a long time. However, besides the genetic and cellular contributions to heart formation, little is known about the molecular and cellular components involved in generating tissue and tension forces required in heart morphogenesis. Embryonic heart tube remodeling requires coordination of actomyosin-dependent tissue forces fundamental to the emergence of cardiac chambers and looped heart. It has been established that cardiac chamber remodeling is coordinated through tissue-scale polarization of actomyosin. Here, using zebrafish as a model, I describe the role of actomyosin in generating and distributing the tension forces necessary across the ventricular myocardium during cardiac looping and chamber formation. I describe the spatio-temporal distribution of phosphorylated myosin during embryonic heart formation. A mathematical model was generated to demonstrate that the tissue-scale supracellular polarization of actomyosin within the myocardial epithelium is essential for heart formation. The mathematical model serves as a predictive tool of cardiac looping and chamber formation and supports its dependence on the proper actomyosin distribution. Examining the molecular mechanisms governing the actomyosin activity along the heart tube, I demonstrate that both Rho-associated Protein Kinase 2a (Rock2a) and cardiac-specific Myosin Light Chain Kinase 3 (Mylk3) regulate the actomyosin-based tissue forces through the phosphorylation state of the Myosin Regulatory Light Chain (MRLC). I show that the preferential basal activity of Mylk3 and the apical activity of Rock2a mediate the proper levels of phosphorylated myosin (pMyo) and its polarized distribution along the apicobasal axis within the myocardium. I propose that the antagonistic force-generating activities of Mylk3 and Rock2a facilitate mechano-molecular control of heart tube morphogenesis. Moreover, I show Mylk3 and Rock2a are under the genetic control of Planar Cell Polarity signaling, identifying Mylk3 as a novel tissue-specific effector, downstream of the Vangl2 branch of this signaling pathway. Altogether, these findings describe for the first time a mechano-molecular mechanism necessary for proper looping and chamber formation during heart development.

II. Zusammenfassung

Das Herz ist das erste funktionelle Organ, das während der Embryonalentwicklung der Vertebraten entsteht und ist über Speziesgrenzen hinweg evolutionär konserviert. Es ist für die korrekte Verteilung essentieller Nährstoffe und Sauerstoff im Embryo unerlässlich. Seine Entwicklung erfordert feinabgestimmte Prozesse auf den Ebenen des Wachstums, der Zelldifferenzierung und der Morphogenese. Zu Beginn bildet sich eine lineare Herzröhre aus, gefolgt von kardialer Schlauchbildung und Reifung. Wie andere Organe auch entsteht das Herz aus einem einfachen Epithel mit planaren Polarisierungseigenschaften. Die genetischen und molekularen Programme, die an der Entstehung des Herzens beteiligt sind, werden schon lange untersucht. Abgesehen von dem genetischen und zellulären Einfluss auf Herzentwicklung, ist bis dato wenig über die molekularen und zellulären Komponenten und deren Beteiligung an Gewebsentwicklung und Gewebedrücken, die zur Herzmorphogenese beitragen, bekannt. Die Krümmung des embryonalen Herzschlauches wird von Aktomyosin-abhängigen Gewebedrücken koordiniert, die elementar für die Entstehung der Herzkammern und der Herzschleife sind. Es wurde bereits gezeigt, dass die Entstehung der Herzkammer durch eine gewebeweite Polarisierung von Aktomyosin koordiniert wird. Mit Hilfe des Zebrafisch als Modellorganismus, beschreibe ich die Rolle von Aktomyosin bei der Ausbildung und Verteilung von Drücken, die während der Entwicklung der Herzschleife und der Herzkammer, über den gesamten ventrikulären Herzmuskel, nötig sind. Weiter beschreibe ich die räumlich-zeitliche Verteilung von phosphoryliertem Myosin während der embryonalen Herzentwicklung. Ein entwickeltes mathematisches Modell zeigt, dass die gewebeweite Polarisierung von Aktomyosin innerhalb des myokardiellen Epithels essentiell für die Entstehung des Herzens ist. Das Modell prognostiziert die Entstehung der Herzschleife und der Herzkammer und stützt deren Abhängigkeit von der korrekten Aktomyosinverteilung. Ich zeige, dass die Rho-assoziierte Proteinkinase 2a (Rock2a) und die herzspezifische Myosin-leichte-Ketten-Kinase (Mylk3) die Aktomyosin-basierenden Gewebedrücke durch den Phosphorylierungszustand der Myosin-regulierenden leichten Kette (MRLC) regulieren. Weiter zeige ich, dass die basale Aktivität von Mylk3 und die apikale Aktivität von Rock2a die richtige Menge an phosphoryliertem Myosin (pMyo) und seine polarisierte Verteilung entlang der apikobasalen Achse innerhalb des Herzmuskels vermitteln. Demnach vermute ich, dass die antagonistischen Druck-generierenden Aktivitäten von Mylk3 und Rock2a die mechano-molekulare Kontrolle der Herzschlauchmorphogenese erlauben. Außerdem zeige ich, dass Mylk3 und Rock2a unter der genetischen Kontrolle der planaren Zellpolarität stehen. Dadurch

identifiziere ich Mylk3 as neuen gewebespezifischen Effektor, unterhalb des Vangl2-Arms dieses Signalwegs. Zusammengefasst beschreiben diese Ergebnisse zum ersten Mal einen mechano-molekularen Mechanismus, der für die richtige Herzschleifenbildung und Herzkammerentstehung während der Herzentwicklung erforderlich ist.

1. Introduction

1.1 The heart

The heart is an evolutionarily conserved organ across species (Figure 1). Its principal function is pumping blood to ensure the proper delivery of vital nutrients and oxygen throughout the embryo's body (Olson, 2006) and it is the first functional organ to form during vertebrate development (D. Li & Wang, 2018; Olson, 2006; Stephenson, Adams, & Vaccarezza, 2017). Vertebrates have a multichambered-heart directly connected to a closed vascular system (Bettex, Prêtre, & Chassot, 2014).

The heart in simple chordates acts as a peristaltic pump connected to an open circulation (Bettex et al., 2014; Monahan-Earley, Dvorak, & Aird, 2013). In fish the circulatory system is single and unidirectional with the gills placed downstream of the heart to oxygenate the blood (Bettex et al., 2014). Fish heart is composed of a single atrium and single ventricle connected through the atrioventricular canal/junction (AVJ). It has a characteristic “S”-shape helping to establish winding circuits in each of the chambers. The contraction is synchronized and sequential from posterior (atrium) to anterior (ventricle) direction. Atrioventricular and outflow valves facilitate unidirectional flow of blood by preventing backflow. Both, trabeculated and compact myocardium is present in fish heart. The conduction system includes the pacemaker tissue in the inflow tract (IFT) and the zones of slow conduction in the AVJ and the outflow tract (OFT) (Bettex et al., 2014; Monahan-Earley et al., 2013; Tessadori et al., 2012; Tota & Gattuso, 1996).

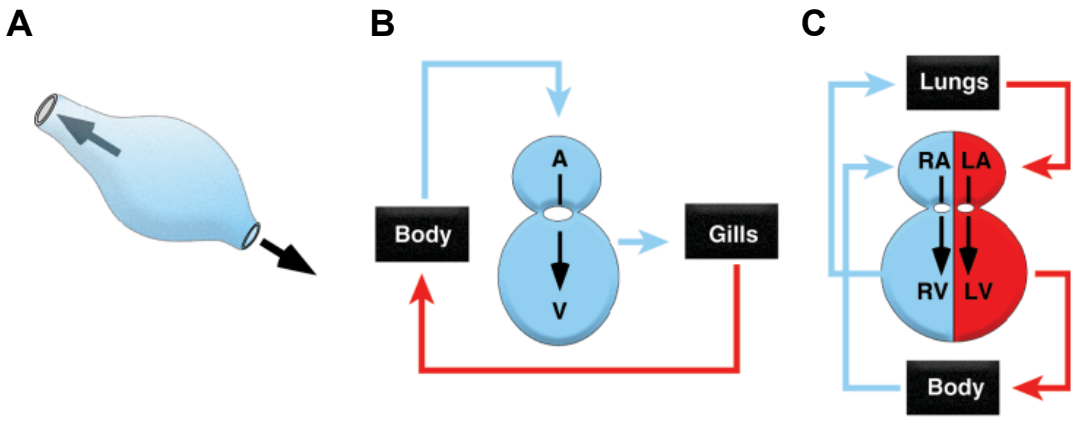

Figure 1. The heart is conserved across species. Simplified scheme of the different types of hearts. A) Linear tube in simple chordates. B) The fish heart consists of one ventricle and one atrium. C) Reptiles, birds, and mammals have four-chambered hearts with two atria and ventricles. A: atrium; V: ventricle; RA: right atrium; RV: right ventricle; LA: left atrium. Arrows indicate blood flow direction; oxygenated blood (red) and unoxygenated blood (blue) (From Olson 2006).

The mammalian heart has a four-chambered heart with two atria and two ventricles, arranged in parallel with a helical shape. A septum between the aortic and the pulmonary valves allows to have two separate circulations. The right atrium is exclusively connected to the right ventricle and the same is true for the left chambers. Both halves beat in synchrony, the right part of the heart pumps the unoxygenated blood from the body through the lungs to the left part where the oxygenated blood is pumped to the rest of the body. Mammals possess only compacted myocardium forming the heart (Bettex et al., 2014). The sinoatrial node represents the pacemaker of the mammalian heart, from which the electrical signals travel to the atrioventricular node, along the His bundle through the Purkinje fibers to finally reach the ventricular walls (Brennan et al., 2020; Burkhard, van Eif, Garric, Christoffels, & Bakkers, 2017; Ehrlich, 1995). The heart arises from the lateral plate mesoderm together with the blood vessels, blood cells, kidney, and the lining of the body cavities (Kemmler, Riemslagh, Moran, & Mosimann, 2021; Scott & Barresi, 2016). Its development is complex and requires fine-tuning processes at different levels involving growth, differentiation, and morphogenesis (Stainier, 2001).

1.2 Early cardiac development in vertebrates

Despite the most obvious structural differences among vertebrates, cardiac development programs at cellular and molecular levels are well conserved between the different species (Olson, 2006; Stephenson et al., 2017). The heart is derived from the mesoderm (Andrés-Delgado & Mercader, 2016; Devine, Wythe, George, Koshiba-Takeuchi, & Bruneau, 2014; Kemmler et al., 2021; Liu & Stainier, 2012; Narumanchi et al., 2021; Vornanen & Hassinen, 2016), the intermediate germ layer of the embryo that lays between the ectoderm and endoderm, which also generates the blood, kidney, gonads, bones, muscles, and connective tissues (Scott & Barresi, 2016).

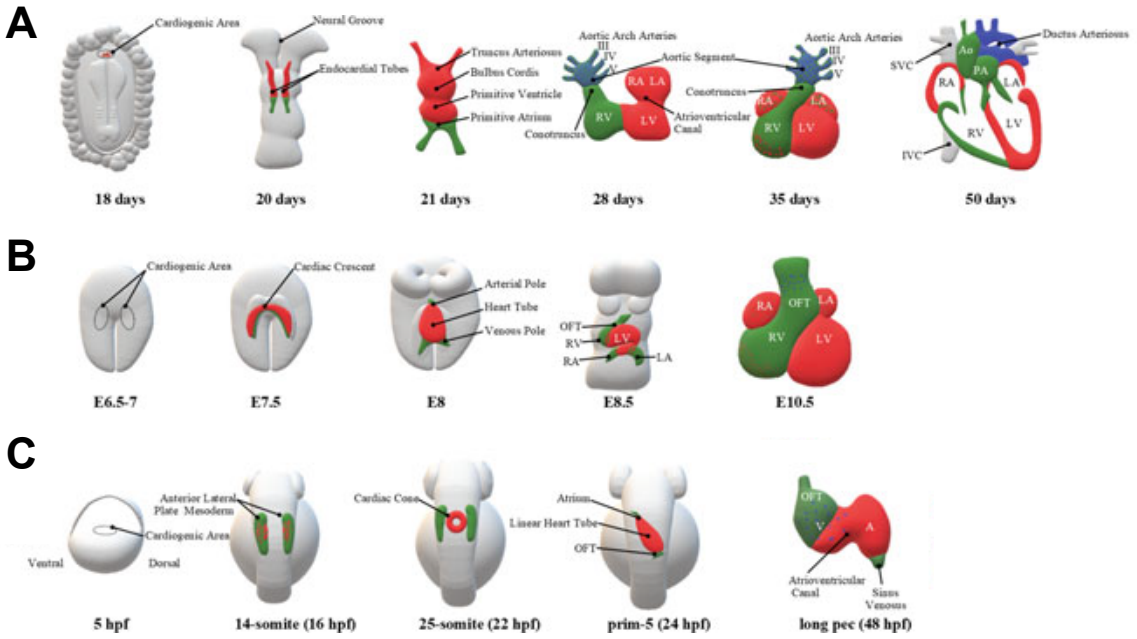

Figure 2. Early cardiac development. The early formation of the heart is a conserved mechanism across vertebrates including A) human, B) mouse and C) zebrafish. Cardiac progenitors are specified early during development, then they migrate bilaterally towards the midline of the embryo to fuse and form the cardiac crescent in amniotes or the cardiac disc in zebrafish. Followed by the elongation and linear heart tube formation, which will undergo the looping process to finally form the multichambered heart. RA: right atrium, RV: right ventricle, LA: left atrium, LV: left ventricle, PA: pulmonary artery, Ao: aorta, SVC: superior vena cava, IVC: inferior vena cava, A: atrium, V: ventricle, OFT: outflow tract, (Adapted from Perl & Waxman, 2020).

The cardiac precursors share a common origin across all the different species derived from the anterior lateral plate mesoderm (ALPM) (Bakkers, 2011; Devine et al., 2014; Staudt & Stainier, 2012). The cardiac progenitors' position is already established in the gastrula stage (Keegan, Meyer, & Yelon, 2004), as they begin to express cardiac specific genes *Nkx2.5* and *GATA4* (Laverriere et al., 1994; Prall et al., 2007). The cardiac progenitors migrate laterally to the midline of the embryo to converge anteriorly to the LPM, guided through signals coming from other adjacent LPM progenitor cells, to finally fuse to form the cardiac disc in fishes or the equivalent in amniotes (including mice and humans), the cardiac crescent (Figure 2). Once the cardiac disc has formed after fusion of endocardial and myocardial progenitors the elongation process occurs giving rise to the cardiac cone, which later becomes the linear heart tube. In amniotes a similar process occurs, crescent forms after the fusion process occurs to form the linear heart tube (DeRuiter, Poelmann, VanderPlas-de Vries, Mentink, & Gittenberger-de Groot, 1992). The linear heart tube (LHT) is a temporary structure composed of an inner endothelial (endocardial cells) layer wrapped by a monolayer of epithelial (myocardial cells) layer that appears during early development (Andrés-Delgado & Mercader, 2016). The LHT originates in humans at 20–22 days of embryonic development, in mice at 8.0

days, in chicken at 1.5 days, and in zebrafish at 22 hours post-fertilization (hpf) (Figure 2) (Stephenson et al., 2017).

1.3 Cardiac looping and chamber formation

One crucial step in the morphogenesis of the heart is the looping process that occurs concomitantly with the formation and the expansion of the cardiac chambers. Despite the main structural differences between fish and mammalian heart, the former being composed of one atrium and one ventricle, while the later comprises two atria (left and right) and two ventricles (left and right), the morphogenetic program is well conserved. The looping process in fish gives rise to the “S”-looped fully formed heart and in mammals the initial "C”-looping continues with the helix maturation and formation of the four chambered heart. After the linear heart tube formation, a series of events lead to the asymmetric orientation of the LHT, chamber formation, ballooning to finally result in a fully functional heart (Figure 3). The events during the looping stage can be divided into intrinsic, cellular behaviors within the organ, or extrinsic, external cues such as mechanical forces or events occurring outside the organ (Desgrange, Garrec, & Meilhac, 2018; Le Garrec et al., 2017). In mouse, the intrinsic processes comprise differential growth as hyperplasia and hypertrophy and oriented growth, while the extrinsic events include hemodynamic forces generated through blood flow, and cardiac jelly swelling combined with the constrain of relative stiff dorsal mesocardium (Shi, Yao, Xu, & Taber, 2014). In addition, cell shape changes and cell rearrangements (through cell neighbor exchange), buckling, and actomyosin polarization contribute to the looping and the cardiac chamber formation (Merks et al., 2018; Shi et al., 2014).

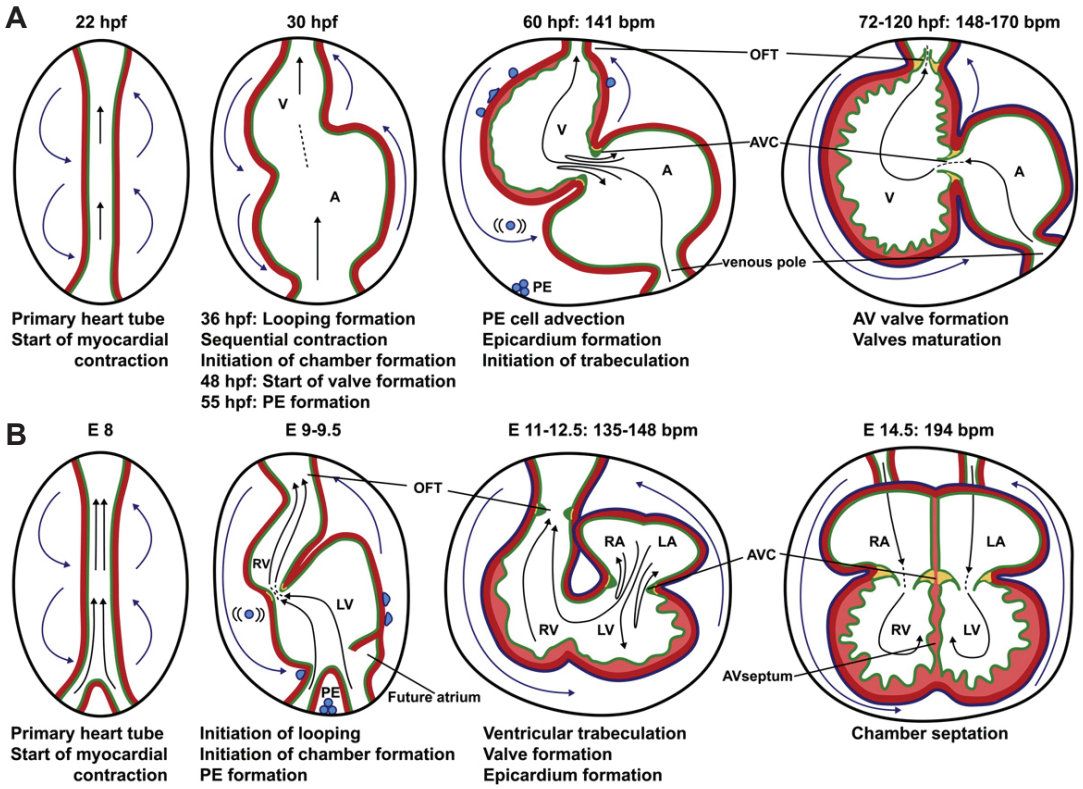

Figure 3. Morphogenetic events of heart development. The time point of development is indicated in hours post fertilization (hpf) and the heart rate in beats per minute (bpm). Blood flow is indicated by the black arrows and the pericardial fluid by the blue arrows. Epicardium, myocardium, and endocardium are indicated in blue, red and green, respectively. Valves in yellow. V: ventricle; A: atrium; OFT: outflow tract; AVC: atrioventricular canal; PE: proepicardium. (Adapted from Andrés-Delgado and Mercader 2016).

For the study of the cardiac looping, it is necessary to understand the intertwined relationship between the mechanics of the cells and tissues and the molecular players involved in such complex process.

1.4 Modeling of the cardiac looping

Cardiac jogging, when the formed LHT moves leftward and away from the dorsal midline, marks the first event establishing the left-right asymmetry in the developing heart as a result of lateral signals (Ahmad, Long, & Rebagliati, 2004). This is followed by the rightward looping and involves the transformation of the linear heart tube into a looped flat S-shape in fish or a helix in amniotes (Buckberg, 2002). The overall mechanism of the heart looping has been studied using different approaches from anatomy, biology, genetics, mechanical processes, and more recently, computational and mathematical tools to generate models (Desgrange et al., 2018; Le Garrec et al., 2017). Respective models of tube deformation have been proposed for both, a 3D looping model for amniotes and a 2D model for fish (C. Gao & Chen, 2010;

Mlodzik, 2016; Sharma, Castro-Piedras, Simmons, & Pruitt, 2018; Theisen et al., 1994; Wharton, 2003) (Figure 4). On the one hand, the intrinsic cues have been considered (Franco & Kelly, 2011; Francou, De Bono, & Kelly, 2017; Kelly, Brown, & Buckingham, 2001; Kelly, Buckingham, & Moorman, 2014; Kelly & Buckingham, 2002; Kelly & Sperling, 2018; Mesbah, Harrelson, Théveniau-Ruissy, Papaioannou, & Kelly, 2008; Mesbah et al., 2012); the differential growth in specific zones varying along the length and the circumference of the tube, but without any change in orientation along the tube axis. The second scenario comprises the oriented growth, where the growth ratio is the same around the circumference of the tube, but in a tilted-oriented fashion (Desgrange et al., 2018; Le Garrec et al., 2017).

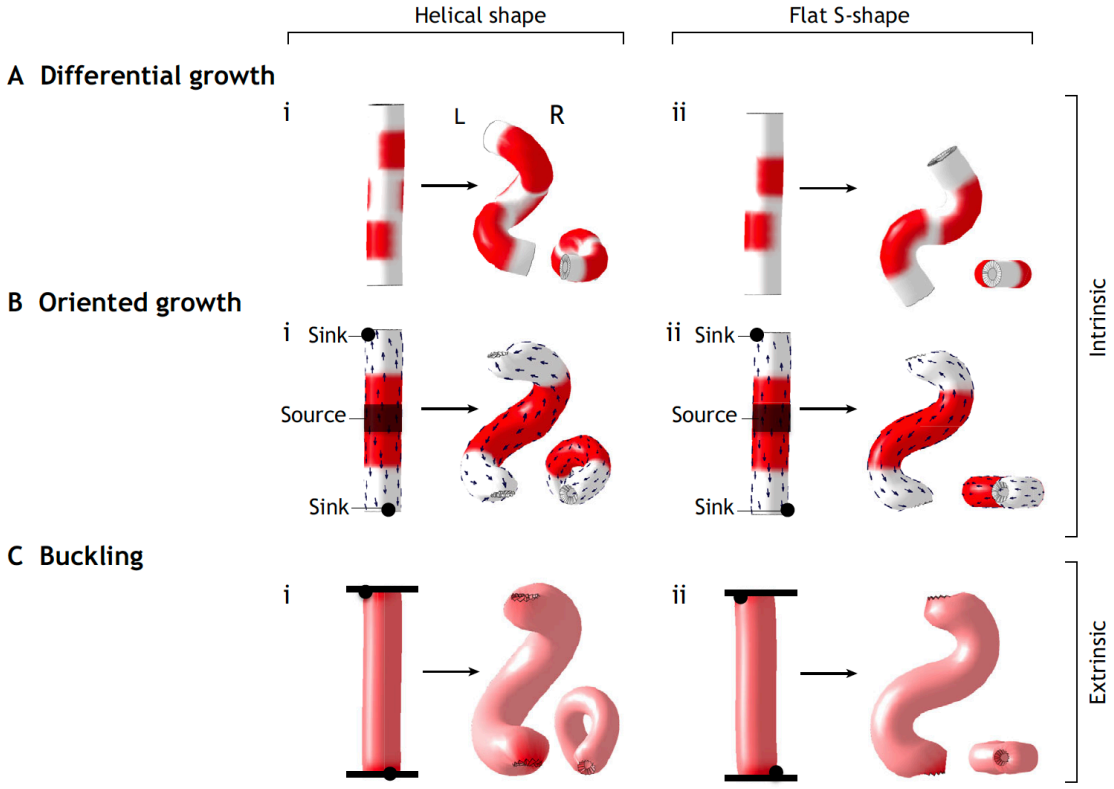

Figure 4. Theoretical models of heart looping considering extrinsic and intrinsic mechanisms. Helical shape for mammalian 3D heart looping (i) and flat S-shape for the fish 2D looped heart (ii). The initial state is shown to the left, and the final output shape is on the right of each condition. A) Differential growth along the tube comes from three differential bands of higher longitudinal growth, intercalated along the tube for the helical shape: while for the flat S-shape from two differential bands of higher longitudinal growth positioned at opposite sides of the tube. B) Oriented growth within the heart tube, the growth rate across the tube's circumference is constant, but in tilted orientation causing the looping. C) Buckling considers the longitudinal growth constant, but the fixed distance between the poles causes deformation leading to looping. (Fom Desgrange, Garrec, and Meilhac 2018).

On the other hand, the extrinsic cue taken into account has been the buckling, a mechanical instability marked by abrupt sideways deformation when the tube is confined between fixed poles forcing it to loop (Desgrange et al., 2018; Le Garrec et al., 2017). As a result, the looping has been proposed as a mechanism to shape the heart since its first description over 100

years ago by Wilhelm His in 1886 (Patten, 1922). Other extrinsic mechanisms have been suggested to explain the regulation of heart looping, which should be also considered for proper cardiac formation, like the cardiac jelly contribution and the hemodynamic forces established from the blood cardiac flow. The looping process is conserved among species, and recently, a theoretical model was developed to simulate the process in amniotes (3D) or fish (2D) looping (Desgrange et al., 2018; Le Garrec et al., 2017). For the heart formation of zebrafish, tissue bending is essential when the looping process occurs since it is a transition from the linear heart tube to a two-chambered heart (Linask & VanAuker, 2007).

1.5 Morphogenesis

During embryonic development, cells, tissues, and whole organisms develop their final shape in a process known as morphogenesis. At the tissue level, morphogenesis comprises bending, narrowing, lengthening, branching, and folding events for organs to reach their final and fully functional form (Papusheva & Heisenberg, 2010a). All the aforementioned processes are dependent on the cellular behaviors, from a collective but also from an individual perspective. Basic cellular mechanisms have been defined during morphogenesis illustrated in Figure 5, including cell proliferation, apoptosis, cell fusion, cell migration, cell-to-cell adhesion/de-adhesion, mesenchymal to epithelial transition (MET), epithelial to mesenchymal transition (EMT), cells becoming wedge-shaped (apical constriction), and cell neighbor exchange (Scott & Barresi, 2016; Trinkaus, 1984). Combination of these cellular processes generates highly specialized tissues and organs (Davies, 2013b; Scott & Barresi, 2016; Trinkaus, 1984; Wolpert, Tickle, & Martinez Arias, 2015).

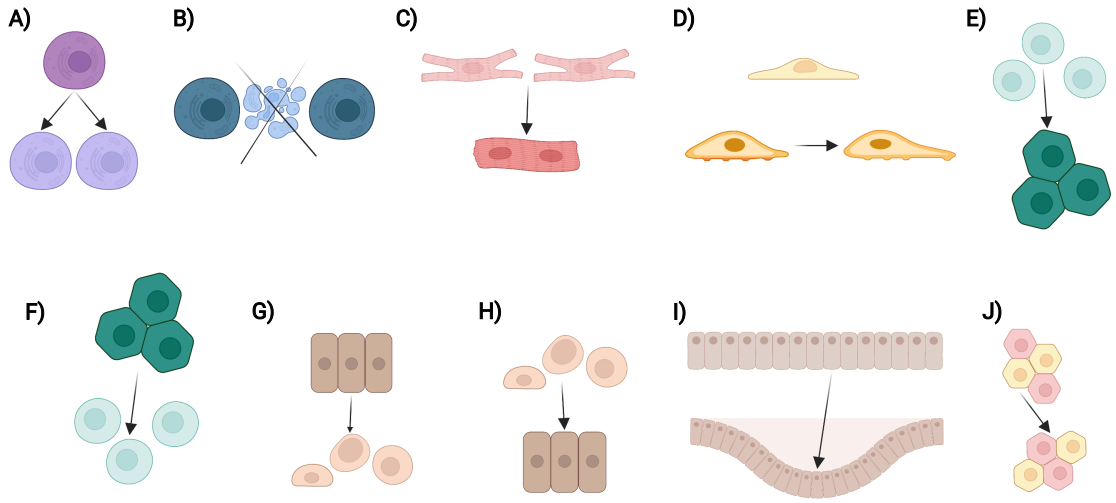

Figure 5. Basic cellular mechanisms of morphogenesis. A) Cell division. B) Apoptosis. C) Cell fusion. D) Migration. E) Adhesion. F) De-adhesion. G) Epithelial to mesenchymal transition (EMT). H) Mesenchymal to epithelial transition (MET). I) Constriction. J) Neighbor exchange (rosette formation).

1.6 Mechanical forces: cellular tension

One of the outcomes of the aforementioned processes during morphogenesis is the physical force generation that at its core is based on the cellular properties. The generated forces are not only driving the tissue shape changes, but are also stabilizing the tissues to acquire their final form. One of these forces comprise tension. In physics, tension is described as the pulling force transmitted axially by different means. In the biological context, tension can arise at different levels, at the plasma membrane level within the lipid bilayer, at the cellular level as well as at the supracellular level across tissues. The cellular tension, which is in the focus of this work, is one of the most studied forces in living organisms since many processes rely on it: from cell migration to cytokinesis, convergent extension, tissue morphogenesis, and organ formation. Recently, the attention has focused on the molecular players required to generate cellular tension. The cytoskeleton is the main component involved in tension generation, particularly the cortical actomyosin complex (Figure 6). The interaction of cortical actomyosin complex with the plasma membrane (PM) has been described as the primary contributor (Sens & Plastino, 2015; Sitarska & Diz-Muñoz, 2020).

In general terms, the cellular tension can be defined as a sum of the membrane and cortical tensions.

$$Cellular\ tension = membrane\ tension + \ cortical\ tension$$

(Equation 1)

The membrane tension is defined by the molecular components of the plasma membrane itself: lipid content, presence of transmembrane proteins, peripheral protein binding, and its interaction with cortical actomyosin, which can influence the tension distribution locally across the PM (Sitarska & Diz-Muñoz, 2020). The cortical tension is defined mainly by the cytoskeletal components localized at the cell periphery: cortical cytoskeleton, where cortical actomyosin is the primary and most studied contributor to tension generation. It enables cells to resist external mechanic stress, controls cellular shape and allows cells to generate force on their neighbors (Kelkar, Bohec, & Charras, 2020).

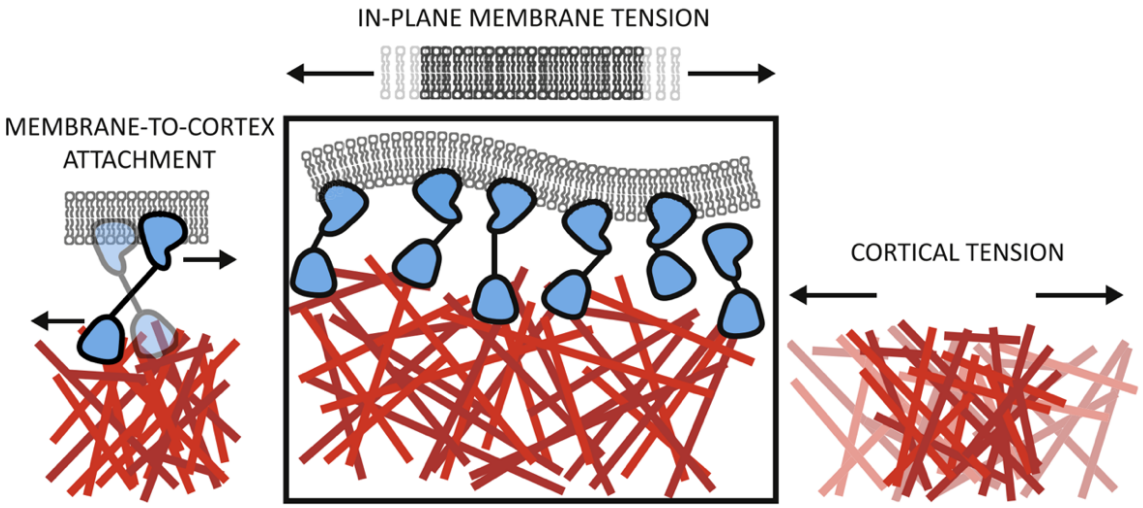

Figure 6. Cellular tension. The membrane and the cortex contribute to generating the cellular tension (left). The membrane tension is defined by the lipid content and the transmembrane proteins contributing to it across the plane (center). The cortical tension is generated by the cortical cytoskeleton, mainly the cortical actomyosin complex (right) (From Sitarska and Diz-Muñoz 2020).

1.7 Actomyosin complex

The actomyosin is a macromolecular complex and one of the main components of the cytoskeleton. It is constituted mainly of actin and myosin proteins (Agarwal & Zaidel-Bar, 2019; Gross, 2017; Levayer & Lecuit, 2012; Murrell, Oakes, Lenz, & Gardel, 2015; Svitkina, 2018; Zaidel-Bar, Zhenhuan, & Luxenburg, 2015). It was first discovered during the 1940s in the muscle fibers when it was observed that actin and myosin form highly organized bundles of filaments that make up more than half of the total protein of the muscle cell (Straub, 1942). Both proteins were detected in other cell types, showing that actomyosin in muscle tissue was a specialized form of a standard macromolecular complex that regulates mechanical forces involving intra and intercellular tension (Cartagena-Rivera, Logue, Waterman, & Chadwick, 2016; Eghiaian, Rigato, & Scheuring, 2015; Munjal & Lecuit, 2014; Peukes & Betz, 2014; Q. Yu, Li, Murrell, & Kim, 2018). In addition, it plays a role in mechanosensing and

mechanotransduction across different cell types (Linask and VanAuker, 2007; Kelkar, Bohec, and Charras, 2020). The contractile properties of the actomyosin are dictated by the interaction of the actin filaments and the motor protein myosin, which possesses ATPase activity to generate the pulling force using the actin filaments as rails (Kamm & Stull, 2011; Sheikh, Lyon, & Chen, 2015). The contractility of the actomyosin complex is responsible for generating the mechanical forces required for different processes, including, among others, cytokinesis, cell migration, tissue morphogenesis, and muscle contraction (Murrell et al., 2015; Vicente-Manzanares, Ma, Adelstein, & Horwitz, 2009)

1.7.1 Actin

Actin belongs to a family of proteins conserved among species and is present in all eukaryotic cells. Actin is a monomeric protein that constitutes mainly two subcellular structures; microfilament, a significant constituent of the cytoskeleton, and thin filaments, part of the contractile machinery in muscle cells (Cooley, Whitaker, Sweeney, Fraser, & Davidson, 2011; Dominguez & Holmes, 2011; Svitkina, 2018). In its monomeric form it is present as an individual subunit called globular actin (G-actin) that can polymerize into actin filaments. Filamentous actin (F-actin) is formed as double molecular strands of polymerized G-actin winding together in a helix conformation (Taylor, Abramova, Charlton, & Adler, 1998). Actin assemblies are highly dynamic and are involved in a wide variety of cellular processes: structural as cytoskeleton component, cell motility (migration), cytokinesis, intracellular trafficking, organelle movement, cell signaling, regulation of cellular junctions, membrane dynamics, and generation of intra and intercellular tension forces as a part of morphogenetic processes required for organ development (Heisenberg & Bellaïche, 2013; Mammoto & Ingber, 2010; Stooke-Vaughan & Campàs, 2018; Yogurtcu, Kim, & Sun, 2012). ATP-dependent actin polymerization intrinsically contributes to establishing tension forces within the cells. Moreover, actin microfilaments serve as rails to establish direct interaction with the motor protein myosin, directly impacting the mechanical properties of the cells and cellular dynamics. Tissue force generation is established with direct interaction with myosin, mainly with the non-muscle myosin II and actin filaments in every cell of the body (C. W. Chang & Kumar, 2015; Conti & Adelstein, 2008; Heissler & Manstein, 2013; Martino, Perestrelo, Vinarský, Pagliari, & Forte, 2018).

1.7.2 Myosin

Myosin is a superfamily of ATP-dependent motor proteins involved in a wide range of motility processes in all eukaryotic cells (Agarwal & Zaidel-Bar, 2019; Gross, 2017; Lecuit, Lenne, &

Munro, 2011; Levayer & Lecuit, 2012; Murrell et al., 2015). To date, myosin proteins have been classified in 19 classes (termed myosin I to XIX) based on their discovery, their localization, and the function they are involved in (Hodge & Cope, 2000). The basic properties of all myosin proteins are actin-binding domains, ATP hydrolysis (ATPase enzymatic activity), and force transduction (Beach et al., 2014; Conti & Adelstein, 2008; Heissler & Manstein, 2013; Hodge & Cope, 2000; Kasza & Zallen, 2011; Sellers, 2000; Somlyo et al., 2004; Vicente-Manzanares et al., 2009). The structure of the myosin is comprised of three domains: head, neck, and tail. The head region is a globular domain at the N-terminus where the ATPase catalytic region is located together with the actin-binding domain. The neck domain interacts with the regulatory chains of the myosin to modulate its activity. It also serves as a leverage arm transducing the generated force and linking the catalytical head with the C'-terminal region. The tail region binds to and moves cargo in a cell; at the same time, the C-terminal domains of other myosin proteins self-associate into filaments, which allow their heads to tether actin filaments and exert tension (Vicente-Manzanares et al., 2009). Myosin genes are conserved across species, and several isoforms have been identified and characterized, with the Myosin II being the most common and abundant class of myosin. Myosin II is the main myosin responsible for the contraction in muscle cells. However, it is also present as a non-muscle myosin (NMII) in all types of cells (Wolff & Rubin, 1998).

The non-muscle myosin II comprises of three pairs of subunits: two heavy chains with the globular head domain with the ATP and actin binding domain, two regulatory light chains (RLC) in the neck of the heavy chain which regulate the activity of the myosin, and two essential chains also in the neck region of the heavy chains which are in charge of stabilizing the two heavy chains (Sellers, 2000; Vicente-Manzanares et al., 2009).

1.8 Actomyosin regulation

Actomyosin contractility is a crucial regulator of cell morphology and tissue morphogenesis (Lecuit, Lenne, and Munro, 2011). First, stability and change of the cell's shapes are generated through a cortex of F-actin meshwork beneath the plasma membrane that resists and generates tension forces (Bovellan et al., 2014). Second, active contractile tension is generated by ATP hydrolysis within myosin to move along these F-actin filaments (Levayer & Lecuit, 2012).

NMII phosphorylation is the main posttranslational modification that regulates its activity. There are many different amino acid residues which are known to be subjected to the phosphorylation. Among all of them, in this work I focused on the Ser18/Thr19 phosphorylation of myosin regulatory light chain (MRLC) because those are the main phosphorylation sites controlling the myosin activity by increasing its affinity to bind actin in vertebrates (Ikebe,

Hartshorne, & Elzinga, 1986; Scholey, Taylor, & Kendrick-Jones, 1980; Sellars, Pato, & Adelstein, 1981; Umemoto, Bengur, & Sellers, 1989).

NMII localization or activity is regulated by phosphorylation and dephosphorylation of its MRLC. The dynamic phosphorylation of MRLC at the highly conserved amino acid residues T18 and S19 (Figure 7) causing a conformational change from a closed to an open state allowing it to interact with actin filaments. This involves a tightly regulated interplay between Rho-associated kinase (ROCK), myosin light chain kinase (MYLK), and myosin phosphatase (MYPT) activity in a complex interaction network where ROCK and MYLK directly phosphorylate MRLC, while MYPT reduces MRLC phosphorylation (Loirand, Guérin, & Pacaud, 2006; Matsumura, Totsukawa, Yamakita, & Yamashiro, 2001; Riento & Ridley, 2003; Totsukawa et al., 2004). Phosphorylation of MRLC involves tight regulation of various processes together, the activity of the kinases, also the phosphatase (MYPT) activity, and Ca^{2+} signaling (Riento & Ridley, 2003). ROCK increases MRLC phosphorylation directly but also indirectly through phosphorylation of MYPT1, which inhibits its phosphatase activity, and results in the elevated pMRLC levels (Somlyo et al., 2004). Previously, the role of MRLC was also described during epithelial remodeling through accumulation at central junctions of cell clusters during cell rearrangements and it has been shown that the phosphorylation of MRLC affects localized tension (Blankenship, Backovic, Sanny, Weitz, & Zallen, 2006; Zallen & Blankenship, 2008).

Other mechanisms upstream of this complex network of kinases and phosphatases comprise the myotonic dystrophy kinase-related Cdc42-binding kinase (MRCK, activated by Cdc42), and leucine zipper interacting kinase (ZIPK) (Vicente-Manzanares et al., 2009). Moreover, activation of MRLC through phosphorylation is controlled via inhibition of myosin phosphatase target subunit 1 (MYPT1) activity that is mediated by its phosphorylation through ROCK (Lecuit, Lenne and Munro, 2011). The induction of small GTPases by Rho GEFs, leading to enhanced ROCK function and activation of Formin and Formin-related proteins such as Daam (Nishimura, Honda, & Takeichi, 2012).

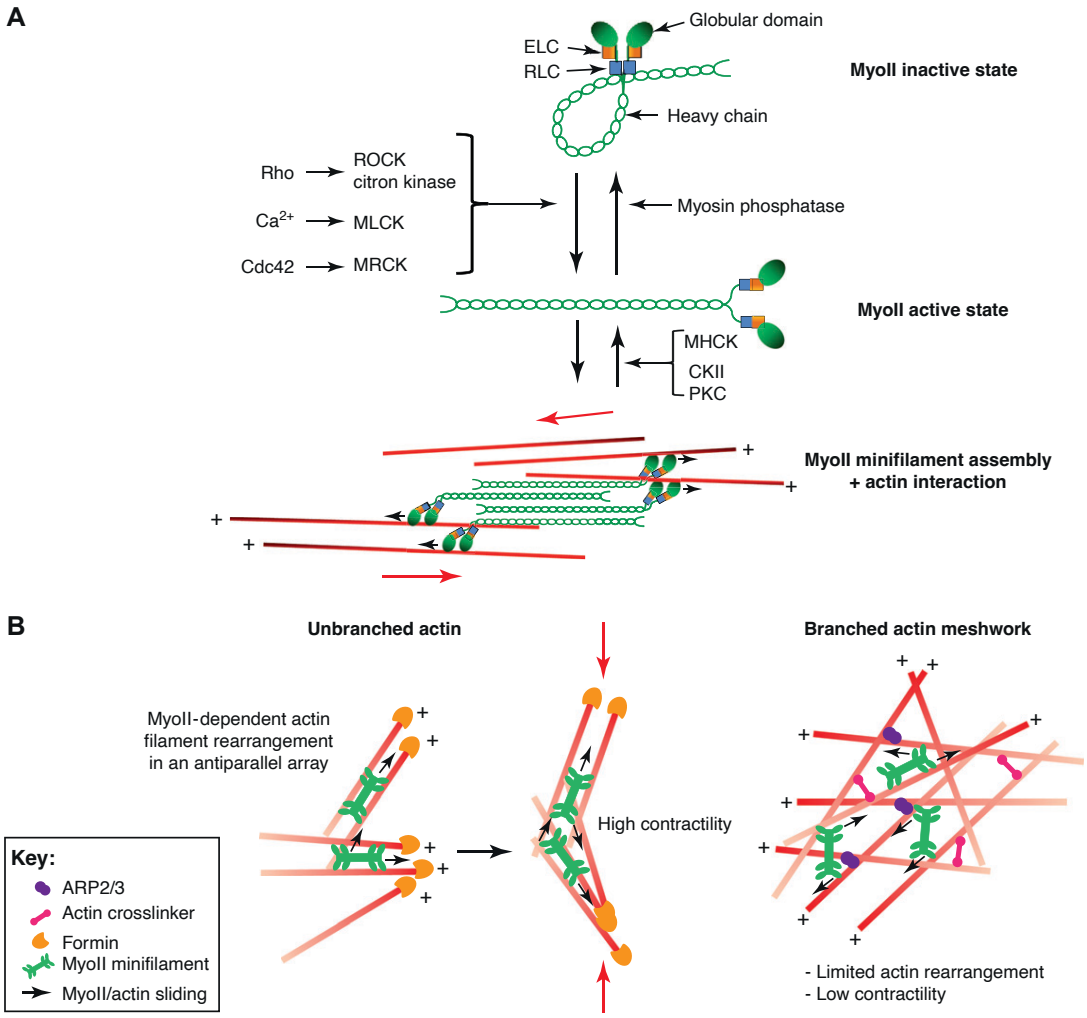

Figure 7. Actomyosin regulation at glance. A) Non-muscle myosin (MyoII) is activated through phosphorylation from diverse proteins causing a conformational change from a closed to an open state allowing it to interact with actin filaments. B) Unbranched and branched (mainly cortical) actin filaments. Actin arrangements build up to tension due to the interaction with MyoII (from Levayer and Lecuit 2012).

1.9 Epithelium

During the formation of the linear heart tube and the looping process, the zebrafish myocardium is made of a single layer of polarized cells. Epithelia are types of tissues made up of layers of similar cells bound closely together and adhering to each other forming coherent cell sheets (Drenckhahn et al., 1993). All metazoans have epithelial tissues, which establish body compartments, engage in the controlled exchange of chemicals and ions, and control homeostasis (Fahey & Degnan, 2010; Nichols, Dirks, Pearse, & King, 2006).

During organ formation, migration of cells, tissue branching, tubulogenesis, and generation of tension forces are orchestrated together. The physical constraints the epithelium is subjected to during organogenesis can be divided in general categories as follows: tissue branching, bending and expansion, and lumen formation (Keller & Shook, 2011; Navis & Nelson, 2016;

Spurlin & Nelson, 2017). These morphogenetic changes must be tightly controlled and are required to achieve the proper epithelial remodeling and organization to achieve the capacity to form organs. The polarity of the epithelium is first established at a cellular level.

1.10 Cell polarity

Cell polarization is crucial for developing multicellular organisms, and aberrant cell polarization contributes to disease conditions (Iden & Collard, 2008). Cell polarity is the asymmetrical organization of the different components of the cell including its intracellular organelles, cytoskeleton, and plasma membrane (Trinkaus, 198 O'Briennnnn, Zegers, and Mostov, 2002; Nelson, 2003; Shin, Fogg and Margolis, 2006; Goldstein and Macara, 2007; Bryant and Mostov, 2008). Cell polarization is achieved by segregating their molecular components, proteins, and lipids, preferentially on the opposite sides of the cell membranes. This asymmetry defines specialized functions, such as maintaining a barrier within an epithelium or transmitting signals (Bryant & Mostov, 2008; Papusheva & Heisenberg, 2010b).

1.11 Apicobasal polarity

Apicobasal polarity is a type of cell polarity specific to epithelial cells (Gibson & Perrimon, 2003), containing a specialized apical membrane facing the outside of the body or the lumen of internal cavities and a specialized basolateral membrane localized at the opposite side, away from the lumen (Assémat, Bazellières, Pallesi-Pocachard, Le Bivic, & Massey-Harroche, 2008; Goldstein & Macara, 2007; Moore et al., 2013; W. J. Nelson, 2003; Rodriguez-Boulan & Macara, 2014; Roignot, Peng, & Mostov, 2013; Shin et al., 2006). Three main protein complexes have been described to be involved in the establishment of apicobasal polarity (Figure 8) in cells: Crumbs, Scribble, and PAR (partitioning defective), with the latter demonstrating the broader activity among them (Assémat et al., 2008; Goldstein & Macara, 2007). These complexes can collaborate or antagonize each other during polarization processes, producing or sustaining cellular asymmetry (Iden & Collard, 2008).

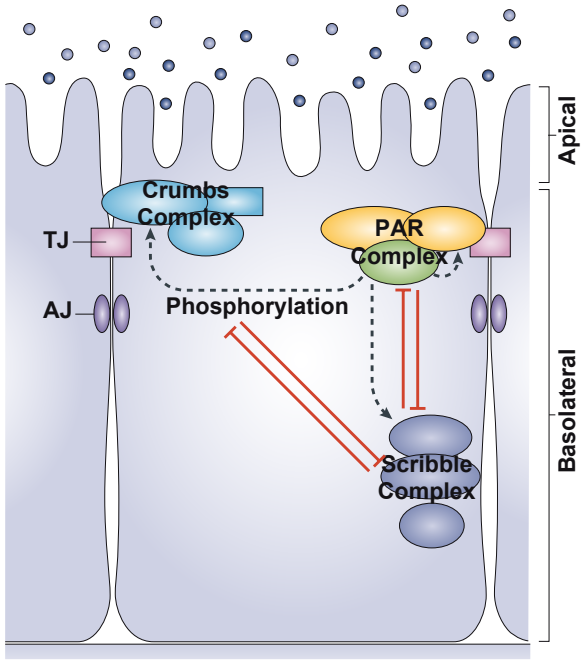

Figure 8. Simplified apicobasal cell polarity. Three conserved apicobasal polarity protein complexes (the partitioning defective (PAR), Crumbs and Scribble complexes). PAR and Crumbs complexes localize predominantly to tight junctions, whereas Scribble complex localizes mainly in the basolateral membrane. Mutual exclusion of the Scribble complex and the apical complexes establishes the apicobasal polarity and maintains the asymmetric distribution of polarity regulators. TJ: tight junction. AJ: adherens junction. (Adapted from Iden and Collard 2008).

The Crumbs complex comprises the transmembrane protein Crumbs and two scaffolding proteins, PALS1 (protein associated with LIN-7 1) and PATJ (PALS1-associated tight junction protein) (Makarova, Roh, Liu, Laurinec, & Margolis, 2003; Roh & Margolis, 2003). Crumbs complex regulates polarity in epithelial cells by determining the apical membrane; this function is conserved from *Drosophila* to mammals (Bulgakova & Knust, 2009). Expression of Crumbs-3, a mammalian homolog of *Drosophila* Crumbs, contributes to the formation of tight junctions (Michel et al., 2005; Tepass, Tanentzapf, Ward, & Fehon, 2001). The Scribble complex consisting of Scribble, Discs large (DLG), and Lethal giant larvae (LGL) was first identified in *Drosophila melanogaster* as being involved in cell polarization since the mutations in any of these genes caused a loss of polarity properties in cells of epithelial tissues (Bilder, Li, & Perrimon, 2000). The PAR complex was also identified and studied at first in *Drosophila melanogaster* and *Caenorhabditis elegans*; these polarity proteins have also homologs in vertebrates (Iden & Collard, 2008). Two *par* genes (*par-3* and *par-6*), discovered in *C. elegans*, are proteins containing a PDZ domain that form a PAR complex interacting with the atypical protein kinase C (aPKC). Isoforms of PAR-3, PAR-6, and aPKC, are expressed ubiquitously in many types of cells where the kinase activity of aPKC mediates the phosphorylation of target proteins required to regulate downstream events of polarity signaling (Iden et al.,

2012).Crumbs-3 and PAR-3 complexes in mammals are localized mainly to tight junctions, and the Scribble complex is mainly located basolaterally (Iden & Collard, 2008). The mutual exclusion of Scribble and the tight junction complexes defines the apicobasal polarity with the phosphorylation of LGL2 and PAR-1 to keep the asymmetric distribution of the polarity components (Bilder et al., 2000; Bilder & Perrimon, 2000).

1.12 Planar polarity

The arrangement of the cells at a global tissue-scale level in an oriented manner over a single 2D plane is known as a planar polarity (Zallen, 2007). It was first identified in *Drosophila melanogaster* by observing the polarized arrangement of bristles and hairs that project from the fly's specific cell surfaces in the abdomen and wings (Jussila & Ciruna, 2017). The uniform orientation, structure, and mobility of cells within the plane of a tissue or organ system is coordinated by the non-canonical Wnt signaling pathway, known as the Planar cell polarity pathway.

1.13 Wnt signaling pathway

Wnt signaling is considered among the most important signaling pathways during embryonic development (Sanz-Ezquerro, Münsterberg, & Stricker, 2017). It controls various developmental processes in the organisms, such as embryonic induction, cell fate specification, and cell polarity (Compass, Vladar, Antic, & Axelrod, 2016; Habas, Kato, & He, 2001; Slusarski, Yang-Snyder, Busa, & Moon, 1997; ten Berge, Brugmann, Helms, & Nusse, 2008; Tran, Sekkali, Van Imschoot, Janssens, & Vleminckx, 2010; Y. Yang & Mlodzik, 2015). In adults, Wnt signaling is required for tissue maintenance and its mis-regulation causes abnormalities and occurrence of disease like osteoporosis, vascular defects, tumor and cancer predisposition (Barber, 1992; Gong et al., 2001; Kinzler et al., 1991; Lammi et al., 2004; Robitaille et al., 2002).

Wnt ligands are a group of highly hydrophobic secreted glycoproteins evolutionarily conserved across metazoan. There are 19 members of Wnt ligands comprising one protein family (Butler & Wallingford, 2017; Compass et al., 2016; Henderson, Long, & Dean, 2018; Karner, Wharton, & Carroll, 2006a, 2006b; Klaus & Birchmeier, 2008; Lawrence, Struhl, & Casal, 2007; Mikels & Nusse, 2006; Niehrs, 2012; Y. Yang & Mlodzik, 2015; Zallen, 2007). Shared features among all the Wnt ligands include several charged amino-acid residues, 22 characteristic cysteine residues distributed along the sequence for the proper protein folding dependent on disulfide bonds, glycosylation sites, and secretion signal sequences (Mikels & Nusse, 2006; Niehrs, 2012). Wnt proteins are highly modified post-translationally; N-linked glycosylation and

lipidation of a palmitoyl moiety in the first cysteine residue contributes to its high hydrophobicity necessary for the proper secretion, transport, recognition, and the overall activation and modulation of their activity across the cells mainly as paracrine or autocrine signaling (Baeg, Lin, Khare, Baumgartner, & Perrimon, 2001; Beckett et al., 2013; Mehta, Hingole, & Chaudhary, 2021; Mulligan et al., 2012; Panáková, Sprong, Marois, Thiele, & Eaton, 2005; Stanganello et al., 2015).

The Wnt signaling has been defined as “canonical” or “non-canonical”. The former involves stabilization and activation of the transcriptional regulator β-catenin, whereas the latter is independent of β-catenin activation (Butler & Wallingford, 2017; Niehrs, 2012).

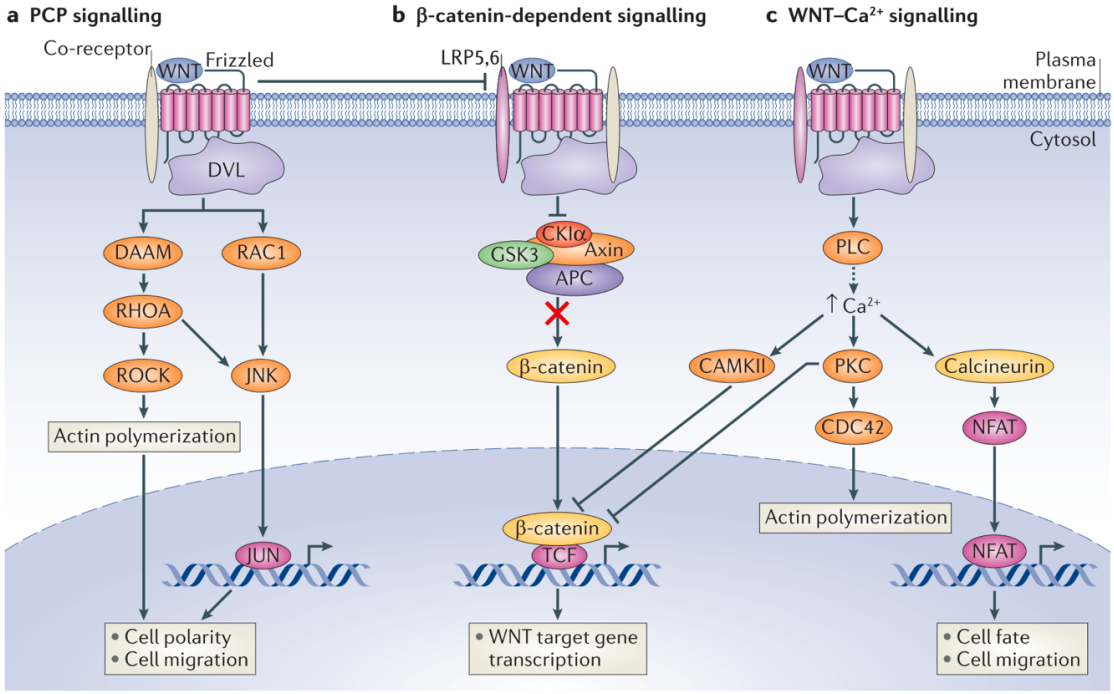

Figure 9. Wnt signaling pathway. A) Planar cell polarity (PCP) signaling: Disheveled (DVL) activates small GTPases (RHOA through DAAM (Disheveled-associated activator of morphogenesis) and RAC1), which then activate RHO kinase (ROCK) and JUN-N-terminal kinase (JNK), to finally lead to actin cytoskeletal changes and expression of cell polarity and cell migration genes. B) β-catenin-dependent signaling in the presence of Wnt ligand, the destruction complex (comprising glycogen synthase kinase 3 (GSK3), casein kinase Iα (CKIα), Axin and adenomatosis polyposis coli (APC)) is inactivated allowing β-catenin to accumulate and translocate to the nucleus, and to promote the expression of target genes. Without the Wnt ligand, GSK3 phosphorylates β-catenin, which marks it for degradation. C) The Wnt-Ca^2 signaling: increase in intracellular Ca^{2+} through the action of phospholipase C (PLC) activates multiple Ca^{2+}-dependent proteins including calcium and calmodulin-dependent kinase (CAMKII), protein kinase C (PKC), and calcineurin, which ultimately results in the activation of the target gene transcription, and promotion of the actin polymerization (From Niehrs 2012).

The canonical Wnt signaling pathway initiates with the recognition of the Wnt ligand by its receptor Frizzled (Fz) and co-receptor LRP-5/6. Then, the cytoplasmic protein Disheveled

(DVL) is recruited to inactivate “the destruction complex” composed of glycogen synthase kinase 3 (GSK3), adenoma polyposis coli (APC), Axin and casein kinase Iα (CKIα) leading to the stabilization and translocation of β-catenin to the nucleus, where it binds two main transcription factors TCF (T cell factor) and LEF (lymphoid enhancer-binding factor) to regulate the expression of genes, mainly involved in cell differentiation and proliferation (Aoki, Sadoshima, & Izumo, 2000; Klaus & Birchmeier, 2008; Le Garrec et al., 2017; Logan & Nusse, 2004; Papusheva & Heisenberg, 2010b).

The non-canonical Wnt signaling pathways do not use β-catenin activation but instead use other modules downstream after Fzd activation. The two main non-canonical branches of Wnt signaling can be classified as the Wnt-Ca^{2+} signaling and the Planar cell polarity pathway.

The Wnt-calcium pathway was identified in Xenopus and Zebrafish (Slusarski, Corces, & Moon, 1997; Slusarski, Yang-Snyder, et al., 1997). The activation of this pathway results in an increase of intracellular Ca^{2+}, which can be caused either by the GPCR-like activity of the frizzled receptor (Slusarski, Corces, et al., 1997) or a more recently described mechanism involving the activation of the L-type Calcium channels (Panáková, Werdich, & MacRae, 2010). The intracellular calcium increase results in the activation of calcium-dependent enzymes like calcium/calmodulin-dependent kinase (CaMK)II, PKC, or calcineurin (Dorn & Brown, 1999). The result is the modulation of gene expression involving different transcription factors like NFAT (nuclear factor of activated T cells) or Nemo-like kinase, which interferes with β-catenin signaling and histone modifications to regulate gene expression (Saneyoshi, Kume, Amsaki, & Mikoshiba, 2002).

The second non-canonical Wnt signaling pathway, the Planar cell polarity pathway, is described in detail below.

1.14 Planar cell polarity pathway

The Planar cell polarity (PCP) pathway was first identified in Drosophila studying the orientation of the hairs and bristles across the body (Figure 10A, B). Six main molecular components of the pathway have been identified as core components: Wnt ligands, Frizzled receptors, the cytosolic proteins Disheveled, Prickle, Diego, and the transmembrane proteins Van Gogh and Flamingo (Table 1) (Butler & Wallingford, 2017; Compass et al., 2016; Fanto & McNeill, 2004; Henderson et al., 2018; Karner et al., 2006b; Lawrence et al., 2007; D. Li & Wang, 2018; Nishimura et al., 2012; Wu, Ge, Huang, Hua, & Mu, 2011; Zallen, 2007). The components are segregated on opposite sides of the cell in a polarized fashion (Figure 10C). On the distal/posterior side of the cells, Fz and Dvl are found, whereas Vangl and Pk are localized on a proximal/anterior orientation. Flamingo is equally distributed across the cellular membrane.

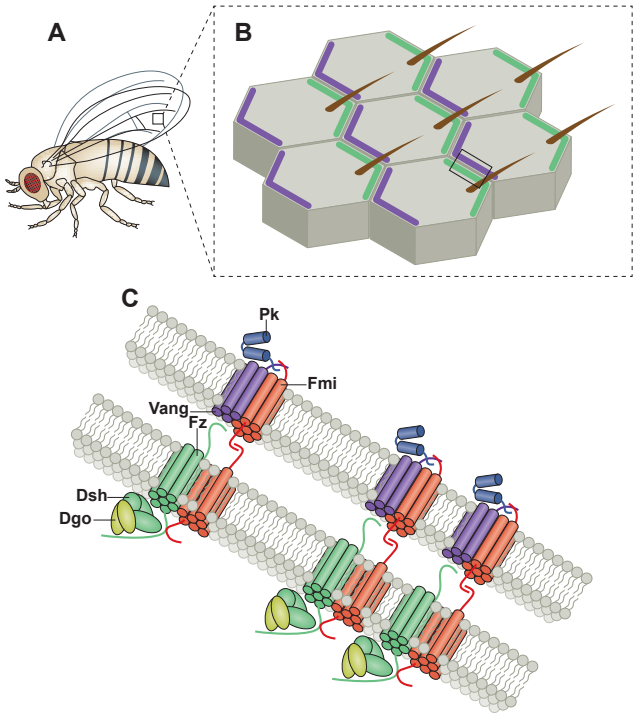

Figure 10. Planar polarity. A) Identified in *Drosophila melanogaster*, planar polarity is manifested by many planar-polarized body features like hairs and bristles on the wings, legs, and notum. B) Cells of the wing epithelium have a single actin-based trichome; asymmetrically patterned by proximal accumulations of Van Gogh (Vang) and Prickle (Pk) (purple) and distal accumulations of Frizzled (Fz), Disheveled (Dsh) and Diego (Dgo) (green). C) Asymmetric PCP signaling components. Fz and Vang are transmembrane proteins that associate with physically linked Flamingo (Fmi) (From Butler and Wallingford 2017).

Frizzled transmembrane proteins serve as receptors of the Wnt ligands. Fz receptors bind also other ligands, including secreted Frizzled-related proteins (SFRPs) and R-spondin. However, the main ligands are the 19 Wnt proteins depending on the Fz receptors (Angers & Moon, 2009; Janda, Waghray, Levin, Thomas, & Garcia, 2012; Klaus & Birchmeier, 2008; Mikels & Nusse, 2006; Rao & Kühl, 2010; Saito-Diaz et al., 2013).

Fz receptors comprise a family of seven transmembrane domains proteins with a length ranging from 500 to 700 amino acids depending on the Fz member (Adler, Vinson, Park, Conover, & Klein, 1990; Dann et al., 2001; Malbon, 2004; Schulte & Bryja, 2007; Vinson, Conover, & Adler, 1989). They are considered unconventional class of GPCRs, the frizzled GPCRs, because the main signal transduction does not correspond to a classical GPCR signaling activation (Dijksterhuis, Petersen, & Schulte, 2014; Foord et al., 2005; Schulte, 2010; Schulte & Bryja, 2007).

Table 1. PCP core components and their localization.

Proximal localization (Anterior)	Both	Distal localization (Posterior)
Membrane: **VANGL** (Van Gogh) **Cytosol:** **PK** (Prickle)	**Membrane:** **CELSR** (Flamingo)	**Membrane:** **FZD** (Frizzled) **Cytosol:** **DVL** (Disheveled) **ANKRD6** (Diego)

Fz receptors contain an N-terminus domain that contains multiple glycosylation sites, followed by seven transmembrane I domains, and an intracellular C-terminus domain, which is subjected to post-translational modifications (PTMs) and interacts with different proteins (Dann et al. 2001; Janda et al. 2012; D. C. Slusarski, Corces, and Moon 1997; Schulte and Bryja 2007; Huang and Klein 2004; Yang and Mlodzik 2015; Wang et al. 2016; Angers and Moon 2009). The Fz N-terminus contains a large extracellular cysteine-rich domain (CRD), which mediates the direct interaction with the Wnt ligands through the hydrophobic pocket, and serves as a cavity for the palmitate moiety of the Wnt proteins (S. Yang et al., 2018). The C-terminus facing the cytosol varies across the different Fz receptors, except for the highly conserved motif (KTXXXW). This motif is required for the recruitment and binding with the scaffold protein Dvl to transduce the signaling after Wnt-mediated activation of the receptor (Angers & Moon, 2009; Dann et al., 2001; H. Huang & Klein, 2004; Janda et al., 2012; Malbon, 2004; Schulte & Bryja, 2007; Slusarski, Corces, et al., 1997; Wang et al., 2016; Y. Yang & Mlodzik, 2015).

Right downstream of the Fz receptor, the cytosolic protein Disheveled is located. It participates in both canonical and non-canonical Wnt signaling depending on interactions that are not yet fully understood (C. Gao & Chen, 2010; Mlodzik, 2016; Sharma et al., 2018; Theisen et al., 1994; Wharton, 2003). In planar polarized cells, the cytoplasmic transducer is localized on the same side of the Fz receptors. Dvl protein was first identified in *Drosophila*, however, it is conserved across the species from hydra to humans (Klingensmith, Nusse, & Perrimon, 1994; Theisen et al., 1994; Wharton, 2003). Disheveled has three conserved domains identified based on the amino acid sequence. The DIX (Disheveled-Auxin) domain, PDZ (Post synaptic density-95/Discs large/Zonula-occludens-1) responsible for the direct interaction with the Fz receptor, and a DEP (Disheveled, Egl-10, Pleckstrin) domain which mediates the interaction with other proteins like DAAM, necessary for the PCP signaling. Another two conserved basic regions are also present in Disheveled. One located between the DIX and PDZ domains rich in serine and threonine. The second one downstream of the PDZ domain rich in proline. These

basic regions mediate protein-protein interactions and are crucial to discern which Wnt signaling to follow. Disheveled also contains a nuclear localization signal (NLS) and nuclear export (NE) signal, both important for the regulation of the cellular localization of the protein (C. Gao & Chen, 2010; Mlodzik, 2016; Sharma et al., 2018; Theisen et al., 1994; Wharton, 2003; X. Zhang et al., 2007).

Van Gogh/Strabismus (Vangl in vertebrates) protein was first identified in *Drosophila* as a novel component of the planar cell polarity (Wolff & Rubin, 1998). Vertebrates have two orthologs, Van Gogh-like protein 1 and 2. Vang/Vangl are four transmembrane domain proteins with multiple functional domains, and it is proposed that they share overlapping and redundant functions (Bailly, Walton, & Borg, 2018; Fanto & McNeill, 2004; Iliescu, Gravel, Horth, Apuzzo, & Gros, 2011; Karner et al., 2006b; Rao & Kühl, 2010; Tada & Kai, 2009; Zallen, 2007). Vangl proteins contains two serine/threonine phosphorylation clusters close to the cytoplasmic N-terminus region upstream of the four transmembrane regions. The C-terminus of the protein is critical for establishing direct interactions with different proteins, including the PCP core components Prickle and Disheveled (Angers & Moon, 2009; Bailly et al., 2018; Compass et al., 2016; Fanto & McNeill, 2004; Henderson et al., 2018; Karner et al., 2006b; Rao & Kühl, 2010; Tada & Kai, 2009; Wang et al., 2016; Y. Yang & Mlodzik, 2015; Zallen, 2007). Three important motifs have been also described to be present in the Vangl2 sequence, a basolateral-sorting motif (YXXF) which is necessary for vesicle transport and sorting to the proper membrane localization (Guo, Zanetti, & Schekman, 2013), a VIM motif (p97/VCP interacting motif) involved in ubiquitination and degradation of it (Feng et al., 2021), and a PDZ binding motif (PBM) (Feng et al., 2021).

As mentioned before the cytoplasmic component localized together with Vangl2 is the Prickle protein (Compass et al., 2016; Fanto & McNeill, 2004; Gibbs et al., 2016; Henderson et al., 2018; H. Huang & Klein, 2004; Karner et al., 2006b; Lim et al., 2016; Rao & Kühl, 2010; Tada & Kai, 2009; Veeman, Slusarski, Kaykas, Louie, & Moon, 2003; Zallen, 2007). It was first identified in *Drosophila* (Taylor et al., 1998), with homologs present in vertebrates including zebrafish, mouse, and human (Katoh & Katoh, 2003; Veeman et al., 2003). The main distinction between isoforms is the length of the C-terminus. Prickle is a cytosolic protein that contains three LIM domains, and it is also known as REST/NRSF-interacting LIM domain protein, which is a putative nuclear translocation receptor (Veeman et al., 2003). Prickle directly interacts with Vangl, which recruits it to the membrane (Bastock, Strutt, & Strutt, 2003; Jenny, Darken, Wilson, & Mlodzik, 2003). This interaction between Vangl and Prickle in a proximal localization within the cells is responsible for the cell planar polarization (Fanto & McNeill, 2004; Henderson et al., 2018; H. Huang & Klein, 2004; Karner et al., 2006b; Rao & Kühl, 2010; Tada & Kai, 2009; Veeman et al., 2003; Zallen, 2007).

From the six PCP core components, Celsr (Cadherin EGF LAG seven-pass G-type receptor) protein is not distributed in a polarized manner but its recruitment is regulated through the signaling cascade depending on the partner interaction required in a time specific manner (Aw, Heck, Joyce, & Devenport, 2016; Devenport, Oristian, Heller, & Fuchs, 2011; Stahley, Basta, Sharan, & Devenport, 2021). Celsr (Flamingo) protein is a member of the cadherin superfamily, however, it does not interact with catenins making it a nonclassical-type cadherin (Gul, Hulpiau, Saeys, & van Roy, 2017). The flamingo cadherins are transmembrane proteins with seven transmembrane regions containing nine cadherin domains, seven epidermal growth factor-like repeats, and two laminin G-like domains in their ectodomain. These proteins are thought to be receptors for contact-mediated communication, with cadherin domains serving as homophilic binding areas and EGF-like domains serving as cell adhesion and receptor-ligand interactions (Fanto & McNeill, 2004; Stahley et al., 2021). It has been shown that all three members of the human CELSR family (CELSR1, CELSR2, and CELSR3) play critical roles in vertebrate PCP during embryonic development in different processes, like vessel formation and rearrangements of cells, while their mis-regulation leads to development of neural and cardiovascular diseases (Compass et al., 2016; Stahley et al., 2021).

Diego is a cytoplasmic protein identified in *Drosophila* (Feiguin, Hannus, Mlodzik, & Eaton, 2001). Its homolog in vertebrates is Diversin or ANKRD6. It has been shown that it interacts with the planar polarity protein Disheveled to activate downstream effectors of the PCP pathway including RhoA or Jun N-terminal Kinase (Feiguin et al., 2001). The PCP pathway is essential for embryonic development (convergent-extension process) and organogenesis (tissue branching and bending) including proper heart formation since specific mouse mutant phenotypes are related to heart looping defects (Desgrange et al., 2018). One of the primary readouts of the PCP pathway is the remodeling and local reorganization of the actomyosin complex through downstream effectors, including small GTPases Rho, Rac, Cdc4, and JNK (Marlow, Topczewski, Sepich, & Solnica-Krezel, 2002; Tada & Kai, 2009; Unterseher et al., 2004). However, the activity of actomyosin complexes, specifically the phosphorylation of myosin, has been thus far attributed solely to Rho-associated protein kinase, Rock (Figure 11) (Compass et al., 2016; Vicente-Manzanares et al., 2009; Y. Yang & Mlodzik, 2015; Zallen, 2007).

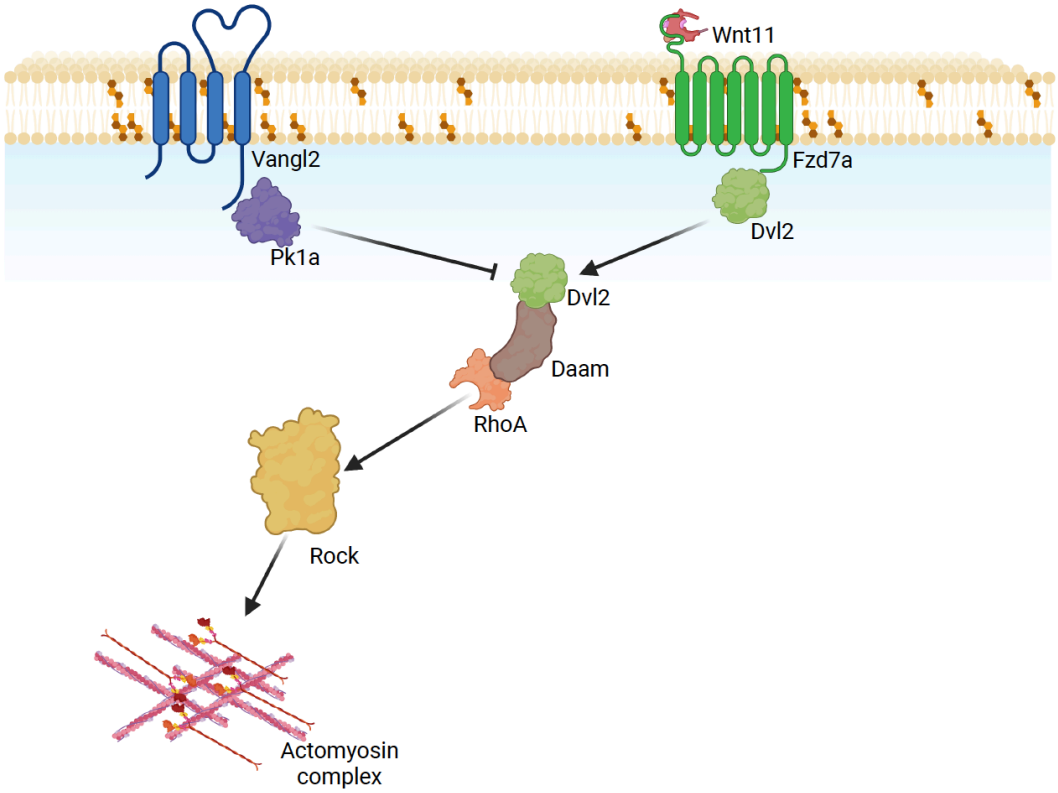

Figure 11. Planar cell polarity pathway. Simplified scheme of the PCP pathway. In zebrafish, the transmembrane receptor Fzd7a and the four transmembrane protein Vangl2 occupy mutually exclusive domains in the plasma membrane of the cells. Fzd7a acts as the receptor of the Wnt11 ligand, recruiting and activating the cytoplasmic protein Disheveled, which activates Daam to transduce the signal to the RhoA GTPase to activate Rock, causing phosphorylation of the non-muscle myosin II resulting in the contraction of cells. Vangl2 interacts with its cytosolic transducer Pk1a, which competes to bind Dvl2 to regulate/inhibit its downstream activity.

Dynamic interactions between PCP core components and the actomyosin cytoskeleton have been described repeatedly (Butler & Wallingford, 2017; Shindo & Wallingford, 2014). PCP signaling regulates actomyosin contractility through activation of the RhoA GTPase and subsequent Rock-dependent phosphorylation of myosin as well as through the regulation of actin polymerization through Rac and Cdc42 in several tissues (Eaton et al., 1996; Lu et al., 2015; Strutt et al., 1997; Winter et al., 2001). PCP is known to be contributing to establishing apicobasal polarity via binding of Dvl to aPKC; through this mechanism, PCP mediates the formation of contractile actomyosin in the cell cortex at apical tight junctions (Zhang et al., 2007).

PCP proteins are required for the phosphorylation of myosin during cell intercalation in Xenopus, chicken, and mice (Lienkamp et al., 2012; McGreevy, Vijayraghavan, Davidson, & Hildebrand, 2015; Nishimura et al., 2012; Shindo & Wallingford, 2014; Williams, Yen, Lu, & Sutherland, 2014). The mechanism by which PCP proteins act on myosin has been attributed specifically to Dvl. Dvl acts via the formin Daam1, the PDZ-RhoGEF, and RhoA to activate

Rock and causing phosphorylation of myosin and inhibition of the myosin phosphatase (Habas, Kato, and He, 2001; Nishimura, Honda and Takeichi, 2012).

Dvl interaction with Rock is mediated by the formin-homology protein Daam1, a critical regulator of the cytoskeleton and cell migration (Raftopoulou & Hall, 2004). Two families of DAAM proteins bind to Dvl: DAAM1 and DAAM2. DAAM1 and 2 catalyze the assembly of unbranched actin filaments and recruit the actin capping protein Profilin (Lecuit et al., 2011; Sinha, Wang, Evans, Wynshaw-Boris, & Wang, 2012). DAAM1 has a low affinity for RhoA (Ajima et al., 2015). However, the binding of Dvl to DAAM1 in the context of the non-canonical Wnt signaling increases its affinity for RhoA and induces actin polymerization (Habas et al., 2001). The DAAM1/Dvl complex also associates with Rho to form an actin remodeling complex through the activation of Rock1 (Nishimura et al., 2012). Alternatively, the Rho/DAAM1/Dvl complex remodels the actin cytoskeleton via the JNK (Jun N-terminal kinase). At the same time, JNK is also regulated by a Dvl/Rac complex (Angers & Moon, 2009; Fanto & McNeill, 2004).

Prickle proteins have been also linked to the indirect regulation of the actomyosin complex, mediating the lateral signaling pathway that coordinates the multiaxial protrusive activities in diverse types of cells (Zhang et al., 2016; L. Zhang & Wrana, 2018). For example, these multiaxial protrusive activities are regulated by Smurf2 and E3 ubiquitin ligase in the PCP pathway (Zhang et al., 2016). In contrast, when Pk1 or the Rho GTPase activating proteins (Arhgap21/23) are downregulated, the phosphorylation patterns of the myosin expand throughout the cell, and focal adhesions are stabilized around the periphery of the cell (Zhang et al., 2016). Arhgap 21 and 23 are two essential effector molecules of Pk1, belonging to the RhoGAP family (Zhang et al., 2016; Zhang & Wrana, 2018). These proteins interact and control the protrusive activity by regulating RhoA and modifying the actomyosin network and the mechanical properties of the cell surface (Zhang et al., 2016; Zhang & Wrana, 2018).

1.15 PCP in morphogenesis and organogenesis

In the morphogenesis of many organs, cell proliferation and patterning are controlled by signaling pathways triggered by diverse ligands including the Wnt family (Foulquier et al., 2017; D. Li & Wang, 2018; Merks et al., 2018; Wu et al., 2011). Directional migration of neural crest cells requires non-canonical Wnt/PCP signaling (Carmona-Fontaine et al., 2008) and proper localization of the apical junctional complex protein Par-3 to the cell-cell contacts (Moore et al., 2013). In neural tube closure, PCP signaling links the two essential morphogenetic processes: convergent extension and apical constriction (Nishimura et al., 2012). Also crucial to the PCP pathway is an asymmetrical distribution of distinct and complementary PCP signaling complexes, either Fz-Dvl or Vang-Pk (Butler & Wallingford,

2017). The defects in morphogenesis caused by PCP signaling are mainly based on deficient adhesion and cytoskeletal rearrangements (Butler & Wallingford, 2017; Wang et al., 2016; Wu et al., 2011). In addition, fibroblasts of Pk1a missense mutants fail to establish a polarized cell morphology or directional migration due to misalignment of F-actin (Gibbs et al., 2016). Wnt5 and Wnt11, known previously as the non-canonical Wnt ligands, along with PCP core components, play an essential role in proper cardiac development (Cohen, Miller, Wang, Moon, & Morrisey, 2012; Foulquier et al., 2017; D. Li & Wang, 2018; Merks et al., 2018; Nagy et al., 2010; Pandur, Läsche, Eisenberg, & Kühl, 2002; Wu et al., 2011). In Vangl2 mutants, for instance, SHF cardiomyocytes fail to migrate in the cardiac cushion tissue since the actin cytoskeleton remains cortical instead of forming F-actin stress fibers allowing polarized protrusive activity (Phillips, Murdoch, Chaudhry, Copp, & Henderson, 2005).

Table 2. PCP mouse mutants with incomplete heart looping (From Desgrange, Garrec, and Meilhac 2018). IL: incomplete looping, sOFT: shortened outflow tract, IRL: incomplete rightward looping.

Mutant description	Stage	Cardiac phenotype	Reference
$Wnt5a^{null/null}$	E9.5	IL, sOFT	(Sinha et al., 2015, 2012)
Wnt5a gain of function	E9.5	IL, sOFT	(D. Li et al., 2016)
$Wnt11^{null}$	E9.5	IL, sOFT	(Zhou et al., 2007)
$Vangl2^{Lp}$	E8.5, E9.5	IRL	(Henderson et al., 2001; Ramsbottom et al., 2014)
$Scrib^{Crc}$	E9.5, E10.5	IRL	(Phillips et al., 2007)
$Dvl1^{null/null}$	E9.5	IRL	(Sinha et al., 2012)
$Dvl2^{null/null}$	E9.5, E10.5	IRL, sOFT	(Kioussi et al., 2002; Sinha et al., 2012)

Defects in PCP signaling correlate with several congenital heart diseases (CHD), mainly associated with defects in the remodeling of the outflow tract during development summarized in Table 2. Previous findings from our lab showed that cardiac chambers expand through epithelial remodeling (Merks et al., 2018). The underlying mechanism involves PCP signaling, which restricts actomyosin contractility in distinct ways in different regions of the cardiac tissue (Figure 12). The nature of this process is, however, unexplored.

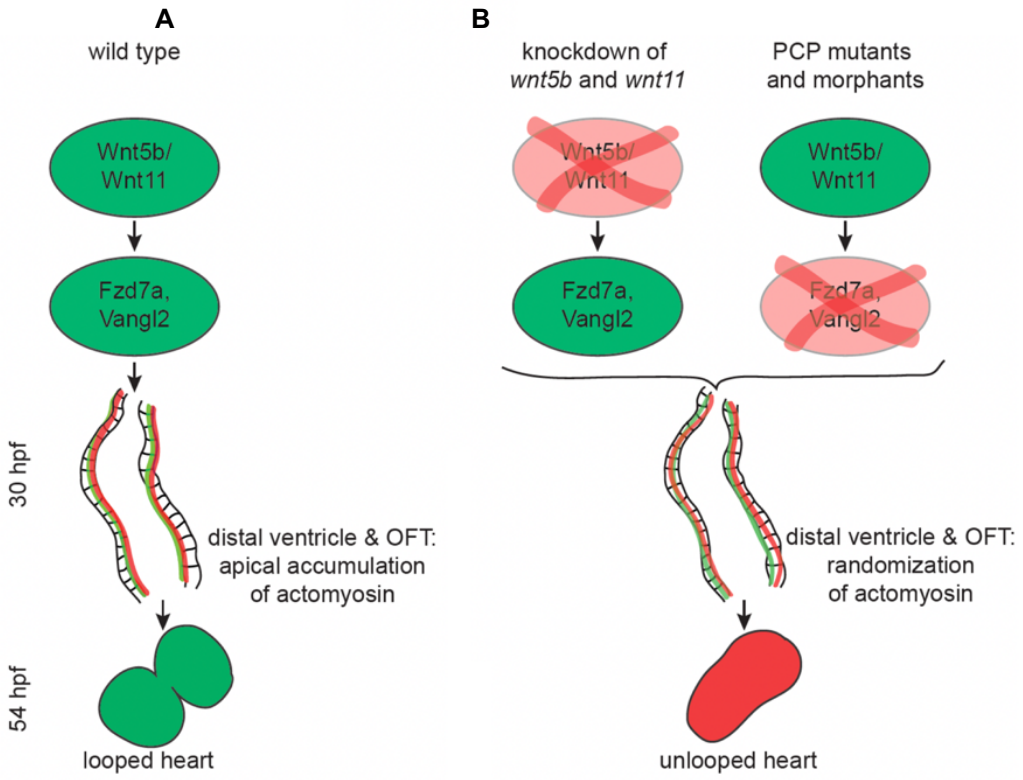

Figure 12. PCP controls the heart looping and chamber formation. A) In wild type developing hearts, Wnt ligands (Wnt5b/Wnt11) activate the PCP pathway resulting in the proper actomyosin (red/green lines) patterning across the cardiac epithelium of the linear heart tube at 30 hpf resulting in a proper looped heart at 54 hpf. B) Disruption of the PCP pathway, by either knocking down the Wnt ligands or the PCP core components (Fzd7a or Vangl2), affects the proper localization of the actomyosin complex across the cardiac epithelium of the linear heart tube at 30 hpf causing an impaired looping, resulting in an unlooped heart (Adapted from Merks 2018).

2. Aims

Like many other organs, the heart undergoes complex changes in shape and size from the cellular scale to the context of the whole organ (Desgrange et al., 2018; Le Garrec et al., 2017). The genetic and molecular programs involved in heart formation have been studied for a long time (Stainier, 2001; Stainier, Lee, & Fishman, 1993). However, it was not until recently and with the advancement of imaging technologies that the focus turned on the cellular processes that drive heart formation. For instance, the migration dynamics of the heart cells have only recently revealed how dynamic the process of heart formation is (Felker et al., 2018; Lombardo et al., 2019; Tessadori et al., 2021). In addition, besides the genetic and cellular contributions to heart formation, little is known about the molecular and cellular components that are involved in generating tissue forces required in heart morphogenesis.

Planar Cell Polarity pathway is indispensable for proper cardiac development. Defects in PCP signaling correlate with several congenital heart diseases, mainly associated with defects in the remodeling of the outflow tract that occurs during development (Wu et al., 2011). Previous findings from our lab showed that cardiac chambers expand through epithelial remodeling (Merks et al., 2018). The underlying mechanism involves PCP signaling, which restricts actomyosin contractility to different regions of the cardiac tissue. The localized activity of actomyosin was required not only for chamber expansion, but also for proper S-looping of the heart. The nature of how PCP regulates the localized patterns of tissue tension in the developing heart tube is, however, unexplored.

In this study, I will examine the mechanical heterogeneities at cellular and molecular level that are established in the linear heart tube. I will focus on the time points when the looping process occurs to gain a comprehensive overview of the mechano-molecular control of cardiogenesis. Given that myosin phosphorylation is critical in determining the actomyosin activity, I will evaluate the expression levels of the cardiac kinases to assess their potential role in the phosphorylation of the non-muscle MRLC during the looping of the heart. I will then determine the role of PCP in regulation of cardiac myosin kinases.

It has been identified that Myosin Light Chain Kinase 3 (Mylk3) is specific to cardiac tissue and its functions has been correlated with the incidence of congenital heart disease and abnormal heart formation (Chan et al., 2008; Seguchi et al., 2007; Tobita et al., 2017).

I hypothesize that Mylk3 might act as a novel effector protein of PCP that modulates the actomyosin complex. I will examine whether the regulation of kinases activity via PCP is required to generate the patterns of tissue tension necessary to shape a fully formed heart.

3. Materials and Methods

3.1 Reagents and resources

3.1.1 Chemical reagents

Table 3. Essential chemicals and reagents

Reagent	Manufacturer	Catalog Number
DreamTaq™ DNA Polymerase	ThermoFisher Scientific™	EP0701
10x DreamTaq™ Buffer	ThermoFisher Scientific™	B65
RedSafe™ Nucleic Acid Staining Solution	iNtRON Biotechnology	21141
GlycoBlue™	Invitrogen™	AM9515
TaqMan™ Gene Expression Master Mix	Applied Biosystems™	10525395
TRIzol Reagent	Invitrogen™	15596026
SeaBlock buffer	Abcam	Ab166951
VECTASHIELD® vibrance anti fade mounting medium with DAPI	Vector Labs	H1800
Pronase	Roche	10165921001
Cas9-EGFP	Sigma	
Flipper TR sensor	Cytoskeleton	CY-SC020
BSA	Sigma	
PFA	Sigma	
Superfrost Plus Microscope Slides	ThermoFisher Scientific™	
TrypLE Express™	Gibco™	12604-013
FACSmax™ Cell Dissociation Solution	Genlantis	T200100
70 µm pluriStrainer Mini	pluriSelect Life Science	43-10070-40
Hank's Balanced Salt Solution	Gibco™	14175095
TRIzol™ LS Reagent	Invitrogen™	10296028
ML-7 Inhibitor	Cayman chemicals	11801
Rockout Inhibitor	Cayman chemicals	17922

All chemical reagents used in this study were of analytical grade from Sigma-Aldrich, Ambion, Applied Biosystems, Biorad, Biozym, Calbiochem, Life Technologies, New England Biolabs, Qiagen, Promega, Roche, Roth, R&D Systems, Thermo-Scientific, and VWR, unless otherwise stated.

3.1.2 Buffers and solutions

Table 4. Buffers and solutions

Buffer/Solution	Composition
E3 Embryo Medium	5 mM NaCl, 0.17 mM KCl, 0.33 mM $CaCl_2$, 0.33 mM MgSO4; pH 7.4
PBST	PBS, 0.1% Triton-X100
Blocking Solution (BS)	Sea Blocking buffer, 1% DMSO, 0.1% Tween-20, 2 mg ml–1 BSA
PEM buffer	0.1 M PIPES (pH 6.95), 2 mM EGTA, 1 mM $MgSO_4$
Saline-Sodium Citrate (SSC) **Buffer, 20x**	3 M NaCl, 300 mM Na3C6H5O7; pH 7.0
Tyrode's Solution (TS)	136 mM NaCl, 5.4 mM KCl, 1 mM $MgCl_2$•$6H_2O$, 5 mM D-(+) Glucose, 10 mM HEPES, 0.3 mM Na_2HPO_4 • 2 H_2O, 1.8 mM $CaCl_2$ • 2 H_2O; pH 7.4
Supplemented L15 culture medium	15% fetal bovine serum, 0.8 mM $CaCl_2$, 1:200 Penicillin-Streptomycin in Leibovitz's L-15 Medium, GlutaMAX™ Supplement

3.1.3 Equipment

Table 5. Equipment

Equipment	Manufacturer
Centrifuge 5427 R	Eppendorf
Centrifuge 5920 R	Eppendorf
Flaming/Brown Micropipette Puller, Model P-97	Sutter Instrument
FemtoJet 4i Microinjector	Eppendorf
M-152 Three-Dimensional Manipulator	Narishige Group
Mastercycler pro vapo protect	Eppendorf
MD33 Brightfield Microscope	Leica
M165 Fluorescent Microscope	Leica
NanoDrop ND-1000 Spectrophotometer	peqLab
ViiA™ 7 Real-Time PCR System	Life Technologies
TCS SP8 Confocal Microscope	Leica
BD FACSAria™ I Flow Cytometer	BD Biosciences
Trimscope II	LaVision Biotec GmbH,

3.1.4 Antibodies

Table 6. Primary antibodies

Antibodies	Host specie	Source	Identifier	Dilution
Myosin light chain (phospho S20)	Rabbit	Abcam	Ab2480	1:50
Zn8	Mouse	Developmental Studies Hybridoma Bank	Zn-8	1:50
EGFP	Chicken	AvesLab	GFP1010	1:50
mCherry	Rat	Thermo	M11217	1:50
Vangl2	Rabbit polyclonal	Customized	Gift, (Roszko et al., 2015)	1:25
MF20	Mouse	Hybridoma Bank	MF-20s	1:50

Table 7. Secondary antibodies

Antibodies	Host specie	Source	Identifier	Dilution
Alexa Fluor® 488 Anti-Mouse	Donkey	Jackson Immunoresearch	715-545-150	1:200
Alexa Fluor® 546 Anti-Rat	Donkey	Invitrogen	A11081	1:200
Alexa Fluor® 594 Anti-Rabbit	Goat	Jackson Immunoresearch	711-585-152	1:200
Alexa Fluor® 633 Anti-Mouse	Goat	Life Technologies	A-21052	1:200
Alexa Fluor® 647 Anti-Rabbit	Goat	Life Technologies	A-21245	1:200
Fluorescein cinjugated Anti-Chicken	Goat	Aves Lab	F-1005	1:100

3.1.5 Critical commercial assays

Table 8. Critical commercial assays

Critical commercial assays	Source	Identifier
Phusion High-Fidelity PCR Kit	ThermoFisher Scientific™	F553L
First-Strand cDNA Synthesis Kit	ThermoFisher Scientific™	K1612
RNAscope multiplex assay	ACD	233130
Megascript	Invitrogen	AM1334
First Strand cDNA Synthesis Kit	ThermoFisher Scientific™	K1612
Gateway BP Clonase II Enzyme Mix	ThermoFisher Scientific™	11789020
Gateway LR Clonase II Plus Enzyme	ThermoFisher Scientific™	12538120

3.1.6 Organism strains

Table 9. Zebrafish lines

Zebrafish Line	Source	ZFIN ID
AB	ZIRC (Zebrafish International Research Consortium)	Wild type
WIK	ZIRC	Wild type
TL (Tupfel long fin)	ZIRC	Wild type
Tg [*myl7*: EGFP]^{twu34}	(C. J. Huang, Tu, Hsiao, Hsieh, & Tsai, 2003)	ZDB-TGCONSTRCT-070117-49
Tg [*myl7*: hMYLK3-mCherry]	This study	N/A
***vangl2*^{m209}**	(Jessen et al., 2002)	ZDB-FISH-150901-11436
mylk3*^{sa18088} *(mylk3*$^{+/-}$*)	ZIRC	ZDB-ALT-131217-14144

3.1.7 Oligonucleotides

Table 10. Oligonucleotides

All the oligonucleotides were ordered and purchased from Biotez company unless stated otherwise.

Primers	Description	Sequence
Mylk3 gRNA #1	sgRNA synthesis	5'-GAAATTAATACGACTCACTATAGGGCTTG AGCTCCAGCAGCCCGGTTTTAGAGCTAGAA ATAGC -3'
Mylk3 gRNA #2	sgRNA synthesis	5'-GAAATTAATACGACTCACTATAGGTCATTAG GAAGAGTGACCTCGTTTTAGAGCTAGAAATAGC -3'
Mylk3 gRNA #3	sgRNA synthesis	5'- GAAATTAATACGACTCACTATAGGGTCATTAGGA AGAGTGACCTGTTTTAGAGCTAGAAATAGC -3'
Mylk3 gRNA #4	sgRNA synthesis	5'-GAAATTAATACGACTCACTATAGGCAGGAGAA TGTTGGCTGCTGGTTTTAGAGCTAGAAATAGC -3'
sgRNA rev	sgRNA synthesis	5'-AAAAGCACCGACTCGGTGCCACTTTTTCAAGTTG ATAACGGACTAGCCTTATTTTAACTTGCTATTTCTAG CTCTAAAAC -3'
Mylk3 exon 3*	sgRNA synthesis	5'-U*C*AUUAGGAAGAGUGACCUC -3'

Mylk3 ex3 seq FWD	Sequencing	5’- AACCAAACGTCGGTTTCTGC -3’
Mylk3 ex3 seq REV	Sequencing	5’- AGGCTTTTGAGCTTTCCCCT -3’
Mylk3 ex11 seq FWD	Sequencing	5’- CCTGTGTGGGAGAGGTTAGC-3’
Mylk3 ex11 seq REV	Sequencing	5’- GGGTGGGGAAAACCTACGTC-3’
hMylk3 FWD	Sequencing	5’- AGGCTTTTGAGCTTTCCCCT -3’
hMylk3 REV	Sequencing	5’- AGGCTTTTGAGCTTTCCCCT -3’
mCherry REV	Sequencing	5’- AGGCTTTTGAGCTTTCCCCT -3’
EGFP C’ FWD	Sequencing	5’- AGGCTTTTGAGCTTTCCCCT -3’
EGFP C’ REV	Sequencing	5’- AGGCTTTTGAGCTTTCCCCT -3’

*Synthesized sgRNA directly ordered and purchased from Synthego.

Table 11. Morpholino oligonucleotides

Morpholino oligonucleotide	Target	Total (ng)	Sequence
MO1-mylk3	ATG	3.5	5' - TACAGCGAGGTCCCCATCATGCCCT - 3'
MO3-mylk3	Ex6 Splicing	3.5	5' - CAAATCGGCCTCTGCAACAACACAC - 3'
MO2-rock2a	ATG	6.0	5' - CTCCTAGCGACATTTTTGTCTCGT - 3'
wnt11f2	ATG	1.2	5' - AAGATCCAGAAGACACTGATGCAGG - 3'
MO1-fzd7a	5’UTR	1.5	5' -ATAAACCAACAAAAACCTCCTCGTC - 3'
MO1-dvl2	ATG	3.5	5' - TAAATTATCTTGGTCTCCGCCATGT - 3'
MO1-vangl2	ATG	2	5' - GTACTGCGACTCGTTATCCATGTC - 3'
MO-pk1a	ATG	1.5	5' - GCCCACCGTGATTCTCCAGCTCCAT - 3'

Table 12. TaqMan™ probes

TaqMan™ Probe	Assay ID	Part Number
eef1α1l1	Dr03432748_m1	4448892
mylk3	Dr03118478_m1	4448892
rock1	ARYMKW7	4441114
rock2a	Dr03144597_m1	4448892
rock2b	Dr03130796_g1	4448892

All TaqMan™ probes were purchased from Thermo Scientific™ and were designed to analyze gene expression in *Danio rerio*. The *eef1α1l1* was used as internal control within the same well as the gene of interest. *eef1α1l1* TaqMan probe was labelled with the covalently bound fluorophore VIC™, all other TaqMan probes were tagged with the reporter dye FAM (6-carboxyfluorescein).

3.1.8 Plasmids

Table 13. Plasmids

Plasmids	Source	Identifier
pENTR5'	Invitrogen	K59120
pDestTol2 cryaa:YFP	(Mosimann et al., 2015)	
p3'E-polyA	Addgene	Tol2kit #302
pDonor™ 221	ThermoFisher Scientific™	Cat#12536017
p5'E-myl7	N/A	N/A
pDONR223-LOC91807 (Hs mylk3)	Addgene	23546
ZE25 Stbm-pCS2+	Addgene	17067
***myl7:* hMYLK3-mCherry**	This study	N/A

3.1.9 Software and algorithms

Table 14. Software and algorithms

Software/Algorithm	Source
FIJI/ImageJ v2.3.0	https://imagej.nih.gov/ij/
GraphPad Prism 9.0	GraphPad Software LLC
Microsoft Office Word	Microsoft
Microsoft Office Excel	Microsoft

Adobe Illustrator 2022	Adobe
Adobe Photoshop 2022	Adobe
APE- A Plasmid Editor v2.0.61	https://jorgensen.biology.utah.edu/wayned/ape/
ViiA™ 7 RUO software	ThermoFisher Scientific™
Mendeley Desktop version 1.19.8	Mendeley Ltd.
CrispantCal: CRISPR-Cas9 Injection Mix Calculator	https://lmweber.shinyapps.io/CrispantCal/
ICE Analysis. 2019. v3.0	Synthego, https://ice.synthego.com/#/
MatLab	MathWorks
FLIMfit software	(S. C. Warren et al., 2013)

3.2 Methods

3.2.1 Zebrafish husbandry

Zebrafish were bred, raised, and maintained in accordance with the guidelines of the Max-Delbrück Center for Molecular Medicine and the local authority for animal protection (Landesamt für Gesundheit und Soziales, Berlin, Germany) for the use of laboratory animals, and followed the “Principles of Laboratory Animal Care” (NIH publication no. 86-23, revised 1985) as well as the current version of German Law on the Protection of Animals. Zebrafish strains AB, Tü LF, and Wik were used for analysis of wild-type phenotypes and for injection of constructs and morpholinos described below.

Embryos were kept in E3 medium under standard laboratory conditions at 28.5°C. Staging was performed as described previously by hours post fertilization (Kimmel, Ballard, Kimmel, Ullmann, & Schilling, 1995).

3.2.2 Generation of expression vectors

Gateway® cloning system was used to generate the expression vectors (Table 13) following the manufacturer's instructions manual. Briefly, attB-modified custom oligonucleotides were used to amplify genes of interest (hMYLK3) from genomic DNA or plasmid DNA Table 13 resulting in a PCR product containing attB sites at both ends of the sequence. The PCR product was recombined with the Gateway pDONR221 vector containing the matching attP sites using the Gateway BP Clonase II Enzyme Mix to create an entry pME clone and a ccdB fragment by-product. Finally, the Gateway LR Clonase II Plus Enzyme was used to combine the pME with a 5’ entry vector containing a *myl7* promoter sequence (p5’E-myl7) and a 3’ entry

vector expressing a poly(A) sequence (p3'E-polyA) to create a destination vector (pDEST; *myl7:*hMYLK3-mCherry).

3.2.3 sgRNA synthesis

Procedure of sgRNA synthesis involved PCR amplification without any DNA template due to a primer combination that overlap and subsequent *in vitro* transcription (Bassett et al., 2013). The forward oligonucleotide (Table 10)comprised a T7 promoter, a specific sgRNA (GGN18) target-site sequence and a portion of the sgRNA stem loops crucial for Cas9 binding. The reverse oligonucleotide (sgRNA rev, Table 10) contained the entire sgRNA sequence after the GGN18 target site. PCR was performed with Phusion High-Fidelity PCR Kit in 100 µl reaction volumes on a Mastercycler pro vapo-protect with the following program: 98°C for 3s, 40 cycles of denaturation at 98°C for 10s, annealing at 60°C for 30s and extension at 72°C for 15s, final extension at 72°C for 10 min, final hold at 4°C infinitely long. 300 ng of the purified PCR product were used as template for *in vitro* overnight transcription at 37°C with MEGAscript™ T7 Transcription Kit. Purification of the sgRNA was implemented by RNeasy Mini Kit and stored at -80°C until used.

3.2.4 Microinjections

Microinjections using a FemtoJet microinjector and a 3D micromanipulator of mRNA, pDEST, or Cas9/sgRNA were performed at one cell stage injected into the cytoplasm of the cell, morpholino oligonucleotides were injected into the yolk at 1 or 2 cell stage. A calibration of the drop was performed to inject a final volume of 1nL in total. 10 pg of expression constructs together with 25 pg of Transposase mRNA or sgRNA combined with Cas9 protein were injected directly into cytoplasm of single-cell embryos. Morpholino oligonucleotides (MO) were injected in the yolk of one- to four-cell stage zebrafish embryos. In case of double knockdown approaches, both MOs were injected sequentially. Embryos were kept in E3 embryo medium under standard laboratory conditions at 28.5°C.

3.2.5 CRISPR/Cas9 Mutagenesis

A mixture of Cas9-EGFP and sgRNA final concentration were calculated using CrispantCal: CRISPR-Cas9 Injection Mix Calculator to optimize the KCl concentration and sgRNA/Cas9 protein ratio of the injection mix (Burger et al., 2016). One-cell stage zebrafish embryos were injected with the injection mix. Conjugated dextran with Alexa 594 fluorophore was used as an indicator if positive injected embryos. After 24 hours, the positive embryos were sorted to proceed either with the isolation of the hearts, or to keep them growing until 54hpf for the

assessment of the phenotype in F0 embryos (Kroll et al., 2021), or to rise them to adult stages to generate a CRIPR/Cas9 mutant line.

3.2.6 Genotyping

To genotype the fish lines, the adult fish were crossed, and the eggs were collected. After 72hpf the embryos were tail clipped following the previously reported protocol (Kosuta et al., 2018; Wilkinson, Elworthy, Ingham, & van Eeden, 2013). Briefly, embryos were anaesthetized in 0.016% Tricaine in E3 medium. After removal of all liquid, the tip of the caudal fin was cut on the pigment gap, avoiding the caudal circulation to prevent bleeding. The biopsy was placed in a microcentrifuge tube containing 30 µl of 50 mM NaOH solution and boiled for 20 min at 96˚C for gDNA extraction. The tubes were placed on ice to cool down the reaction and neutralized with 3 µl of 1 M Tris-HCl (pH 8.0). Samples were vortexed, stored at 4˚C, until used for PCR amplification. The PCR mixture containing 2 µl gDNA, 4 µl 10x DreamTaq Buffer, 1 µl dNTPs mix (10 mM of each), 0.5 µl forward primer [50 µM], 0.5 µl reverse primer [50 µM] and 0.2 µl DreamTaq Polymerase in a final volume of 40 µl. Amplification was performed on a Mastercycler pro vapo protect with the following PCR cycling parameters: initial denaturation at 94°C for 3min, 40 cycles of denaturation at 95°C for 30s, annealing at 58°C for 30s and extension at 72°C for 30s; final extension at 72°C for 7min, final hold at 4°C. PCR products were analyzed on an 1.5% agarose gel containing 1X Redsafe. The PCR products were purified using the PCR clean up protocol, diluted to 100ng/ml and sent for sequencing.

3.2.7 Inference of CRISPR Edits (ICE) analysis to identify knock out efficiency

The analysis of CRISPR/CAS9-based mutagenesis was adapted from previous protocols used in cells (Brinkman, Chen, Amendola, & Van Steensel, 2014; Conant et al., 2022; Moreno-Mateos et al., 2015). Briefly, after 2dpf from the injection of the embryos at one-cell stage with the Cas9/sgRNA mix, the embryos were genotyped as described in previous section using specific primers Table 10 flanking the region of mutagenesis. Sanger sequencing was performed of the PCR products and analyzed online with ICE tool from Synthego to calculate the efficiency of mutagenesis and to obtain an approximate percentage of cells mutated to correlated with the presence of cardiac phenotype in the corresponding embryos.

3.2.8 Whole embryo imaging for phenotypic analysis

For *in vivo* whole embryo imaging, wild type or *Tg[myl7:EGFP]* embryos were anesthetized at 54hpf with 0.016% Tricaine and embedded in 2% methylcellulose for immobilization on glass

slides. For the analysis of the zebrafish heart looping, embryos of *Tg[myl7:EGFP]* or *Tg[myl7:hMYLK3:mCherry]* were fixed with 4% formaldehyde in PEM (100mM PIPES, 2mM EGTA, 1mM $MGSO_4$, pH 7.0) solution at 2dpf. Imaging was performed using a Leica Fluorescent Microscope M165, including an attached camera system. Images were analyzed with the ImageJ/Fiji software.

Ventral images of the embryos were acquired with a Fluorescent Microscope to image the hearts of embryos at 54hpf, embryos were placed in 3% methylcellulose to keep it steady while acquisition. The angle measurements were performed using FIJI software, taking as a reference the midline of the body axis between the eyes and the AVJ line in the hearts using the measure angle function.

3.2.9 Immunofluorescence staining

Zebrafish embryos were dechorionated using 50ug/ml Pronase in E3 water. Embryos were transferred into Tyrode's solution with 20 mg/ml BSA (Bovine Serum Albumin) for heart isolation following a previous published protocol (Geoffrey Burns & MacRae, 2006; Lombardo, Otten, & Abdelilah-Seyfried, 2015) . Isolated hearts were fixed with 4% PFA for at least 20 minutes at room temperature (RT) and washed with PBST three times for 10 minutes each wash. Then, they were blocked overnight at 4˚C. Subsequently, hearts were incubated with primary antibodies diluted in blocking buffer overnight at 4°C. After three washing steps in blocking buffer (3x30 minutes at RT), hearts were incubated with Alexa conjugated secondary antibodies diluted in blocking buffer for 4 hours at RT. Last, hearts were mounted with Vectashield® antifade mounting medium with DAPI on a Superfrost Plus Microscope Slides (Thermo Scientific), curated for one hour at RT and kept at 4°C for long-term storage.

3.2.10 Fluorescent-Activated Cell Sorting (FACS) from zebrafish embryos

Dechorionated zebrafish embryos of the required stage were placed in a 2 ml tube and washed three times with PBS and following a variation of previous protocol (Samsa, Fleming, Magness, Qian, & Liu, 2016). After removal of PBS, 1 ml TrypLE Express™ (Cat#12604-013; Gibco™) was added and cell dissociation was carried out at 28°C for 10 min with gentle resuspension every 5 min through a 1 ml filter tip. The suspension was centrifuged for 30 sec at 6000 rpm at RT. Supernatant was removed and the remaining cell pellet resuspended with 1 ml FACSmax™ Cell Dissociation Solution (Cat#T200100; Genlantis). Cell dissociation was continued at 28°C with gentle resuspension every 5 min through a 1 ml filter tip until homogenous cell suspension was achieved. The subsequent operations were performed on ice. A 70 µm pluriStrainer Mini (Cat#43-10070-40; pluriSelect Life Science) was placed in a 2

ml tube, wetted with 100 µl Hank's Balanced Salt Solution (HBSS; Cat#14175095; Gibco™) with 2% FBS. Cell suspension was passed through the cell strainer and after rinsing with 200 µl of 2% FBS in HBSS, centrifuged by 6000 rpm for 30 s. Supernatant was removed and pellet washed with 1 ml of 2% FCS in HBSS. After centrifugation at 6000 rpm for 30 s, the pellet was resuspended in 500–1000 µl sterile 1x PBS. For subsequent fluorescence-activated cell sorting (FACS), the cell suspension was filtered through 5 ml polystyrene round-bottom tube with cell-strainer cap (12 x 75 mm, Cat#10585801; Corning™) to prevent clogging. Unlabeled cell suspension from wild type embryos that were prepared in parallel were used to adjust the machine and the cut-off of the BD FACSAria™ I Flow Cytometer (BD Biosciences). GFP-labelled cardiomyocytes and non-cardiomyocytes were collected in 2.0 ml tubes containing 100 µl TRIzol™ LS Reagent (Cat#10296028; Invitrogen™) and snap-frozen in liquid nitrogen and stored at -80°C.

3.2.11 Total RNA isolation from FACS-sorted cells for qPCR

To isolate total RNA from FACS-sorted cells to perform qPCR, the aliquots of FACS-sorted cells were thawed on ice, and either pooled and/or scaled up with TRIzol™ LS Reagent (Cat#10296028; Invitrogen™) to a volume of 500 µl. Samples got shaken for 5 min at 25°C and 1400 rpm and resuspended five times with a sterile 1 ml filter tip. 100 µl ice-cold chloroform were added and the tubes were shaken vigorously for 20 s in between the fingertips. After incubation for 5 min on ice, full speed centrifugation was performed for 15 min at 4°C to achieve phase separation into a lower red phenol-chloroform phase, an interphase, and a colorless upper aqueous phase that contains the RNA. The upper phase was transferred to another 1.5 ml tube, diluted 1:2 in ice-cold isopropanol, mixed well and 2.5 µl GlycoBlue™ Co-precipitant were added to aid RNA visualization. Precipitation of RNA took place overnight at –20°C followed by 30 min full speed centrifugation at 4°C. After removal of supernatant without disturbing the RNA pellet, it was washed with 500 µl 75% Ethanol/H_2O (RT, freshly prepared), with 1400 rpm for 10 min at 4°C. The pellet got air-dried for 10 min at RT, resuspended in 10 µl H_2O and stored at -80°C or used directly for qPCR.

3.2.12 cDNA Synthesis and qPCR

On-column DNase I treatment (DNase Digestion of RNA before RNA Cleanup), cleanup and concentration of RNA were performed according to the RNeasy Mini Kit. After determination of RNA quantity and quality with the NanoDrop ND-1000 spectrophotometer (peqLAB), mRNA was transcribed into cDNA using First-Strand cDNA Synthesis Kit (Cat#K1612 ThermoFisher) manufacturers protocol. Due to combined random hexamer and oligo(dT) primed synthesis

(1:2), the reverse transcription reaction was incubated for 5 min at 25°C followed by 60 min at 37°C in the Mastercycler® pro vapo protect (eppendorf). 10–100 ng of the reverse transcription reaction product was immediately used for qPCR with FAM™ dye-labeled TaqMan™ MGB probes (

Table ***12***) and TaqMan™ Gene Expression Master Mix on a ViiA™ 7 Real-Time PCR System. The qPCR reaction was performed in technical with following conditions: annealing at 50°C for 2 min; denaturation at 95°C for 10 min; denaturation at 95°C for 15 s; amplification at 60°C for 1 min. qPCRs were performed for 55 cycles. The threshold cycle (CT) values and baseline were reported by the ViiA™ 7 RUO software. The CT represents the cycle number (C) in the early phase of the exponential growth at which the detected fluorescence crossed a threshold (T). *eef1α1l* labelled with VIC™ dye was used as an internal reference gene and pipetted in the same well as genes of interest.

3.2.13 Fluorescent *in situ* hybridization (RNAscope®)

Fluorescent RNA *in situ* hybridization was performed using the RNAscope® kit following the manufacturers instruction manual with modifications previously published (Gross-Thebing, Theresa;, Paksa, & Raz, 2014). In brief, after fixation the hearts were dehydrated through sequential incubations of 25%, 50%, and 75% of methanol in PBST for 5 min each, followed by one more incubation in 100% methanol for 5 mins. Then the hearts were rehydrated through a series of 75%, 50%, 25% methanol in PBST for 5 mins each. The hearts were washed and incubated in PBT at least for 20 mins and then they were transferred for protease treatment to a well containing Pretreat 3 for 30 min, then rinsed 3 times with PBT 10 min each. After the hearts were incubated in a preheated mixture of the C1, C2 and C3 (50:1:1) and incubated overnight at 40˚C. Following recovering the probes, the hearts were washed three times with 0.2x SSC buffer for at least 5 mins each. An additional fixation step was performed using 4% PFA at RT for 10 mins.

The signal amplification steps consisted of in hybridization using the Amp buffers from the kit sequentially (Amp1, Amp2 and Amp3) at 40˚C, the hearts were washed three times with 0.2x SSC buffer in between each hybridization step. After the last three washes one more incubation with DAPI solution was performed to label the nuclei for 30 mins RT and finally three washing steps with PBST were performed. The hearts were mounted on a coverslip with Vectashield antifade mounting medium without DAPI.

3.2.14 Drug treatments

Zebrafish embryos at 25 somite stage (19hpf) were dechorionated using protease at a final concentration of 1mg/ml for 10 minutes, they were washed 3 times with E3 water to proceed with the drug treatment. 100 embryos were placed per dish with either DMSO (0.1%V/V), or ML-7 30uM, or Rockout 70uM until the embryos reach Prim15 developmental stage (30hpf) then the embryos were washed 3 times with E3 water. The hearts were isolated and immunostained as described in methods before.

3.2.15 Flipper-TR ® tension sensor staining

Stainings were performed according to manufacturer's instruction with slight modifications. The Flipper TR probe was solubilized using DMSO to reach the stock concentration 1mM and store at -20˚C. The isolated hearts were kept in Tyrode's with BSA, then transferred to a L-15 medium supplemented with 10% FBS, and then incubated for one minute in supplemented L-15 medium containing 1uM Flipper TR membrane sensor dye, the hearts were washed once with supplemented L-15 medium and fixed in 4% PFA electron microscopy grade in PBS followed by one wash with PBS and store in PBS overnight to perform the FLIM imaging and measurements on the following day.

3.2.16 Confocal Microscope Imaging

Confocal laser scanning microscopy system, which combines high-resolution optical imaging with depth selectivity allowing for optical sectioning, was used in this study. Stained fixed hearts were analyzed using the Leica TCS SP8 confocal laser scanning microscope with 63x (N.A.=1.3) oil immersion objective. Images of the heart ventricle were acquired with a Z-stack function with an optical slide size of 0.33 to 1 µm in a resolution of 1024x1024 pixels.

3.2.17 Fluorescence intensity and linear plot profile analysis

Images were analyzed with the ImageJ/Fiji software. All the images were converted to 8-bit image and to gray scale. For total fluorescent analysis the Z projections summing the total gray values was used to quantify the total levels of signals as a gray value and averaging it per pixel number, then the mean value of the control, samples was used to normalize to 1 and compare with the experimental conditions.

To perform the linear plot profile analysis the line tool was used in FIJI, with a 10 pixels thickness value. The Z projection of 3 contiguous Z-planes was generated (3 µm optical section) and line was manually drawn along the apical or basal edge of the cells using the Zn8

signal as a reference of lateral membranes to generate plots of the intensity over the ventricular region of the embryonic hearts.
The pixel intensity was plotted against the distance (microns) along the defined line for pMyo (phosphorylated non-muscle myosin II). The intensity values were normalized to the lowest and highest intensity within the selection and plotted with Prism software.

3.2.18 Fluorescence lifetime imaging (FLIM)

Imaging was performed by Dr. Anca Margineanu (Advanced Light Microscopy Facility, MDC, Berlin) the next day after fixation. The hearts were embedded in 0.25% low-melting-point agarose. Fluorescence lifetime imaging (FLIM) of hearts stained with the Flipper dye was done using a two-photon microscope and the TCSPC (time correlated single photon counting) technique. Excitation was set at 920 nm using a Titanium: Sapphire laser (Mira 900, Coherent, USA) and emission was collected with a bandpass 628/40 nm filter. A water immersion Nikon 20x, 1.1 NA, 2 mm working distance objective dedicated for multiphoton microscopy was used for imaging. Images of the heart ventricle were acquired with a pixel size of 0.16 µm, while the *Z* planes were spaced at 1 µm.

3.2.19 FLIM analysis.

FLIM data analysis was done by Dr. Anca Margineanu (Advanced Light Microscopy Facility, MDC, Berlin) in the open source software *FLIMfit* (S. C. Warren et al., 2013) (https://flimfit.org/) using a double exponential decay model and convolution with the instrument response function (IRF). The IRF was measured by acquiring the second harmonic generation of a sample consisting of urea crystals. The two decay times in the analysis correspond to the possible configurations of the dye molecule: a short lifetime when the two dithienothiophene rings adopt a perpendicular orientation and a long lifetime when the molecule is planarized and intramolecular charge transfer occurs (Colom et al., 2018). As FLIM data in microscopy are acquired with relatively low number of photon count per pixel, a 5x5 pixel binning was used in the analysis. Additionally, a global analysis strategy was applied over all the stacks imaged for one heart to improve the precision in determining the two decay times. This means that only one value of the short component and one value of the long component are calculated and reported for a given sample, but their contributions (i.e., amplitudes within the fluorescence lifetime decay) can vary from pixel to pixel. FLIM images are also shown using the weighted mean lifetime, calculated according to the formula:

$$\tau_{mean} = \frac{\alpha_{long}\tau_{long}^2+\alpha_{short}\tau_{short}^2}{\alpha_{long}\tau_{long}+\alpha_{short}\tau_{short}} = f_{long}\tau_{long} + f_{short}\tau_{short},$$

where α is the amplitude and τ is the decay time for the long and the short components in the fit, and f_{long}, f_{short} are the corresponding fractions of the two lifetime components (with $f_{long} + f_{short} = 1$).

To extract the fitting parameters corresponding only to the cardiomyocytes, regions of interest (ROIs) were manually drawn in ImageJ/Fiji (https://fiji.sc/) on each *z* plane in the acquired volumes of hearts and the average value per ROI was considered. The imaged samples are: control *n* = 41 hearts, *z* = 1032 planes; *rock2a* morpholino: *n* = 25 hearts, *z* = 639 planes; *mylk3* morpholino: *n* = 27 hearts, *z* = 644 planes; *rock2a* + *mylk3* morpholino: *n* = 8 hearts, *z* = 167 planes.

3.2.20 Mathematical modeling of heart tube remodeling

In close collaboration with Dr. Motahareh Moghtadaei (MDC, Berlin) the mathematical model of the cardiac tube ballooning was build using MATLAB software, starting with a double layered cylinder. Within the cylinder, 12 circles sitting on top of each other form 12 planes (P) sitting on top of each other, 6 at atrium and 6 at ventricle. The space between the two cylinders models the thickness of the cardiac tube (myocardium), where the inner layer with smaller radius (r1) models the basal and the outer layer with bigger radius (r2) models the apical side of the tube. The outer circles expand outwards, and the inner circles shrink inwards leading to ballooning of the tube over time. If there is no restriction, this will lead to formation of a 3D oval-shaped tube. However, there are mechanical factors restricting the ballooning of the tube. Among all, we have considered the phosphorylated non-muscle myosin II (pMyo) as the only physical restriction exerted on the growing tube in our model (Equation 1). At each plane (P), the space between r1 and r2 is considered as a medium for continuous distribution of pMyo. More specifically, at each plane, the pMyo distribution is localized at a specific radius r1<r<r2 with a specific intensity inferred from the confocal images of the zebrafish wild type heart tube.

$$\begin{cases} \Delta r_{\mathrm{Apical}} = +\mathrm{constant} \times \frac{1}{\mathrm{pMyo}_{\mathrm{Apical}}} \\ \Delta r_{\mathrm{Basal}} = -\mathrm{constant} \times \frac{1}{\mathrm{pMyo}_{\mathrm{Basal}}} \end{cases} \quad \text{(Equation 1)}$$

This forms a 3D surface of pMyo between the two layers of the heart tube (shown with blue color in the snapshots). Through numerical analysis, we show the physical restriction enforced by pMyo, contributes to the normal ballooning of the heart tube. A linear transition from a straight centerline to an S-shape centerline of the heart tube was assumed to model the cardiac looping, without any dependence on the pMyo distribution. To evaluate the model, we compare the diameter of the tube in control condition at each plane with the data collected

from confocal images of the tube in WT embryos (Equation 2). This simple model with just one parameter (pMyo distribution) can model the cardiac looping with a 10% error. The error is calculated as given in equation 2, where r_p is the radius of the outer cylinder at plane *p* in the model, and R_p is the radius of the cardiac tube obtained from experiments at plane *p*, *1<p<P*.

$$Error = \sum_{p=1}^{P} \frac{r_p - R_p}{R_p} \quad \text{(Equation 2)}$$

Table 15. Model Parameters

Model Parameters	
PARAMETERS	**ORIGIN**
Tube length at 24, 30, and 54hpf	Experimental data
Thickness of the tube at 24, 30, and 54hpf	Experimental data
Looping "S"-shape geometry	Assumption

Table 16. Model variables

Model variables	
INPUTS	**ORIGIN**
pMyo at inner curvature apical at 24 and 54hpf	Experimental data
pMyo at outer curvature apical at 24 and 54hpf	Experimental data
pMyo at inner curvature basal at 24 and 54hpf	Experimental data
pMyo at outer curvature basal at 24 and 54hpf	Experimental data
INITIAL CONDITION	**ORIGIN**
Initial geometry of the tube (radius at various planes) at 24hpf	Experimental data
OUTPUT	**ORIGIN**
Geometry of the tube (radius at various planes) after 24 hpf until 54 hpf	Model output (prediction)

3.2.21 Statistical analysis

GraphPad prism 9 was used to do the statistical analysis. No randomization, test for outliers or test for normal distribution were performed. Ordinary two-way ANOVA with Dunnett's multiple comparisons test was conducted for statistical analysis. Results are described as means and standard deviation (SD) or standard error (SEM) indicated in each figure. N

represents the number of independent biological experiments and n represents the total number of measurements.

Statistical graphs of the FLIM analysis (average lifetime, long lifetime, and fraction of the long lifetime) are shown using the averaged values per heart, which were normalized using the mean value for the corresponding control hearts imaged in each experiment. Statistical significance was estimated using the Kruskal-Wallis test and the Mann-Whitney and Dunn post-hoc tests.

For the qPCR analysis all CT values were normalized to that of the reference gene in the same well, fold induction (fold change, FC) was calculated using the ΔΔCT method (Livak & Schmittgen, 2001) and plotted as log2(FC) with GraphPad Prism 9. Unless otherwise stated, statistics were done with GraphPad Prism 9 on the ΔCT values comparing the untreated control situation to the treated situation using unpaired t-test with Welch's correction.

4. Results

4.1 Transient polarized supracellular distribution of actomyosin along the ventricular myocardium

Previously, the distinct patterns of tissue-scale polarization of actomyosin were identified along the developing myocardium of the linear heart tube in zebrafish at 30 hpf (Merks et al., 2018). Phosphorylated non-muscle myosin II (designated as pMyo henceforth) accumulates at the apical plasma membranes in the cells of the OFT region at this developmental stage. Therefore, I wondered whether the actomyosin pattern occurs transiently or whether it is maintained throughout the heart morphogenesis.

I therefore isolated zebrafish hearts at three different time points: at 24 hpf after the linear heart tube forms, at 30 hpf when the heart looping initiates, and at 54 hpf when the cardiac chambers are formed, and looping is terminated (Figure 13). Throughout these stages, the heart muscle cells are organized in a single-layered epithelium with abluminal apical membranes facing the pericardial cavity and luminal basal membranes facing the endocardium (Jiménez-Amilburu et al., 2016).

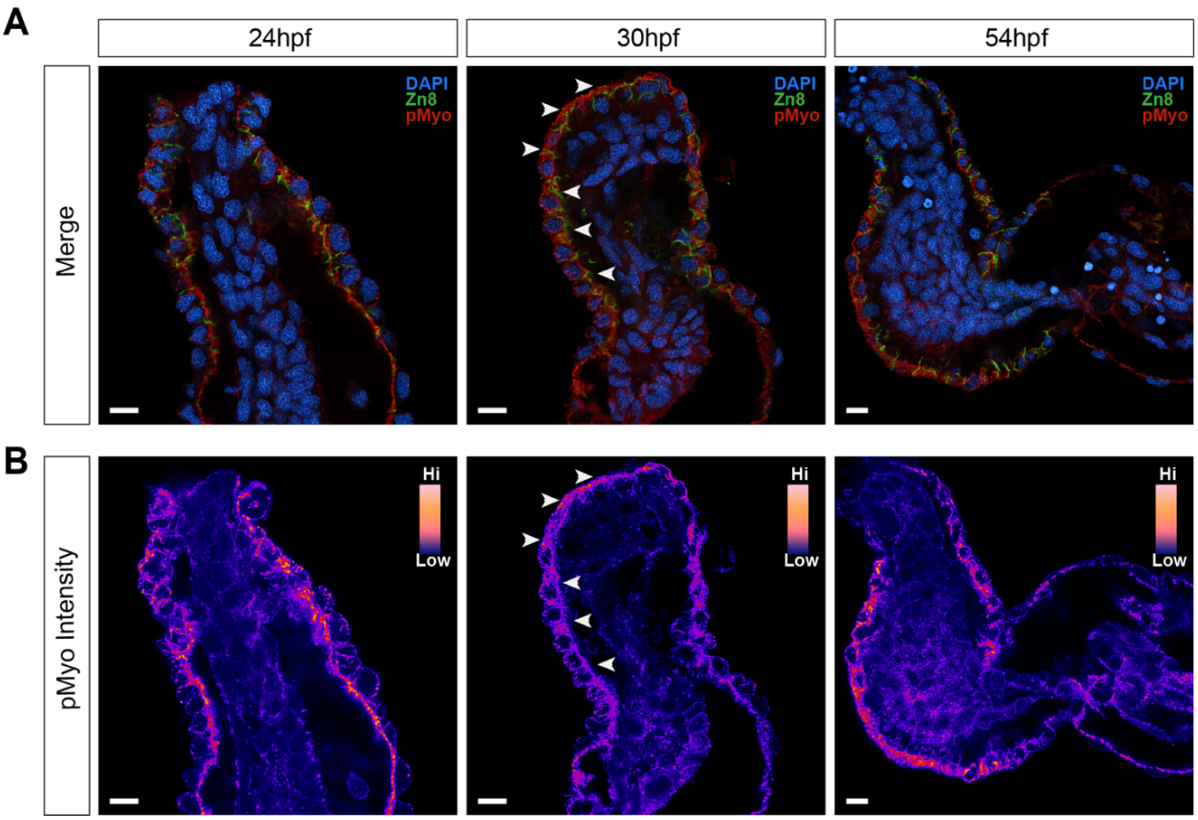

Figure 13. Distribution of pMyo across the ventricular myocardium during cardiac chamber formation and looping. A) Representative images of the merged channels of immunostaining of mid-sagittal sections of the linear heart tube at 24 hpf (left panels), 30 hpf (middle panels) and 54 hpf (right

panels). DAPI (blue), membrane marker Zn8 (green) and pMyo (red). B) Same midsagittal sections immunostained against pMyo and pseudocolored to highlight the pMyo fluorescent intensity, the intensity scale goes from low levels (dark/purple) to high levels (bright/yellow) in insets. At 30 hpf the switch of the distribution from apical to basal localization is indicated with the white arrowheads. Scale bar: 10µm.

At the linear heat tube stage at 24hpf, the pMyo is evenly distributed across the myocardium without an observable pattern or specific localization but the basal increase of intensity in the proximal ventricle and the atrium (Figure 13, 24 hpf, left panels).

I corroborated the previous observations (Merks et al., 2018) showing the pattern of the localized pMyo at 30 hpf (Figure 13, 30 hpf, middle panels). I examined the localization of pMyo along the apicobasal axis of the myocardium in the optical mid-sagittal sections from the outflow tract (OFT) to the atrioventricular junction (AVJ). pMyo exhibits apical localization in the distal ventricle (closer to the OFT) and basal localization in the proximal ventricle (closer to the AVJ) as indicated by the white arrowheads in the merge (Figure 13A, 30 hpf, middle panel) as well as in the pseudocolored panel showing the pMyo fluorescent intensity projection (Figure 13, B), 30 hpf, middle panel).

Finally, after the completion of the cardiac looping, when the two chambers ballooned and are already formed, the pMyo appears to be evenly distributed without any noticeable specific pattern across the ventricle (Figure 13, 54 hpf, right panels).

Taking into consideration all the observations together, my data suggests that the pMyo seems to acquire a specific pattern at 30hpf.

To corroborate these observations, I performed a quantitative plot profile analysis from the images corresponding to the pMyo stainings, to quantitatively determine the localization and levels of pMyo in both outer (Figure 14A) and inner (Figure 14B) ventricular curvatures over the defined time course.

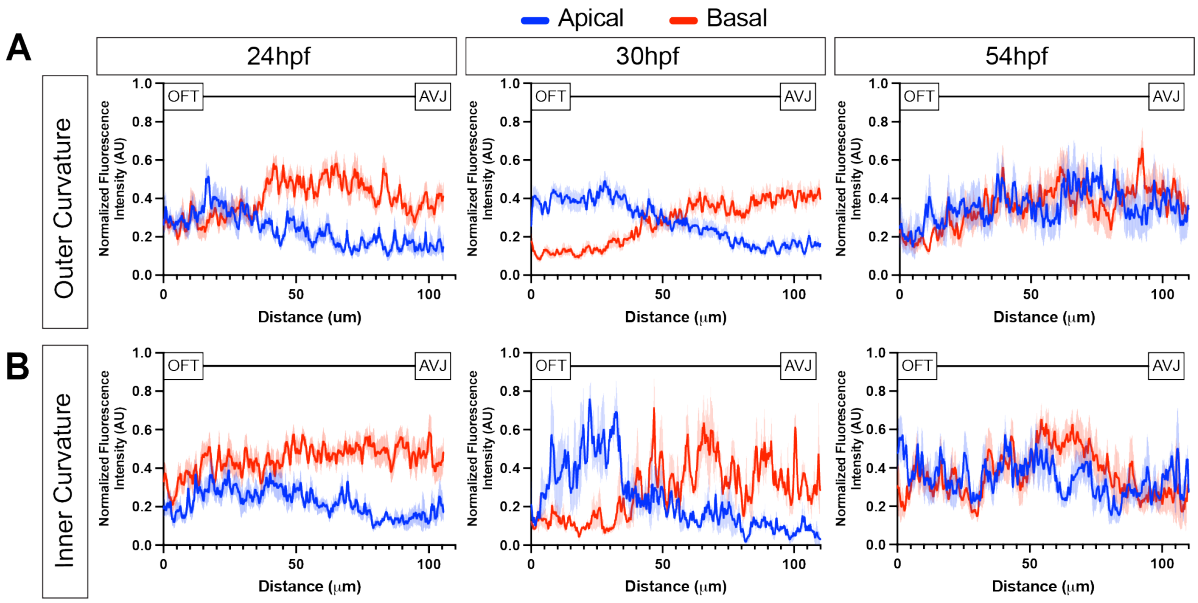

Figure 14. Plot profiles of pMyo across the ventricular myocardium. Linear analysis of plot profiles of the representative images in Figure 15B showing the distribution and the levels of pMyo corresponding to the fluorescence intensity of the midsagittal sections starting from the outflow tract (OFT) towards the atrioventricular junction (AVJ) at 24 hpf (left panels), 30 hpf (middle panels) and 54 hpf (right panels). A, B) pMyo plot profiles at the apical side of the myocardium (blue) and at the basal side of the myocardium (red) in the outer curvature (A) and in the inner curvature (B). The averaged normalized fluorescence intensity from pMyo immunostainigs is plotted and the SEM is indicated by the shaded area. (N=3; n≥9).

At 24hpf, pMyo is evenly distributed along the apical and basal myocardial membranes in the distal ventricle. In the proximal ventricle, the pMyo is more highly localized to the basal membranes as compared to the apical membranes of the ventricular myocardium (Figure 14, 24 hpf, left panels). However, at 30hpf, there is a marked change in the distribution of pMyo (Figure 14, 30 hpf, middle panels); starting from the OFT in the distal ventricle, the signal is higher in the apical side of the epithelium, followed by a noticeable switch in the localization to the basal side in the proximal ventricle close to the AVJ. This switch occurs approximately midway between OFT and AVJ and is highly reproducible. Finally, at 54hpf, the pMyo is homogenously distributed across the myocardium (Figure 14, 54 hpf, right panels). Although the switch in the pMyo localization occurs in both curvatures, it is more evident in the outer curvature of the myocardial epithelium.

The schematic representation of the observed data in Figures 15 and 16 are illustrated in Figure 17 and consider the experimental data of the pMyo levels at three different time points. Remarkably, the switch of the pMyo from apical to basal localization in the ventricle occurs specifically at 30hpf.

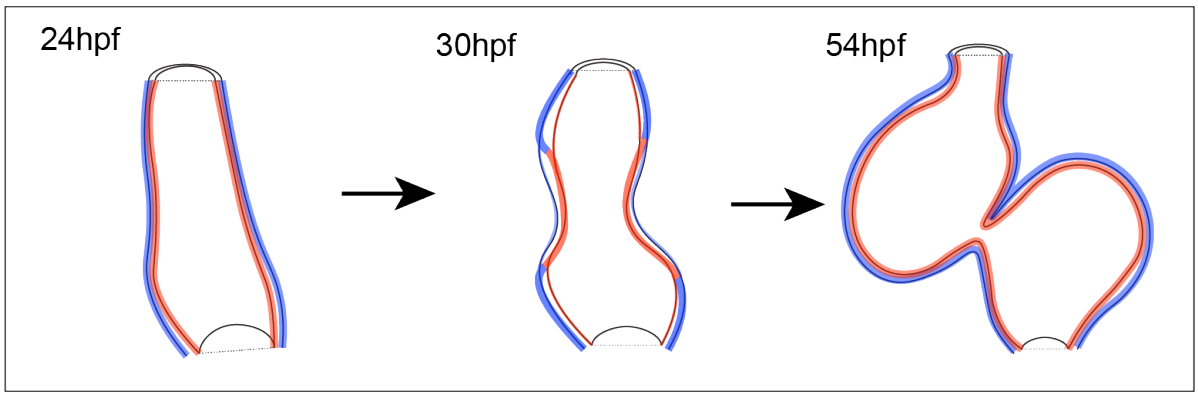

Figure 15. Schematic representation of the pMyo patterning during cardiac development. Apical (blue) and basal (red) localization of pMyo across the cardiac epithelium during cardiac development. Starting from the linear heart tube (24hpf), pMyo levels are low and localized evenly at OFT, and increasing basally at AVJ of the myocardium. During the looping stage (30hpf), the pMyo is localized apically in the distant ventricle and becoming basal as approaching the proximal ventricle. The fully formed two-chambered heart (54hpf) does not display any pMyo spatial polarity, it is equally distributed across the cardiac epithelium.

All the data together show that pMyo distribution is transiently and specifically patterned across the myocardial epithelium at 30 hpf, suggesting its localization is tightly controlled in a spatio-temporal manner. Physiologically, this time point is characterized by the initiation of the heart tube looping and when the chamber expansion occurs.

4.2 How to build a heart? A mathematical model

To date, there have been different approaches to build models of the heart formation (Le Garrec et al., 2017; Shi et al., 2014). However, none of the previous models are solely based on molecular events occurring during the looping process. A mathematical model for cardiac chamber expansion and looping was built in close collaboration with Dr. Motahareh Moghtadaei (MDC, Berlin). Our model takes the advantage of my thorough characterization of the molecular changes in the pMyo patterning across the myocardial epithelium during heart formation as showed previously in Figure 13 and Figure 14.

The model considers the real-life geometrical changes of the heart tube during the cardiac chamber expansion and looping over the developmental time points: 24, 30, and 54hpf. To obtain the respective values, I measured the morphometric indices at these time points that were used as input data to build the mathematical model of the zebrafish heart tube remodeling (Table 15).

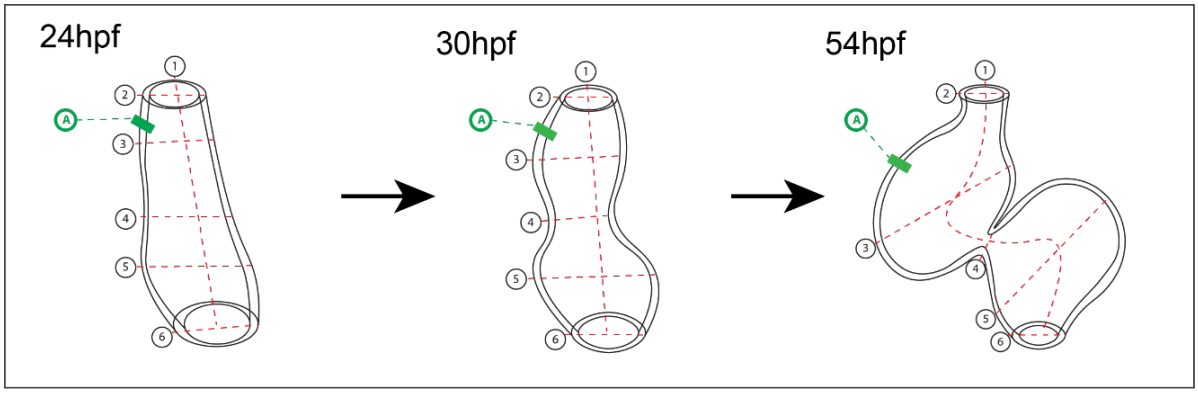

Figure 16. Scheme of the morphometric indices considered for building the mathematical model. The dimensions of the hearts at different time points were measured to use them as input to build the mathematical model: at the linear heart tube (24hpf), during the looping process (30hpf) and after the chamber formation and the heart looping have been completed (54hpf). Represented with the red dashed lines, the length (1) and width at 5 sites along the heart tube (2-5) were measured and one additional measurement was done for the thickness (A, green) of the myocardium in the outer curvature of the ventricle.

The morphometric indices included the heart tube length from the most proximal to the most distal end (Figure 16, (1)), and the outer and inner width of the myocardial tube at 5 different topologies: at the OFT, mid ventricle, AVJ, mid atrium, and sinus node (Figure 16, measurements (2-6), respectively) and one additional measurement for the thickness of the myocardium in the outer curvature of the ventricular region (A). The model considers one assumption that the heart tube undergoes S-shape looping and considers the linear heart tube with its geometries at 24hpf as an initial state. The model input parameters are summarized in Tables: Table 15 and Table 16.

We used the experimentally acquired pMyo distribution along the apicobasal axis of the myocardium in the inner and outer curvatures at 24, 30, and 54hpf as the variable parameter (Figure 15, 16, 19A). The output of our model (Figure 19A) predicts the geometry of the tube from the initial state (Figure 19A, t_i) through the intermediate state (Figure 19A, $t_{1/2}$), and terminates with the fully formed S-looped heart with the two cardiac chambers, ventricle, and atrium (Figure 19A, t_f). Remarkably, the model, using the changes in the pMyo distribution as the only variable, was sufficient to recapitulate the chamber expansion (ballooning) and chamber remodeling occurring during the normal cardiac development in the zebrafish embryos *in vivo* (compare Figure 13 with Figure 17A). Then, we explored the possibility of modeling different conditions when the pMyo patterning is disrupted (Figure 17, B-D). The pMyo distribution was arbitrarily modified from the reference values (Figure 17A'). When either the apical or basal pMyo levels were reduced to half of the maximum value and kept constant across the whole ventricle (Figure 17B' and C', respectively), the ballooning of the chambers

was affected, the expansion of the chamber was defective, and the constriction close to the AVJ appeared incomplete and not as prominent as in the WT conditions (Figure 17B and C). Finally, we used the model to simultaneously reduce the apical and basal pMyo levels and kept them constant across the myocardial epithelium (Figure 17D'). As a result, the defective cardiac chamber ballooning was more pronounced, the chambers do not expand to acquire their characteristic kidney bean-like shape, and the AVJ constriction is missing (Figure 17D). Using the pMyo as the only variable parameter, our mathematical model predicts that the proper polarized distribution of the pMyo across the epithelium is sufficient and required to achieve the proper shape of the heart with the fully expanded chambers with their characteristic shape and the formation of the AVJ. Taking all together, I concluded that pMyo distribution and levels are required to be tightly controlled in a spatio-temporal manner. The correct pMyo patterning is indispensable for the proper looping of the heart and the chamber expansion. If this pattern is disrupted, it could lead to a defective heart formation according to our predictive model.

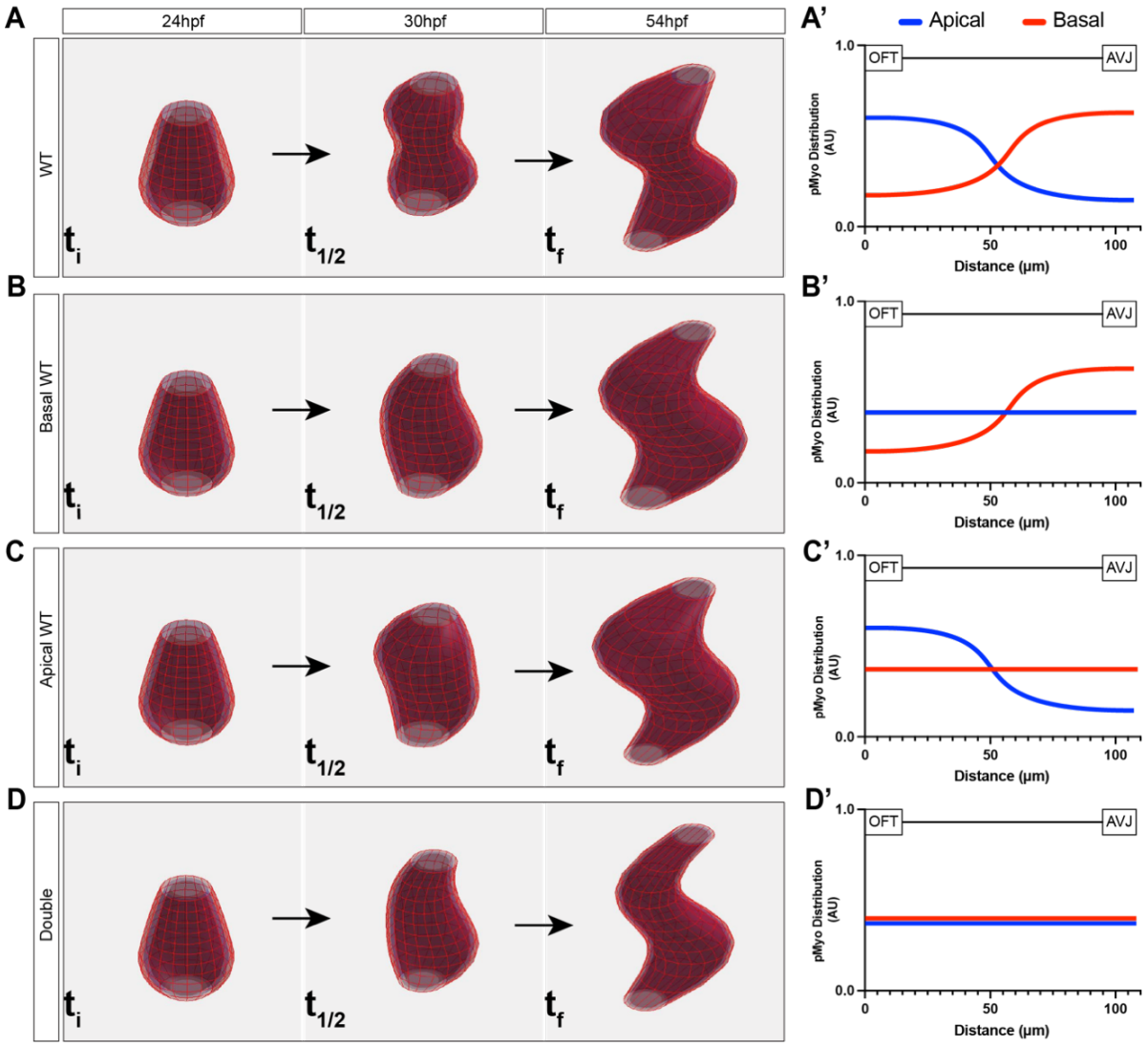

Figure 17. Mathematical model of cardiac remodeling. (A) The model was built using the experimental data from the wild type (WT) condition and predicts the changes in geometry over the process of the tube remodeling with the normal pMyo distribution showing the switch from apical to basal side of the myocardial epithelium (A'). The snapshots from the model at t_i, $t_{1/2}$ and t_f show the heart geometries that mimic the wild type changes of the heart tube remodeling as shopwn in Figure 15. (B-D) Arbitrary change of the pMyo distribution across the cardiac epithelium was used to predict the changes in the heart tube remodeling. (B) The basal distribution of pMyo was kept unchanged (Basal WT) while the apical pMyo was evenly distributed along the whole myocardium(B'). (C) The apical distribution of pMyo was kept unchanged (Apical WT) while the basal pMyo was evenly distributed along the whole myocardium. (D) Both apical and basal distribution (Double) of pMyo were changed to be evenly distributed along the whole myocardium. t_i: initial time used in the models, corresponding to 24hpf; $t_{1/2}$: intermediate time point used in the model, corresponding to 30hpf; t_f: final time used in the model, corresponding to 54hpf.

4.3 Rock2a and Mylk3 are two of the most abundant kinases in the heart

Contractility of cells and tissues is dependent on the actomyosin dynamics, more specifically on the phosphorylation state of the non-muscle myosin II (Kasza & Zallen, 2011; Vasquez,

Tworoger, & Martin, 2014; Zaidel-Bar et al., 2015). To this extent, I assessed the expression levels of four of the main kinases that could regulate the phosphorylation of the myosin in the myocardial epithelium; *rock1, rock2a, rock2b and mylk3*. I decided to focus on theses kinases since the Rock and the Mylk kinases are mainly regulating the Ser18/Thr19 phosphorylation of MRLC resulting in an increase of its affinity to bind actin in vertebrates (Ikebe et al., 1986; Scholey et al., 1980; Sellars et al., 1981; Umemoto et al., 1989). First, using qPCR analysis, I evaluated the expression levels of the four aforementioned kinases in the FACS-isolated cardiomyocytes from 30hpf embryos (Figure 18A). The most abundant kinase in the cardiomyocytes according to the expression levels was *mylk3* with the mean 16-fold higher expression compared to the non-cardiac cells, followed by the *rock2a* with the mean 6-fold higher expression compared to non-cardiac cells (Figure 18B). The expression levels of *rock1* and *rock2b*, a paralog of *rock2a*, were also assessed. However, the levels of *rock1* were very low and for *rock2b* there was no detection level reached in two of the biological independent experiments (Figure 18B). This data was the first evidence that *mylk3* and *rock2a* are the two highest expressed kinases in the embryonic heart.

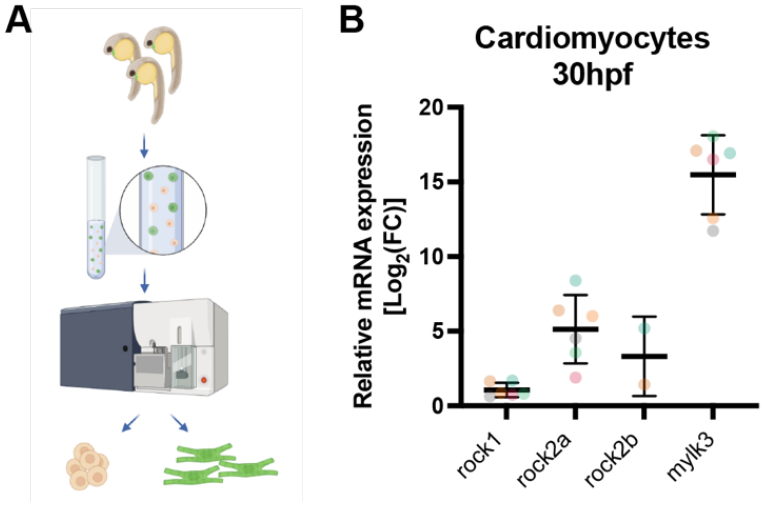

Figure 18. Expression levels of the main kinases in the heart. A) Graphical representation of the experimental approach, GFP expressing cardiomyocytes (Tg[*myl7:*EGFP] line) were isolated from 30hpf zebrafish embryo lysates using FACS. B) qPCR analysis to determine the expression levels of four different myosin kinases in zebrafish cardiomyocytes at 30 hpf. The average values are shown with the SD, each color of the dots represents an independent experiment (N=5). Data plotted as log2 fold change (FC).

Next, I assessed the spatial expression of *rock2a* and *mylk3* kinases using fluorescent *in situ* hybridization (RNAscope®) in embryonic hearts at 30hpf (Figure 19). My data showed that *mylk3* signal was more abundant than *rock2a*; this is in accordance with the qPCR results showing *mylk3* is the highest expressed kinase. However, neither of both kinase transcripts were restricted to a specific region of the heart. They were detected in the endocardium as

well as myocardium at 30hpf embryonic hearts (Figure 19, labeled as **e** and **m**, respectively in merge panel).

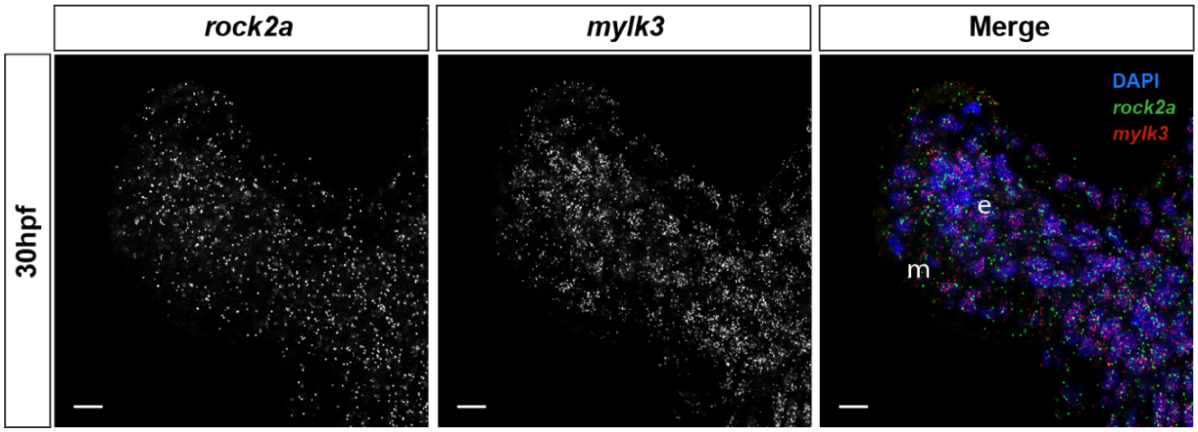

Figure 19. Spatial expression of r*ock2a* and *mylk3* in the embryonic heart. Spatial localization of *rock2a* (greyscale in the left panel, green in the merge panel) and *mylk3* (greyscale in the middle panel, red in the merge panel) transcripts in isolated hearts at 30hpf using RNAscope® fluorescent *in situ* hybridization, nuclei counterstained with DAPI (blue in the merge panel). Both transcripts are localized across the heart in the myocardium (m) and endocardium (e). Scale bar: 10µm.

Altogether, I showed that *mylk3* and *rock2a* are the main kinases expressed in the myocardial epithelium at 30hpf. However, the expression is not preferentially localized in any particular region of the ventricle. It is worth to note that both kinases are expressed not only in the myocardium, but also in the endocardium.

4.4 The tug-of-war between Rock2a and Mylk3 in the cardiac epithelium

After showing that *rock2a* and *mylk3* are the two main kinases expressed in the cardiac epithelium, the next step was to evaluate their contribution to the pMyo levels (Figure 20). Using a pharmacological approach (see methods section for details), embryos were treated either with Rockout, an unspecific inhibitor of the Rho-associated protein kinases, or ML-7, an unspecific inhibitor of the myosin light chain kinases. The treated hearts were isolated and immunostained against pMyo. Rockout- (Figure 20A, middle panel) and ML-7-treated (Figure 20A, right panel) hearts showed a reduced intensity in the signal of pMyo compared to the control hearts (Figure 20A, left panel). Next, the pMyo levels were quantified, normalized, and compared to the control hearts as a sum of total fluorescent intensities. The Rockout-treated hearts showed an average decrease of 40%, and the ML-7-treated hearts showed an average decrease of 35% in pMyo mean fluorescent intensity levels compared to the controls (Figure 20B, yellow and blue dots, respectively). Presuming the additive action of these two kinases, the reduction in pMyo levels would be up to 75%. Hence, these findings suggest a substantial

contribution of these two kinases in the total levels of phosphorylated myosin in the cardiac tissue at 30hpf, while it is not completely abolished the phosphorylation of the myosin the residual pMyo could be attributed to other kinases involved.

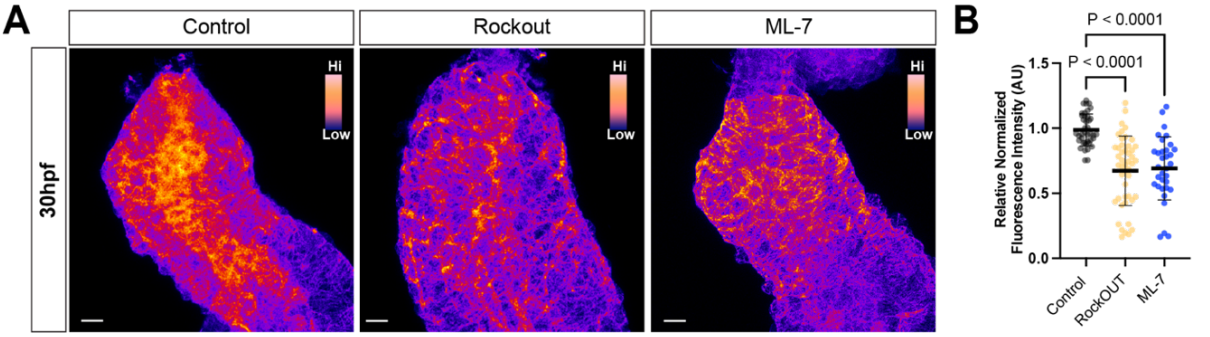

Figure 20. Rock and Mylk phosphorylate pMyo in the embryonic hearts. A) Representative Z-projections of pMyo immunostaining pseudocolored to show the pMyo intensity of isolated 30hpf embryonic hearts in control (left panel), Rockout- (middle panel) and ML-7-treated (right panel) conditions. The intensity scale goes from low levels (dark/purple) to high levels (bright/yellow) in insets. B) Quantification and comparison of the relative normalized pMyo fluorescence intensity levels in control (gray dots), Rockout-treated hearts (yellow dots) and ML-7-treated hearts (blue dots). Ordinary one-way ANOVA with Dunnett's multiple comparison test, with a single pooled variance. (N≥5; n≥20). Scale bar: 10μm.

Since I have previously shown that pMyo is regulated in a spatio-temporal manner across the myocardial epithelium of the ventricle (Figure 13 and Figure 14), I have decided to explore further the effect of the kinases inhibition on the distribution and levels of the pMyo across the myocardial epithelium using the same pharmacological approach as aforementioned. For this purpose, mid-sagittal sections of the hearts were evaluated in the same way as previously described in the section 4.2. The pMyo localization was altered after both drug treatments (Figure 21).

Interestingly, the inhibition of Rock kinase resulted in the reduction of pMyo on the apical plasma membranes of the distal ventricle and OFT cells in the cardiac epithelium (Figure 21A, B, middle panel). At the same time, the basal pMyo pattern close to AVJ and the proximal region remained unaffected (Figure 21A, B, middle panel, white arrowheads).

The opposite effect occurred in the ML-7-treated hearts (Figure 21A, B, right panel). The reduction of pMyo was on the basal side in the proximal ventricle near the AVJ of the myocardium (Figure 21A, B, right panel). At the same time, the pMyo on the apical side of the epithelium was unaffected near the OFT in the distal ventricle (Figure 21A, B, right panel, white arrowheads).

The results obtained from both treatments were then quantitatively analyzed using the linear analysis of the plot profiles along the ventricular myocardium (Figure 21C). The plots show the characteristic patterning in the control conditions; apical pMyo in the distal ventricle close

to the OFT shifting to the basal pMyo as the region approaches the proximal ventricle next to AVJ (Figure 21C, left). Meanwhile, the inhibition of Rocks disrupts the shift since there is no apical pMyo close to the OFT (Figure 21C, center), and the inhibition of Mylks also prevents the shift from occurring with a noticable lack of basal pMyo near the AVJ (Figure 21C, right). The data obtained from these drug treatments showed evidence that the kinases regulate the pMyo levels in a preferential way across the cardiac myocardium. The activity of Rock kinases is mainly in the distal ventricle close to the OFT at the apical membranes of the cardiomyocytes. On the contrary, Mylks are active mainly in the proximal ventricle, close to the AVJ, on the basal side of the cardiac cells. The observations indicate that the kinases phosphorylate the myosin on opposites sides of the cardiac cells of the epithelium in defined regions, i.e., Rocks are more active in the distal ventricle, while Mylks are more active in the proximal ventricle.

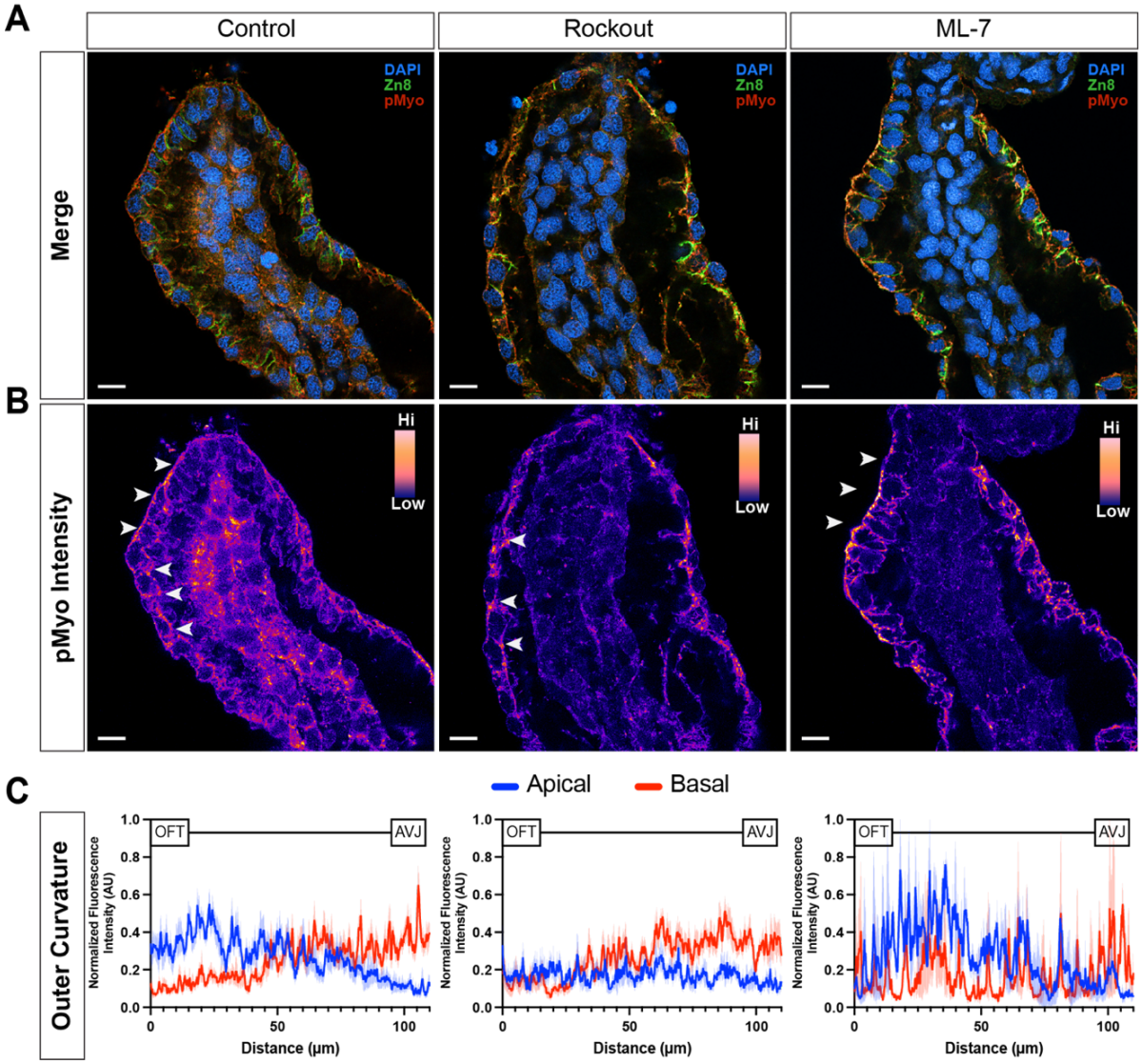

Figure 21. The activity of the Rock and Mylk kinases is preferentially localized across the ventricular myocardium. A) Representative images of merged channels of immunostaining of mid-sagittal sections of the linear heart tube at 30hpf in control (left), Rockout- (center) or ML-7-treated (right) conditions. DAPI (blue), membrane marker Zn8 (green) and pMyo (red). B) Same midsagittal sections of pMyo channel pseudocolored to highlight the pMyo fluorescent intensity. The intensity scale goes from low levels (dark/purple) to high levels (bright/yellow) in insets. In control conditions the switch of the distribution from apical to basal localization is indicated with the white arrowheads, in Rockout-treated hearts the remaining basal pMyo is indicated by the white arrowheads and in ML-7-treated hearts the apical remaining pMyo is indicated by the white arrowheads. Scale bar in A, B: 10µm C) Linear analysis of the plot profiles of the representative images in A, B showing the distribution and the levels of pMyo corresponding to the fluorescence intensity of the midsagittal sections starting from the OFT towards the AVJ. The averaged normalized fluorescence intensity from pMyo immunostainigs is plotted and the SEM is indicated by the shaded area. (N≥5; n≥15).

4.5 Rock2a and Mylk3 are responsible for the proper distribution of pMyo in the cardiac epithelium

Using the pharmacological approach revealed preferential activity of Rock and Mylk kinases but fell short to determine which specific kinases were responsible for the myosin phosphorylation. Therefore, I decided to test the role of the kinases expressed in the cardiac cells that I have identified, *rock2a* and *mylk3*. To specifically reduce the expression of these kinases, I used a morpholino (MO) based strategy targeting each of the kinases. MOs are short modified antisense oligonucleotides complementary to a mRNA molecule blocking its splicing or translation by stearic impediment causing the knock down of a gene of interest (Nasevicius & Ekker, 2000; Summerton, 1999; Summerton & Weller, 1997). I have first determined the knock-down efficiency of both morpholinos and showed that the lack of both kinases causes cardiac defects as previously reported (Lisowska et al., 2018; Seguchi et al., 2007) (Figure 22).

The *rock2a* MO was validated and reported before to cause cardiac malformations in zebrafish (Lisowska et al., 2018; Marlow et al., 2002). However, to validate the *mylk3* effects in cardiac looping I used a mutant *mylk3*$^{-/-}$ line as well as the *CRISPR/Cas9* approach to generate a knockout line for mylk3. First, visual evaluation of the body phenotype (Figure 22A) of the *mylk3* MO-injected embryos had a noticeable cardiac edema (middle panel), the pericardial cavity was filled with liquid in line with the previously reported data (Seguchi et al., 2007). However, the *rock2a* MO-injected embryos had no abnormal body phenotype apart from a very subtle cardiac edema (lower panel). Then, the percentage of the embryos showing a cardiac looping phenotype was quantified and compared (Figure 22B). The full-dose injection of *rock2a* MO caused a cardiac phenotype in 35% of the total embryos analyzed compared with the control group while in the full dose injection of *mylk3* MO, 69% of the embryos showed a phenotype. Splicing *mylk3*^{ex6sd} MO-injected, F0 *mylk3* CRISPR/Cas9 knock out (mylk3^{ex3} CRISPR/Cas9) and the *mylk3*$^{-/-}$ mutant embryos were evaluate to quantify the cardiac phenotype penetrance, 68%, 79%, 91% and 25% of the embryos, respectively, showed a cardiac phenotype (Figure 22B). It is worth noting that only 25% of the *mylk3*$^{-/-}$ displayed a phenotype as expected according to a mendelian ratio (1/4) of homozygous recessive mutant embryos (Bateson, Mendel, & Leighton, 1909).

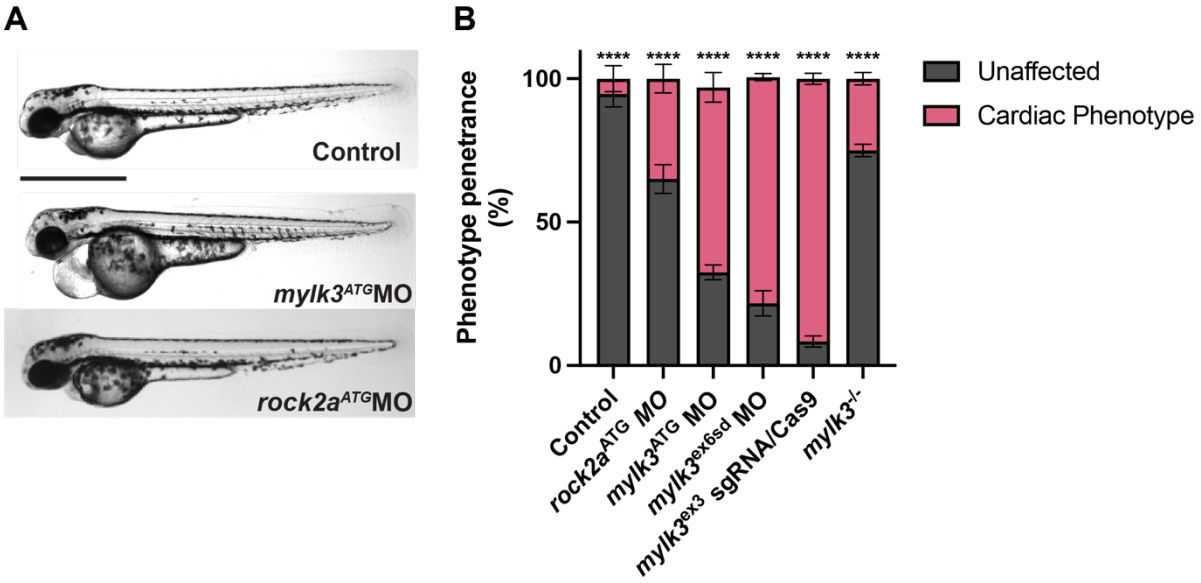

Figure 22. Phenotypic analysis of *mylk3* or *rock2a* knock down embryos. A) Representative brightfield images of the embryos for the phenotypic analysis comparing the uninjected control embryos with the embryos injected with a full dose of *mylk3*^{ATG} or *rock2a*^{ATG} MO. Scale bar: 500µm. B) Quantification of the phenotype percentage of embryos injected with *mylk3*^{ATG} or *rock2a*^{ATG} MO. Ordinary one-way ANOVA, Dunnett's multiple comparison test with a single pooled variance. (N≥3; n≥300).

I have then isolated 30hpf hearts of uninjected control, and *rock2a*^{ATG} MO- and *mylk3*^{ATG} MO-injected embryos and immunostained for pMyo to check the overall levels of pMyo in the ventricle of the embryonic hearts (Figure 23). The embryonic hearts isolated from embryos injected with rock2a MO (Figure 23A, second panel), *mylk3* MO (Figure 23A, third panel) or co-injected with both MOs (Figure 23A, fourth panel) showed reduced levels of the pMyo signal in the immunostainings when compared to control hearts (Figure 23A, first panel). Then, the pMyo levels were quantified and plotted for comparison with control hearts (Figure 23B); hearts from *rock2a* MO-injected (yellow dots) embryos had an average reduction of 25%, an average reduction of 10% was observed in *mylk3* MO-injected hearts (blue dots), and an average of 25% less pMyo was detected when both MOs were co-injected (red dots). This evidence supports the previous results of the pharmacological treatment. Moreover, these findings show that the specific kinases, Rock2a and Mylk3, which are the most abundant kinases in the embryonic zebrafish heart, play a central role in phosphorylating myosin in the developing myocardium. These findings suggest a substantial contribution from each of the two kinases in the total levels of phosphorylated myosin in the cardiac tissue at 30hpf.

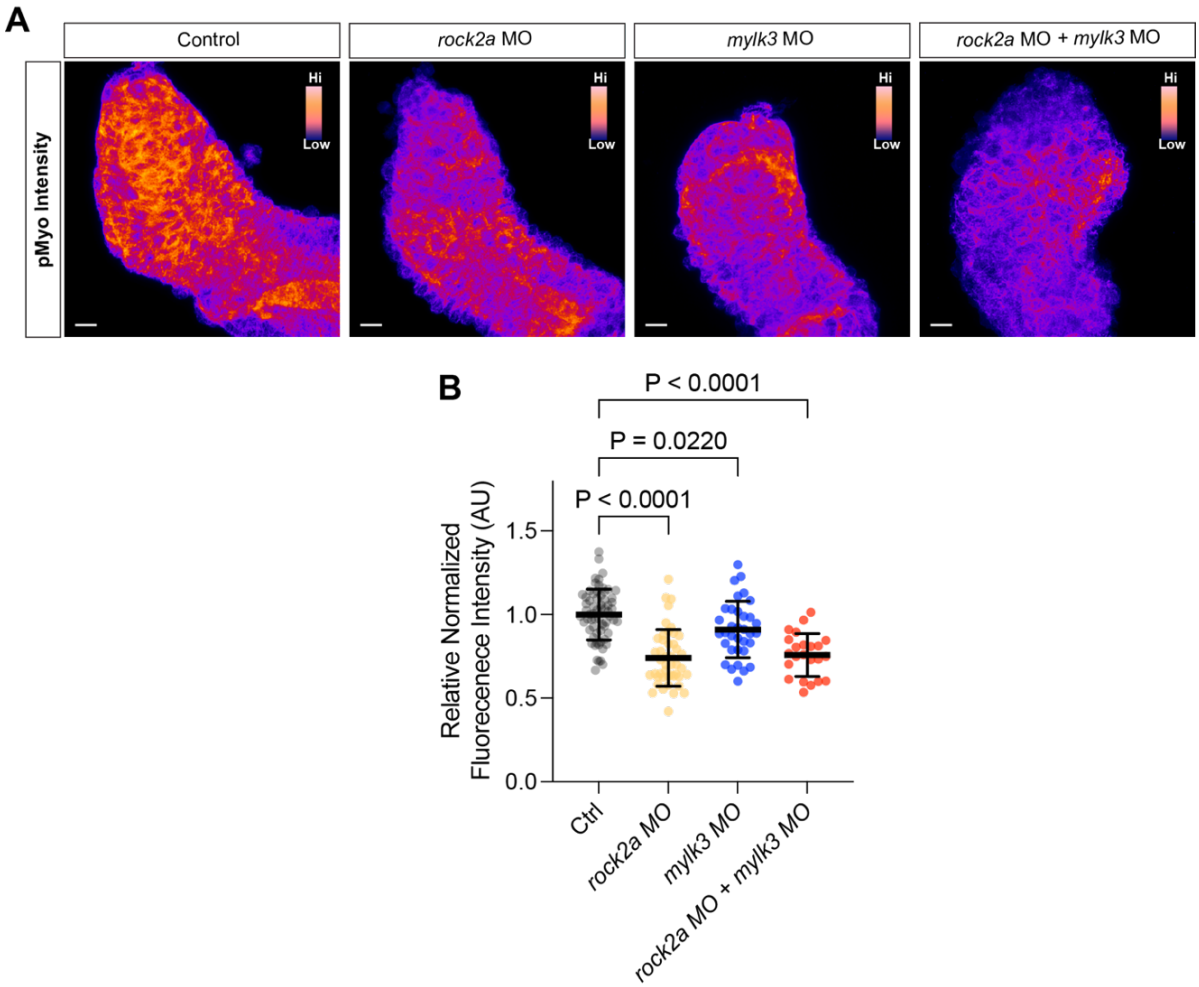

Figure 23. Rock2a and Mylk3 contribute to the pMyo levels in the ventricular myocardium. A) Representative Z-projection images of pMyo immunostaining pseudocolored to show the pMyo intensity of isolated 30hpf embryonic hearts of control embryos (left), *rock2a* MO-injected embryos (second panel), *mylk3* MO-injected embryos (third panel) and embryos co-injected with both MOs (*rock2a* and *mylk3*). The intensity scale goes from low levels (dark/purple) to high levels (bright/yellow) in insets. Scale bar: 10µm. B) Quantification and comparison of normalized pMyo fluorescence intensity levels in control (gray dots), *rock2a* MO injected hearts (yellow dots), *mylk3* MO injected hearts (blue dots) and double *(rock2a* and *mylk3)* MOs injected hearts (red dots). Ordinary one-way ANOVA, Dunnett's multiple comparison test, with a single pooled variance. (N≥3; n≥8)

Next, I assessed the localization of pMyo along the apicobasal axis of the myocardium in the optical mid-sagittal sections from the OFT to the AVJ. I performed a quantitative plot profile analysis to determine the patterning and the levels of pMyo in the outer ventricular curvature (Figure 24). I observed a decrease in the signal coming from the apical side of the epithelium of the distal ventricle near the OFT in the hearts of *rock2a* MO embryos (Figure 24, A. and B, second panels). The opposite effect was observed for the *mylk3* MO hearts (Figure 24, A and B, third panels). The pMyo fluorescence corresponding to the basal portion of the proximal ventricle close to the AVJ was diminished. Additionally, knocking down both genes together, *rock2a* MO + *mylk3* MO, resulted in the decrease and loss of any patterning of the pMyo across the ventricular myocardium on both sides (Figure 24, A and B, right panel).

From the images corresponding to the pMyo stainings, I performed a quantitative linear plot profile analysis to determine the distribution and levels of pMyo in the outer ventricular curvature (Figure 24, C). In the *rock2a* MO hearts, pMyo levels are diminished and distributed evenly along the apical myocardial membranes (Figure 24, C second plot). The basal localization of the pMyo is not affected since the high levels are preserved in the proximal myocardium close to the AVJ. The opposite effect was observed for the *mylk3* MO hearts. The pMyo on the cell's apical membrane along the myocardium remained high and apically in the distal ventricle close to the OFT. However, the basal levels of the pMyo were distributed evenly across the whole myocardium (Figure 24, C, third plot). The knockdown of both genes together, *rock2a* MO and *mylk3* MO, resulted in a loss of any pattern of the pMyo across the ventricular myocardium, and the distribution remained unchanged (Figure 24C, right plot), surprisingly resembling the pattern of the pMyo observed and plotted for the linear heart tube at 24hpf (Figure 14A, upper left panel).

Altogether the data showed the importance of Rock2a and Mylk3 kinases in establishing the proper distribution of pMyo in the cardiac epithelium when the looping process occurs at 30hpf. Rock2a is mainly active on the apical membrane of the cells located in the distal ventricle next to the OFT while the activity of Mylk3 is mainly responsible for phosphorylating myosin in the proximal ventricle close to the AVJ, in the basal membrane of the cells. In conclusion, at the tissue level, the kinases act preferentially in defined regions, Mylk3 in proximal and Rock2a in distal portion of the ventricle. Second, at the cellular level, they act at the opposite sides of the membrane of the cardiac cells in the apicobasal axis within the epithelium, Mylk3 being active basally while Rock2 phosphorylates myosin apically.

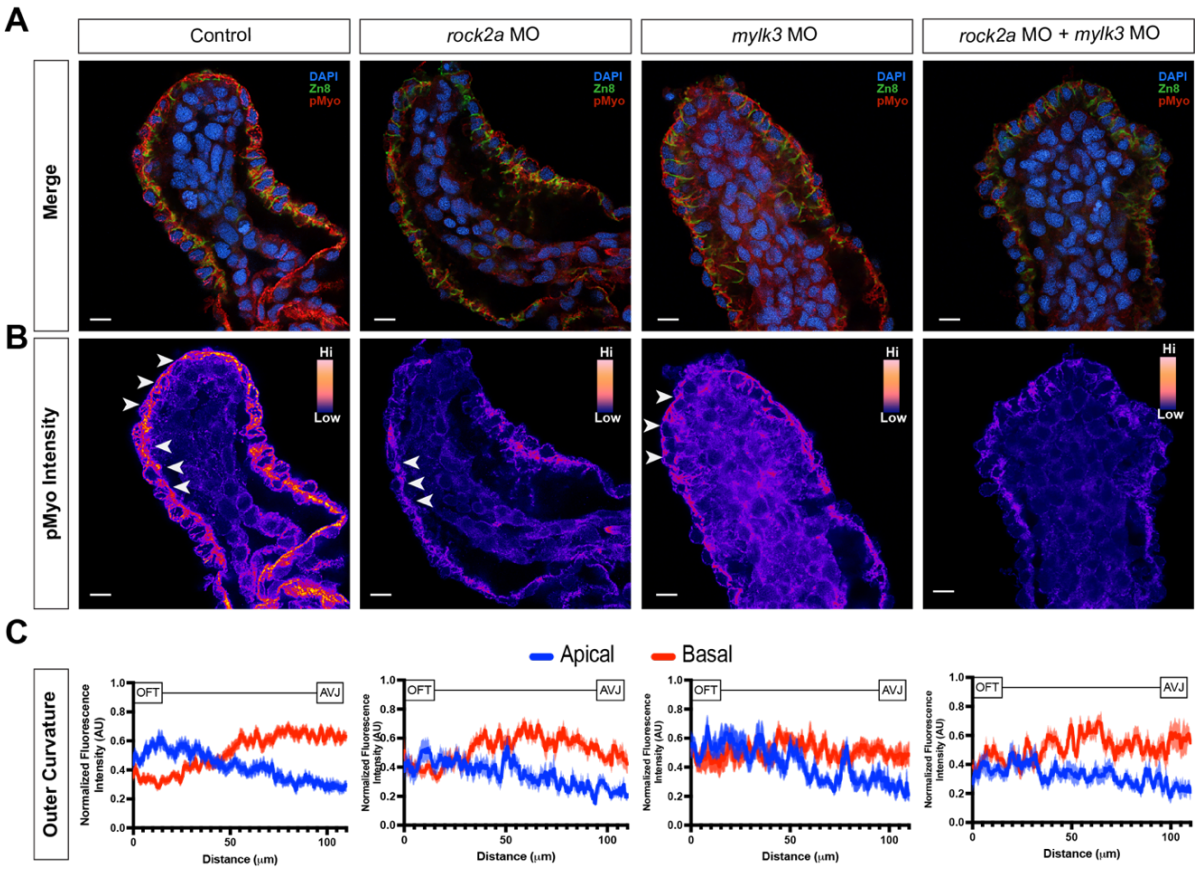

Figure 24. Rock2a and Mylk3 activity is preferentially localized across the ventricular myocardium. A) Representative image of immunostaining of midsagittal sections of isolated hearts at 30hpf in control (left), *rock2a* MO (second to the left), *mylk3* MO (second to the right) or double (*rock2a* and *mylk3*) MOs injected embryos, DAPI (blue), membrane marker Zn8 (green) and pMyo (red). B) Pseudocolored pMyo staining to show the intensity levels from the same midsagittal sections from above showing the pMyo fluorescence intensity from low levels (dark/purple) to high levels (bright/yellow) across the cardiac epithelium at 30 hpf. Midsagittal sections showing the pMyo fluorescence intensity across the cardiac epithelium at 30 hpf, in control conditions the switch of the distribution from apical to basal localization is indicated with the white arrowheads, in *rock2a* MO injected hearts the remaining basal pMyo is indicated by the white arrowheads, in *mylk3* MO injected hearts the apical remaining pMyo is indicated by the arrowheads and in double MO injected hearts there is no switching of the pMyo localization remaining distributed evenly across the myocardium. C) Linear analysis of plot profiles showing the distribution and the levels of pMyo corresponding to the normalized fluorescence intensity of the midsagittal sections in the outer curvature starting from the OFT towards the AVJ for each of the conditions indicated in the panels above. The average normalized fluorescence intensity is plotted with SEM as the shaded area. (N≥5; n≥15) Scale bar: 10μm.

4.6 Rock2a and Mylk3 regulate the tension distribution along the heart tube during the looping process

After characterizing the molecular dynamics of pMyo across the cardiac epithelium during cardiac formation and the identification of two kinases responsible of the regulation of pMyo patterning, I decide to explore the possible effects of the pMyo distribution regarding the cellular tension generated across the cardiac epithelium. Then the question was whether there

are implications of this supracellular pMyo in the tension distribution on a tissue scale. Recently, a specific probe was developed to assess the cellular tension; Flipper-TR® tension sensor probe was used for this purpose (Figure 25) (Colom et al., 2018). The probe changes its fluorescence lifetime depending on the properties of the plasma membrane (tension, pressure, and the viscosity of the lipid bilayer), i.e. the increases in the fluorescence lifetime of the Flipper® sensor are being proportional to the increases in the tension or the viscosity of the membrane (Figure 25A, B). The cellular tension across the ventricular myocardium was evaluated using a FLIM approach, these experiments were done in close collaboration with Dr. Anca Margineanu (MDC Berlin).

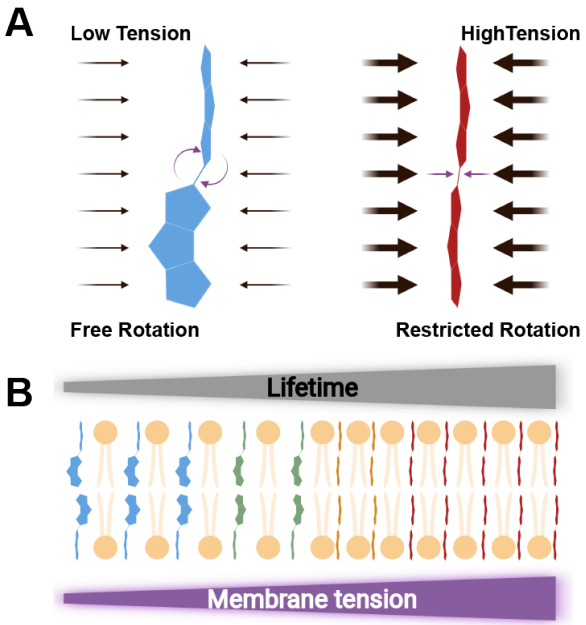

Figure 25. The Flipper-TR® tension sensor probe. The probe consists of two large dithienothiophene flippers. A) In a low membrane tension state (non-confining environment) the two flippers are twisted out of conjugation (blue) while in high membrane tension state (confined environment) the flippers are aligned in a planar fashion (red), the intramolecular rotation is responsible of the fluorescence lifetime change of the molecule. B) The lifetime of the probe is proportional to changes in the membrane tension. The higher the values for the lifetime the higher the membrane tension.

We measured the average lifetime (Tau average), the long lifetime (Tau long), and the short fraction of the lifetime (Tau short) in isolated hearts (Figure 26 and Figure 27). After quantifying the fluorescence lifetimes, the *rock2a* MO (yellow violin plots) hearts showed the increased spread in the distribution of the short lifetime component compared with the control, consequently broadening the average lifetime distribution (Figure 26A). The Tau short only shows a shift towards higher values (Figure 26B). The spread in the distribution of values coming from the *rock2a* MO group suggests high variability in the membrane tension in myocardial cells across the epithelium. These changes in the distribution could be explained because of all the possible effectors of Rock2a, which could influence the membrane tension

in different proportions, among all of them the cortical cytoskeleton and the phosphorylation of the myosin being a plausible explanation.

For the *mylk3* MO hearts, the average lifetime values were broadened and showing higher values for the lifetime when compared with the distribution on the control group (Figure 26A). The long component (Tau long) showed the distribution displacing towards higher values for *mylk3* MO (Figure 26B). The same increase in the short lifetime component was measured for the *mylk3* MO hearts compared with the control hearts (Figure 26C).

When both *rock2a* and *mylk3* are knocked down at the same time, we observe an important reduction of the long lifetime component value (Figure 26B), which seems to be the main factor driving the reduction of the mean lifetime (Figure 26A) and not the fraction of the short fraction of the long component, which shows an actual increase (Figure 26C); this can be related to the reduction of the membrane tension in this condition.

In summary, the signal corresponding to the Flipper dye corresponding to the averaged lifetime was variegated along the cardiac tube in all experimental group conditions. Noticeable changes were more prominent in the long component of the lifetime (Figure 26B).

From the images acquired corresponding to the lifetime measurements (Figure 27), we observed that the average lifetime in the isolated hearts was a combination of increase and decrease in FLIM values distributed all over the myocardium (Figure 26A). The main difference we found from the fluorescent lifetime imaging was the difference in the long lifetimes (Figure 27B), where *rock2a* MO showed a reduction, *mylk3* MO an increase, and the combination of both, a reduction even more pronounced than the one observed for *rock2a* MO. The images corresponding to the fraction of the long time (Figure 26C) were similar for that observed in the average lifetime measurement, showing a combination of increase and decreased FLIM values in the ventricular myocardium.

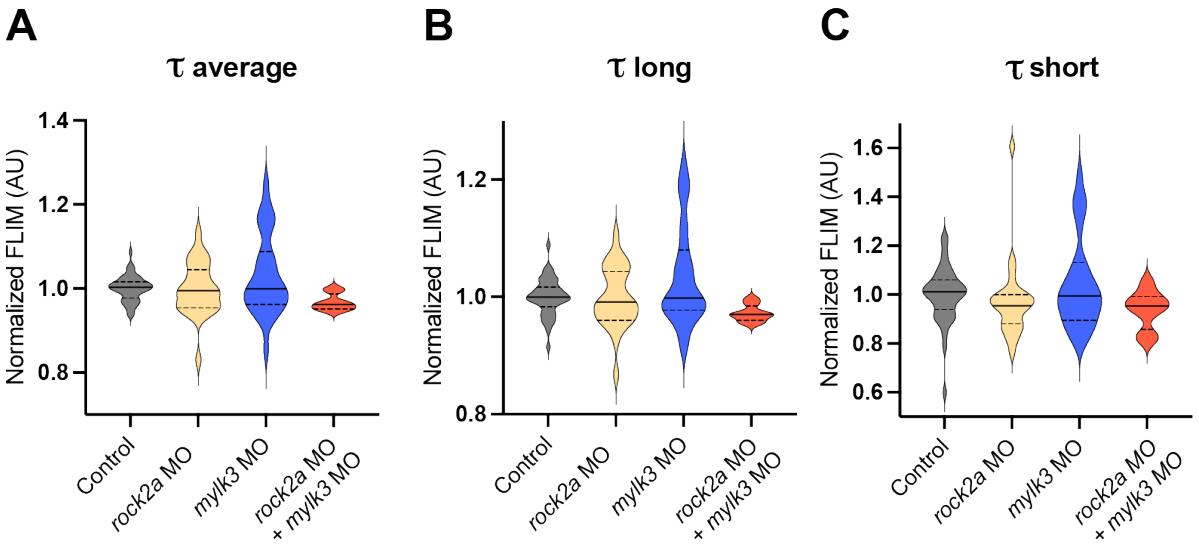

Figure 26. Rock2a and Mylk3 modulate the membrane tension. Violin plots of cardiomyocytes average lifetimes calculated per heart for all groups. Normalization was done relative to the average value calculated for the corresponding control hearts in each experiment. A) Violin plot of the average lifetimes obtained from global analysis fit for the hearts in all groups. B) Violin plots of the long lifetime determined for the myocardium per heart in all groups. C) Violin plots of the fractions of the long lifetime determined for the myocardium per heart in all groups. Control hearts in grey, *rock2a* MO-injected hearts in yellow, *mylk3* MO-injected hearts in blue and double co-injected MOs (*rock2a* and *mylk3* MO) in red. (N≥3; n≥3).

We calculated the average lifetime in each heart individually from all the optical planes per heart. Then, we compared the frequency distribution for the average FLIM in all the hearts corresponding to each group. We observed a change in the averaged FLIM values distribution in hearts from MO-injected groups (Figure 27D). Comparing to the control (gray histogram), the injected hearts with *rock2a* MO (yellow histogram) showed a wider frequency distribution, the same was observed for the *mylk3* MO-injected hearts (blue histogram), but the frequency distribution was even wider when compared to the controls. However, intriguingly, the co-injection of both (*rock2a* and *mylk3*) MOs (red histogram) showed a reduction in the variability resulting in a narrow frequency distribution. This could be explained by the overall cancellation of difference in tension between both kinases. Since the analysis of the measurements were performed in the whole ventricle, this opens the possibility of having regions in the ventricle where the tension is higher and some other areas where the tension is lower, achieving an overall nullifying effect in the tension distribution. This is in line also with our mathematical model.

Our results show that membrane tension variations after knocking down the gene function of either of the kinases qualitatively follow the disruption of phosphorylation of myosin affecting the cortical tension. Since we are not modifying the actin polymerization, the observed effects are only due to the loss of activity modulated through the phosphorylation of the myosin

regulatory light chain. This could explain the high variability and the subtle change in the membrane tension measurement because it is an indirect perturbation of the cortical cytoskeleton and does not interfere directly with the main component, which is the cortical actin filaments.

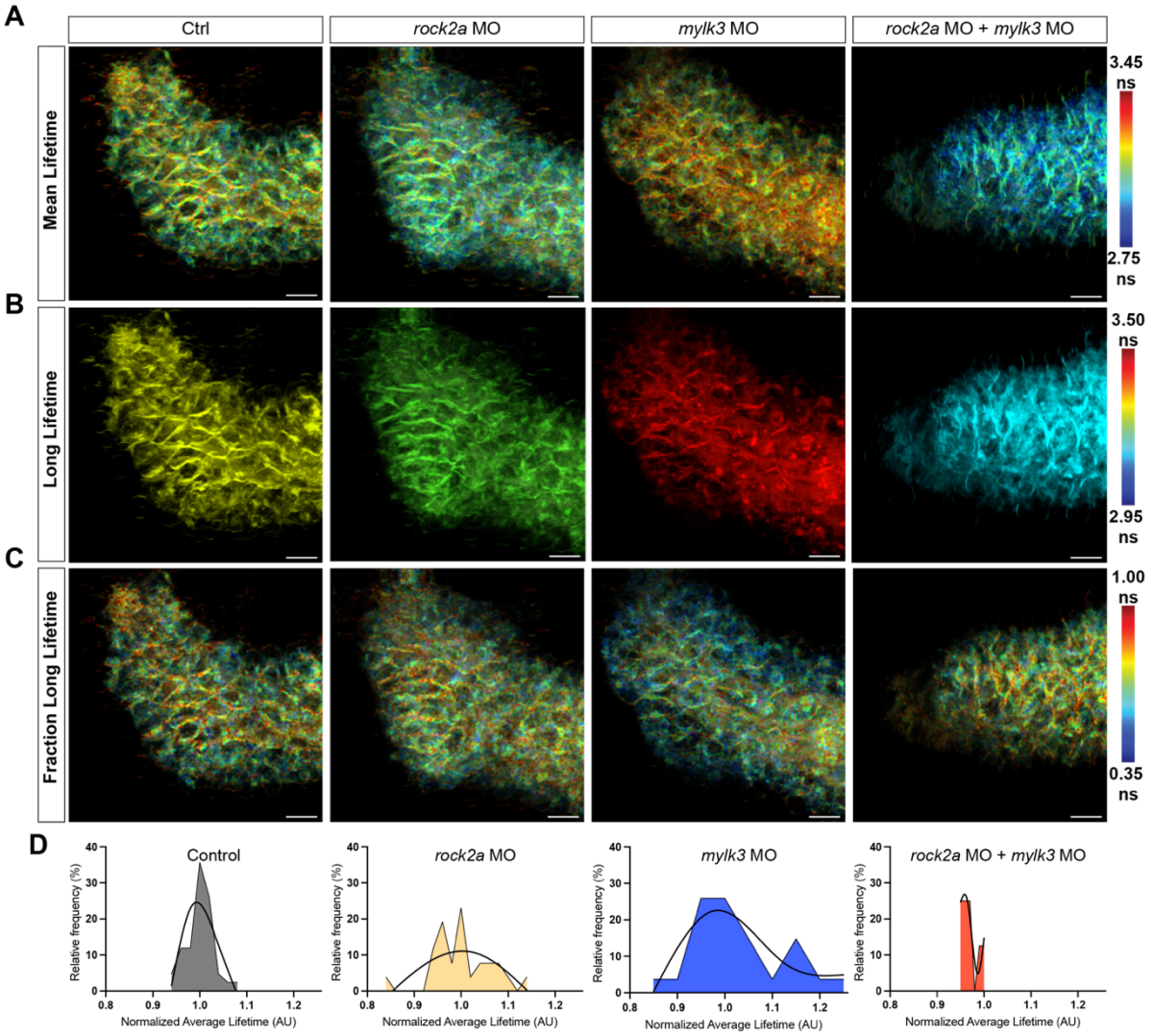

Figure 27. FLIM measurements. Representative images of Z projection of isolated hearts at 30hpf stained with the Flipper-TR tension probe. A) Mean lifetime values (average Tau). B) Long lifetime values (long Tau). C) Fraction of the long lifetime values (short Tau). Control heart (left panels), *rock2a* MO-injected hearts (second panels), *mylk3* MO-injected hearts (third panels) and double MO-injected (*rock2a* and *mylk3*) hearts (fourth panels). The lifetime in ns is represented in color code with the blue pixels correspond to lower lifetime values and the red pixels correspond to higher lifetime values. Note the different scale depending on the measurement. Scale bar: 10µm. D) Histograms showing the frequency distribution of the normalized average lifetime for each of the conditions indicated above each plot, for *rock2a* MO- and *mylk3* MO-injected hearts the distribution is wider, while in the double MO-injected hearts the distribution is narrower. (N≥3; n≥9).

4.7 Rock2a and Mylk3 are required for proper cardiac looping *in vivo*

Once I demonstrated that both kinases play a main role in the modulation of pMyo levels and localization in the heart tube, I used an *in vivo* approach to translate the findings from the molecular cellular and tissue levels to the heart formation process. Our mathematical model and the tissue tension measurements suggested the activity of these two kinases may be required to generate forces that coordinate the heart chamber ballooning and looping. To examine this possibility, I went one step further in the analysis of the phenotypes in the embryos lacking the function of both kinases, focusing specifically on the cardiac looping phenotype (Figure 28B). Ventral images were acquired and analyzed to determine the looping angle that indicates how successful the morphogenetic process of the cardiac looping process is and is measured as angle between the embryo midline and AVJ (Figure 28B, left upper panel). Embryos injected with *mylk3* (Figure 28B, left lower panel) or *rock2a* MO (Figure 28B, right lower panel) showed an incomplete cardiac looping when compared to the control hearts (Figure 28B, right upper panel). When the angle was measured, plotted, and compared (Figure 28C) the average angle for control embryos (gray dots) was 29°, while in *mylk3* MO-injected embryos (blue dots) the angle was wider with an average of 43°, and the same was observed in the *rock2a* MO injected embryos (yellow dots) having an increased value in the angle with an average of 46°. Taking this data together, I showed that both of the kinases are necessary for the proper cardiac looping in zebrafish embryos.

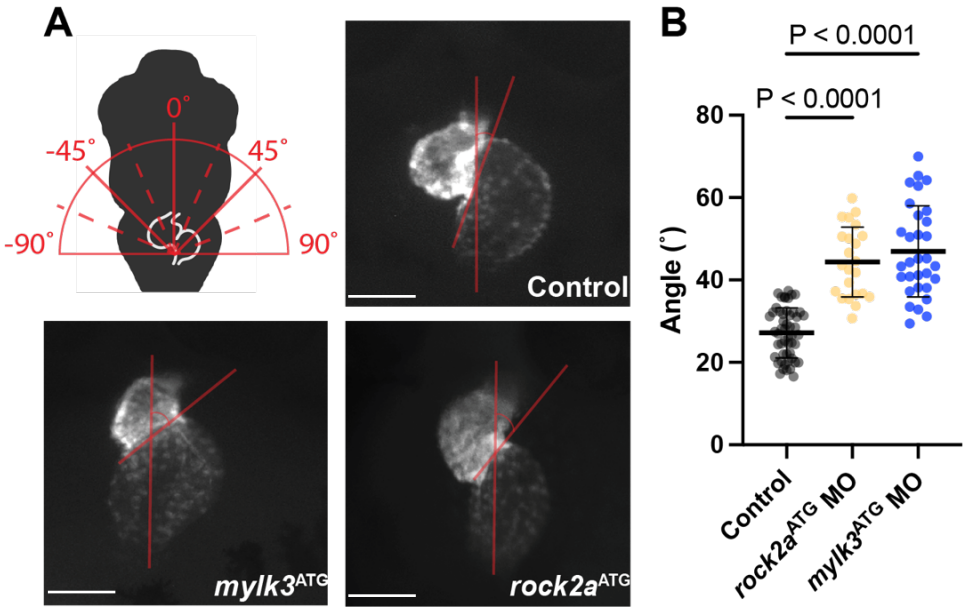

Figure 28. Rock2a and Mylk3 are necessary for proper cardiac looping. A) Cardiac looping analysis scheme illustrating the angle measured as an angle between the midline of the embryo and the AVJ (upper left panel). Representative fluorescent images of the heart from the ventral view of the embryos for control (upper right panel), *mylk3* MO- (lower left panel) and *rock2a* MO-injected (lower right panel) embryos. Scale bar: 500μm. B) Quantification of the looping angle in control (gray dots), rock2a MO-

(yellow dots) and mylk3 MO-injected (blue dots) embryos. Ordinary one-way ANOVA, Dunnett's multiple comparison test with a single pooled variance. (N≥3; n≥30).

4.8 Rock2a and Mylk3 are effectors of the PCP Pathway

After demonstrating the role of Rock2a and Mylk3 in tissue force generation and heart tube remodeling due to the pMyo pattern regulation, I investigated the possibility of Mylk3 being an effector protein of PCP pathway. This was hypothesized because PCP pathway is one of the main morphogenetic signaling pathways that has been showed to be required in cardiac development (Foulquier et al., 2017; Gibbs et al., 2016; Merks et al., 2018; Phillips et al., 2005; Ramsbottom et al., 2014; Sinha et al., 2015, 2012; Wu et al., 2011). I also took in account that the main effect of the PCP signaling is on the cytoskeleton remodeling including the actomyosin complex, in which Rock kinase has been described as the only PCP effector kinase regulating the phosphorylation of myosin (Marlow et al., 2002; Phillips et al., 2005; Vivancos et al., 2009; Winter et al., 2001; Wu et al., 2011).

I used an assessment of genetic epistasis, in which morpholino subthreshold strategy is used (Figure 29) to determine the possible genetic interactions between the kinases and the PCP core components. Injecting subthreshold concentration of either the *rock2a* MO or *mylk3* MO is not enough to cause any phenotype. However, when the respective kinase MOs in subthreshold concentration were co-injected with individual MOs targeting each of the PCP core components in subthreshold concentrations as well: *wnt11f2*, *fzd7a*, *dvl2*, *vangl2 and pk1a*, the phenotype occurs only when the two genes are in genetic epistasis. Meaning, I expected to observe a phenotype only in case of a synergistic effect after the MOs co-injection, indicating there is a genetic interaction between the two respective genes (Figure 30).

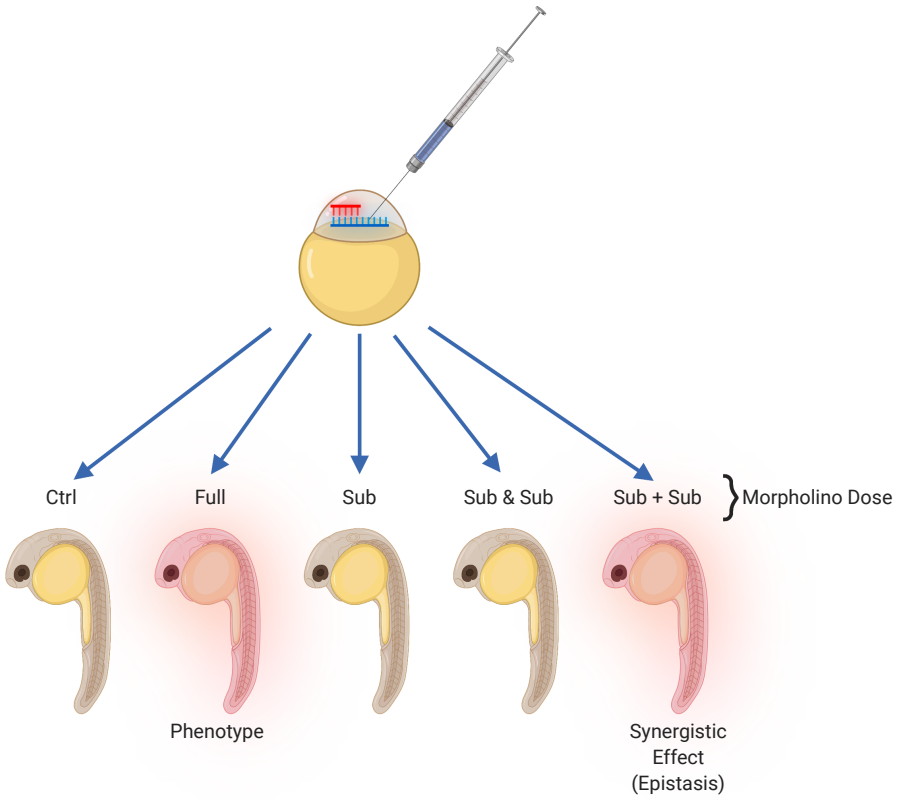

Figure 29. Assessment of genetic interaction: the experimental approach. Control uninjected embryos are used as a control to compare with single cell stage morpholino injected embryos with a full dose (full) causing a phenotype. The injection with MO subthreshold (sub) concentration is not enough to cause a phenotype. The injection of two morpholinos of non-interacting genes (sub& sub) in subthreshold concentrations do not cause any phenotype. The injection of two morpholinos of interacting genes have a synergistic effect causing a phenotype due to the epistatic effect. Ctr: control; Full: full dose MO; Sub: subthreshold MO concentration.

I injected subthreshold concentration of the *rock2a* MO or *mylk3* MO, which is not enough to cause any phenotype in the embryos, and then co-injected with morpholinos targeting each of the PCP core components in subthreshold concentrations: *wnt11f2*, *fzd7a*, *dvl2*, *pk1a*, *vangl2*. After two days, I evaluated the phenotype of the embryos in each condition, which will only show a phenotype in case of a synergistic effect of the co-injection (Figure 30). The planar cell polarity phenotype is characterized by shortening of the body length due to defects during the convergent extension process in early embryonic development (Jessen et al., 2002; Topczewski et al., 2001). For all the subthreshold concentrations co-injected, there was no evident body phenotype in the embryos (Figure 30). Furthermore, neither of the full dose of the *rock2a* nor the *mylk3* morpholinos caused a body phenotype. However, they both caused cardiac defects as quantified in Figure 29.

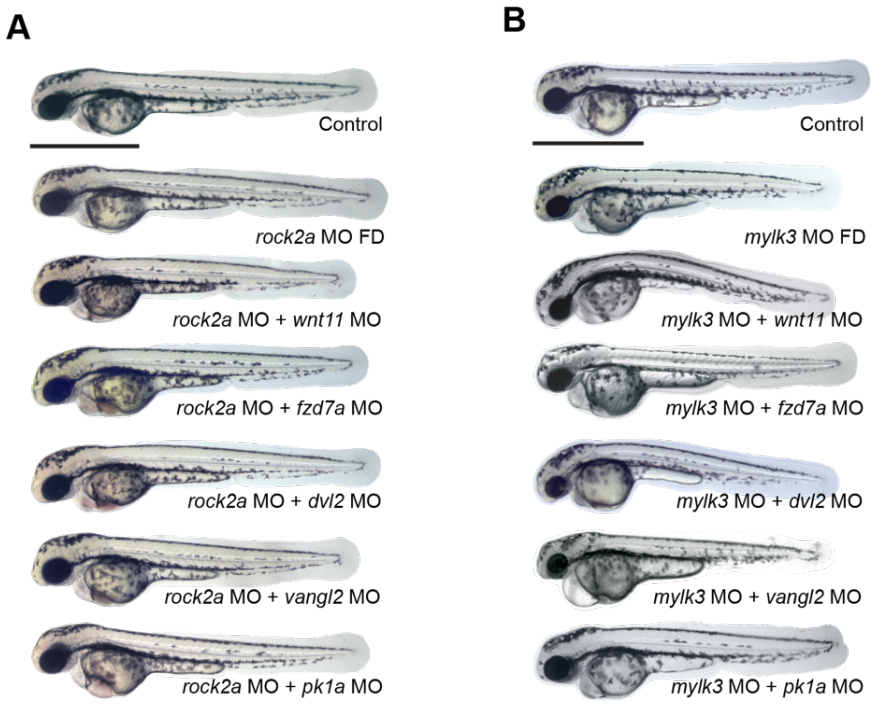

Figure 30. Embryo phenotypes in the analysis of the genetic interaction. A) Representative brightfield images of embryos at 54 hpf to perform the visual phenotypic analysis injected with: A) *rock2a* MO in combination with MOs targeting each of the PCP core components. B) *mylk3* MO in combination with MOs for each of the PCP core components. All MOs concentrations co-injected in combination were subthreshold and not causing any observable phenotype. MO: morpholino; FD: full dose morpholino; Scale bar: 500 µm.

I therefore focused on examining the cardiac phenotype, manifested as the presence of cardiac edema and looping defects (incomplete looping in the heart at 54hpf), when deciding whether two tested genes are genetically interacting or not (Figure 31).

Then, from the different combinations of *rock2a* MO or *mylk3* MO and the respective PCP core components MOs, the percentage of the embryos showing a cardiac phenotype was quantified and compared (Figure 31A). In the full dose injection of *rock2a* MO, 40% of the embryos showed a phenotype; in the combination of *rock2a* MO with *wnt11f2* or *fzd7a* MO, 30% and 25% of the embryos, respectively, showed a cardiac phenotype, this was expected since those are the ligand and the receptor respectively. In the combination of *rock2a* and *dvl2* MOs, 38% of the embryos had a cardiac phenotype. Surprisingly, in the combination of *rock2a* MO with either *vangl2* or *pk1a* MO, a higher percentage of embryos had cardiac phenotype, on average up to 65% in both cases (Figure 31A).

The same analysis was performed by combining *mylk3* MO and the PCP core components MOs in subthreshold concentrations (Figure 31B). The full dose injection of *mylk3* MO caused a cardiac phenotype in 65% of the total embryos analyzed compared with the control group. The co-injection of subthreshold concentrations of *mylk3* MO with either *wnt11f2* or *fzd7a* MO resulted in up to 85% of the embryos with a cardiac phenotype in both cases. Interestingly,

the combination with *dvl2* MO did not significantly affect the percentage of embryos displaying a cardiac phenotype, only 25% showed the cardiac phenotype. However, when *mylk3* MO was injected in combination with *vangl2* MO or *pk1a* MO, it caused a high percentage of embryos with cardiac phenotype, 90%, and 80 %, respectively (Figure 31B).

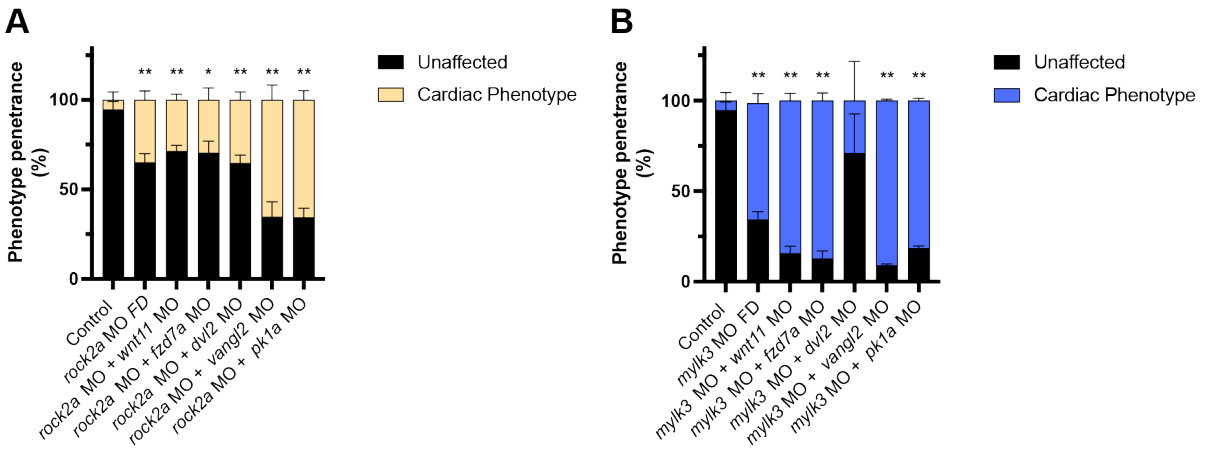

Figure 31. Phenotypic analysis of the genetic interaction. Quantification of the phenotype percentage of embryos injected. A) *rock2a* MO full dose (FD) or in subthreshold concentrations in combination with the PCP core components MOs. B) *mylk3* MO full dose (FD) or in subthreshold concentration combined with the PCP core components MOs. Ordinary one-way ANOVA, Dunnett's multiple comparison test with a single pooled variance. (N≥3; n≥300).

Altogether, the data of *rock2a* MO injections show the genetic interaction between the Rock2a and the core components of the PCP pathway in accordance to previous findings (Marlow et al., 2002; McGreevy et al., 2015) and also serves as a validation of this interaction in the cardiomyocytes. Surprisingly, the co-injection of *rock2a* MO with *vangl2* and *pk1a* MO showed a stronger penetrance in the cardiac phenotype suggesting that Vangl2-Pk1a branch has a stronger genetic interaction with Rock2a in cardiac cells, in contrast with previously reported data showing the main control of the Rock kinase is through the Dvl transducer (Marlow et al., 2002; Winter et al., 2001).

Moreover, here is the first time the genetic interaction between the cardiac myosin kinase Mylk3 and the PCP core components is shown. Interestingly, it is worth noting that the co-injection of *mylk3* MO and *dvl2* MO caused only a minor cardiac phenotype, raising the possibility to partially define the branch of PCP through which the *mylk3* activity is regulated. In other words, my data indicate the Mylk3 activity may be under the Vangl2-Pk1a branch regulation in the cardiac tissue.

4.9 Mylk3 is a novel effector protein under the regulation of the PCP signaling pathway

After establishing the genetic interaction of both kinases, Rock2a and Mylk3, with the PCP core components, the evidence suggests Mylk3 could be regulated by PCP, and it can have a potential role as an effector protein. To assess this, I generated a transgenic line expressing the human MYLK3 fused with a mCherry fluorescent protein under the control of a cardiac-specific promotor for cardiomyocytes, *myl7,* indicated as *Tg[myl7:hMYLK3-mCherry]*. This line was used to perform rescue experiments of the cardiac phenotype caused by downregulation of PCP core components (Figure 32).

First, the new transgenic line was evaluated to determine the possible negative effects of the kinase in the cardiac cells. The body and cardiac phenotype of control embryos (Figure 32A, top) were compared with the transgenic embryos (Figure 32B, top) for a phenotypic analysis. There was no phenotype found when compared the embryos. I proceeded to perform the rescue experiment of the cardiac phenotype caused by the PCP anomalies; embryos of *Tg[myl7:EGFP]* transgenic line were used as controls. Embryos injected with a MO targeting the *wnt11f2* ligand (Figure 32A, B, middle) or *vangl2 (*Figure 32A, B, bottom) were compared. The embryos injected with the *wnt11f2* MO showed a shorten body and cyclopia in the control (Figure 32A, middle) and in the hMYLK3-mCherry expressing embryos (Figure 32B, middle). The embryos injected with the *vangl2* MO also showed a shorten body in the control (Figure 32A, bottom) and in the hMYLK3-mCherry expressing embryos (Figure 32B, bottom). The characteristic body phenotype from the CE disruption was noticeable in both groups of embryos. This phenotype was expected taking in consideration that the overexpression of the hMYLK3 is just limited to the cardiomyocytes due to the cardiac specific promotor, *myl7*, driving its expression. However, while the control embryos exhibited cardiac edema, the presence of cardiac edema in the transgenic *Tg[myl7:hMYLK3-mCherry]* embryos was markedly reduced, suggesting that the cardiac phenotype could be rescued due to the overexpression of the transgene.

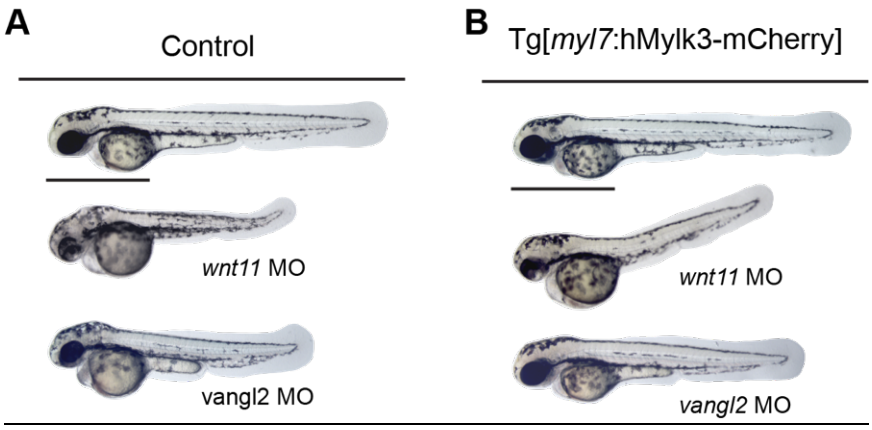

Figure 32. Overexpression of human Mylk3 rescues the cardiac phenotype. Representative images of the (A) control embryos (top) and (B) embryos overexpressing human MYLK3 fused with mCherry in the cardiomyocytes (Tg[*myl7*:hMYLK3-mCherry]) (top). Respective embryos injected with *wnt11f* morpholino or *vangl2* morpholino (A and B, middle and bottom panels, respectively). Scale bar: 500µm.

To further focus on the assessment of the cardiac phenotype, the looping defects were evaluated measuring the looping angle of the hearts at 54hpf (Figure 33), as previously described (see Figure 28B and methods section). Each of the conditions were comparing the embryos of control (Tg[*myl7*:EGFP]) and the hMYLK3-mCherry expressing transgenic line (Tg[*myl7*:hMYLK3-mCherry]). In uninjected embryos (Figure 34B), there was no difference indicating that the kinase overexpression did not cause any defect in the embryos. I hypothesized that if MYLK3 is indeed an effector in Wnt/Vangl2 branch of the PCP pathway, then its overexpression in the heart, should suppress the phenotype caused by the loss of either *wnt11f2* or *vangl2*. The rescue experiments were performed and compared with the control looped hearts (Figure 33A, B). The injection of the morpholino targeting the *wnt11f2* ligand caused a heart looping defect (Figure 33C, upper left panel), but when compared to the hMYLK3-mCherry expressing line injected with the *wnt11f2* MO, the looping was partially recued (Figure 33C, upper right panel). Similarly, the *vangl2* MO injection caused a cardiac looping defect in the control embryos (Figure 33C, lower left panel), but in the hMYLK3-mCherry expressing embryos the cardiac phenotype was also partially recued (Figure 33C, lower right panel). The looping angle values were plotted and compared (Figure 33D). The mean value for the cardiac looping angle in the control embryos was 29°, while in the *wnt11f2* MO-injected embryos it was wider, having a mean value of 57°, and for the *vangl2* MO-injected embryos, the angle was increased to 60°. However, when I quantified and compare the average cardiac looping angle in the hMYLK3-mCherry expressing embryos injected with either of the morpholino, the partial rescue was confirmed, the average looping angle of the hMYLK3-mCherry expressing embryos injected with *wnt11f2* MO was 43° and with *vangl2* MO it was 38°. These values were not statistically significant when compared with the average in the control group indicating the MYLK3 can suppress both *wnt11f2* and *vangl2* phenotypes.

Taking all together, the specific overexpression of the hMYLK3 in the cardiac cells is enough to rescue the cardiac phenotype caused by the disruption of PCP signaling due to the reduction of the expression levels in the *wnt11f2* or vangl2 genes.

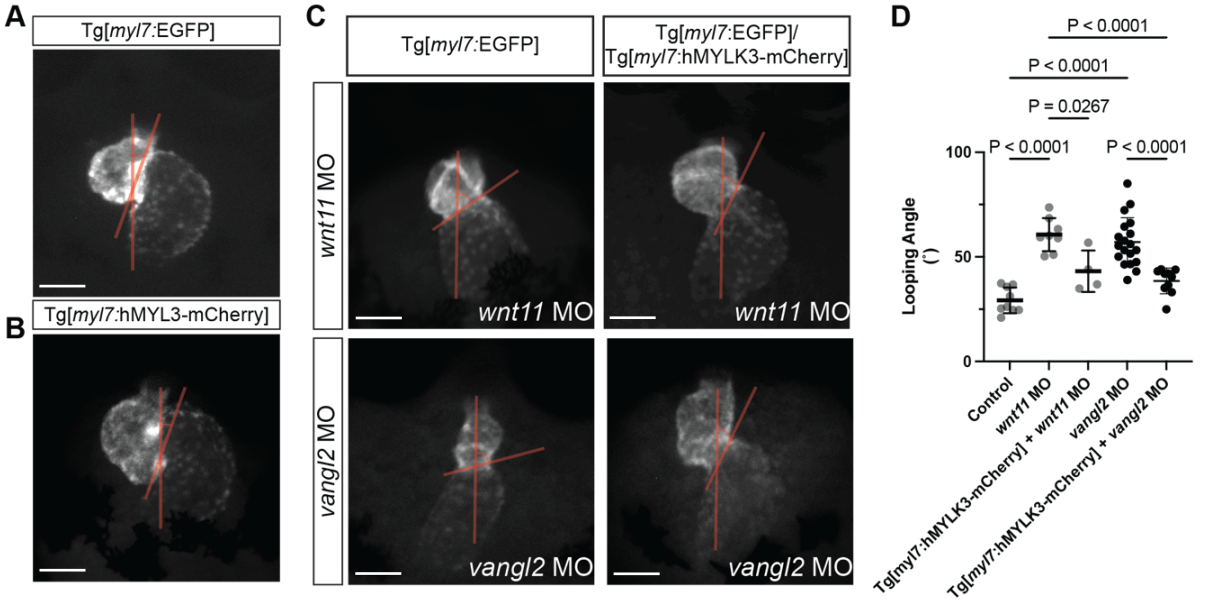

Figure 33. Evaluation of the cardiac phenotype in genetic rescue experiment. Scheme showing the approach for cardiac looping angle measurements using as a reference the midline of the body and the AVJ A). Representative image of a control heart (using the transgenic line Tg[myl7:EGFP]). B) Representative image of the uninjected transgenic line overexpressing human MYLK3. C) Representative images for comparison of the cardiac looping angles between the Tg[*myl7*:EGFP] transgenic line and Tg[*myl7*:hMYLK3-mCherry] injected either with *wnt11f2* MO or *vangl2* MO. Scale bar: 50µm D). Quantification of the looping angle in all the conditions. Ordinary one-way ANOVA, Dunnett's multiple comparison test with a single pooled variance. (N≥2; n≥10).

4.10 Vangl2 regulates Mylk3 localization/activity

After identifying PCP as a pathway modulating the Mylk3 activity via Vangl2 during the development of the heart, I proceeded to check the spatial expression of *vangl2* across the cardiac tissue (Figure 34A) and the protein localization (Figure 34B). The expression of *vangl2* was observed in the whole embryonic heart (Figure 34A, right panel, green in merge), including the myocardium and endocardium, together also with the transcripts of *mylk3* (Figure 34A, middle panel, red in merge). No preferential localization of the *vangl2* transcripts was observed in any specific region of the myocardium.

To assess the protein localization, Vangl2 immunostainings were performed to check its distribution across the heart. Vangl2 was found across the heart in the plasma membrane, as expected (Figure 34B, left panel, green in merge). Surprisingly, nuclear signal was also observed for the immunostainings; however, this observation was not further addressed.

Importantly, the plasma membrane distribution of Vangl2 protein appears homogeneous across the ventricle, i.e., no preferential localization of Vangl2 in the proximal vs distal ventricle was observed. In the midsagittal sections, Vangl2 localizes to the region of apical tight junctions (data not shown).

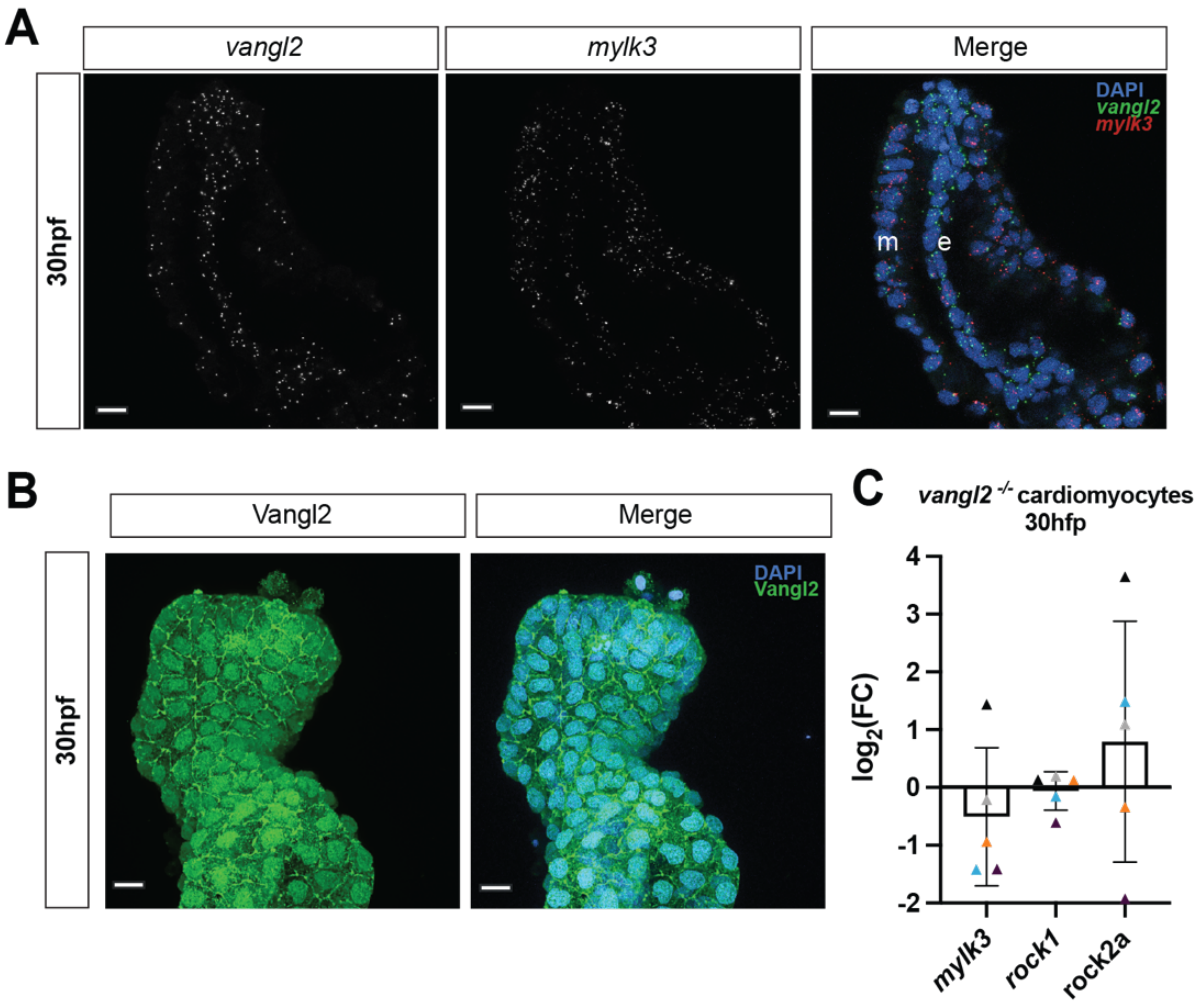

Figure 34. Distribution of Vangl2 across the cardiac tissue. A) Spatial localization of *vangl2* and *mylk3* transcripts in isolated hearts at 30hpf using RNAscope® fluorescent *in situ* hybridization. *vangl2* transcripts in grey in left panel and green in merge, *mylk3* transcripts in grey in the middle panel and red in merge, DAPI (blue) stains nuclei in merge. myocardium (m) and epicardium (e). B) Immunostaining for Vangl2 (green) in isolated hearts at 30hpf using a customized anti-Vangl2 antibody, DAPI (blue) stains nuclei in merge. Scale bar in A, B: 10µm. (N=5). C) qPCR analysis to determine the expression levels of three different kinases, *mylk3, rock1, rock2a* in *vangl2*$^{-/-}$ mutant in FACS-sorted zebrafish cardiomyocytes in comparison with WT zebrafish cardiomyocytes at 30hpf. The average values are shown with the SD, each color of the dots represents an independent experiment (N=5). Data plotted as log2 fold change (FC).

Since neither the *vangl2* transcripts nor Vangl2 protein were spatially restricted in its localization across the myocardium, I perform qPCR analysis to evaluate whether Vangl2 may regulate the *mylk3* expression levels (Figure 34C). Comparing the expression levels between

the isolated cardiomyocytes from WT embryos and *vangl2*$^{-/-}$ embryos showed no difference in mRNA expression for the kinases evaluated: *mylk3*, *rock1* and *rock2a*, indicating that Vangl2 does not exert any transcriptional control on the expression of *mylk3* in cardiac cells during heart development.

Then, I addressed the possibility of *mylk3* being regulated through Vangl2 at posttranscriptional level. Using the transgenic line, Tg[*myl7:* hMYLK3-mChery], I injected *vangl2* MO to evaluate the possible changes in the localization or levels of hMYLK3 (Figure 35). There were no changes in the distribution and localization of the hMYLK3 (Figure 35A). However, quantifying the levels of fluorescence, my results indicated that decreasing the expression of *vangl2* causes a decrease of the hMYLK3 present in the myocardium (Figure 35B).

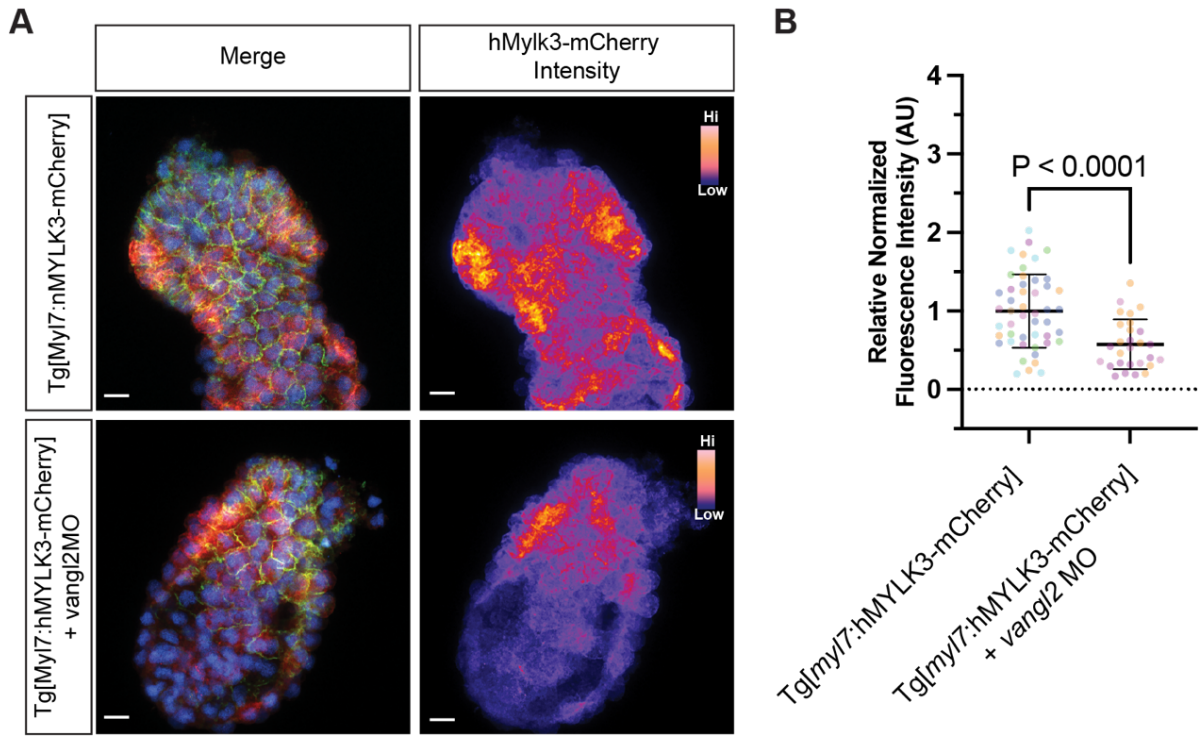

Figure 35. Vangl2 regulates the levels of Mylk3. A) Z-projections of immunostaining of all Z-stacks of the total fluorescence intensity corresponding to mCherry signal from the transgenic line Tg[*myl7*:hMYLK3-mCherry] uninjected (top) and injected with *vangl2* MO. B) Relative normalized fluorescence intensity corresponding to the mCherry signal for each of the conditions aforementioned. Unpaired t-test with Welch correction. (N≥3; n≥3) Scale bar: 10µm.

The data suggests the Vangl2 may regulate the Mylk3 in at the posttranslational level.

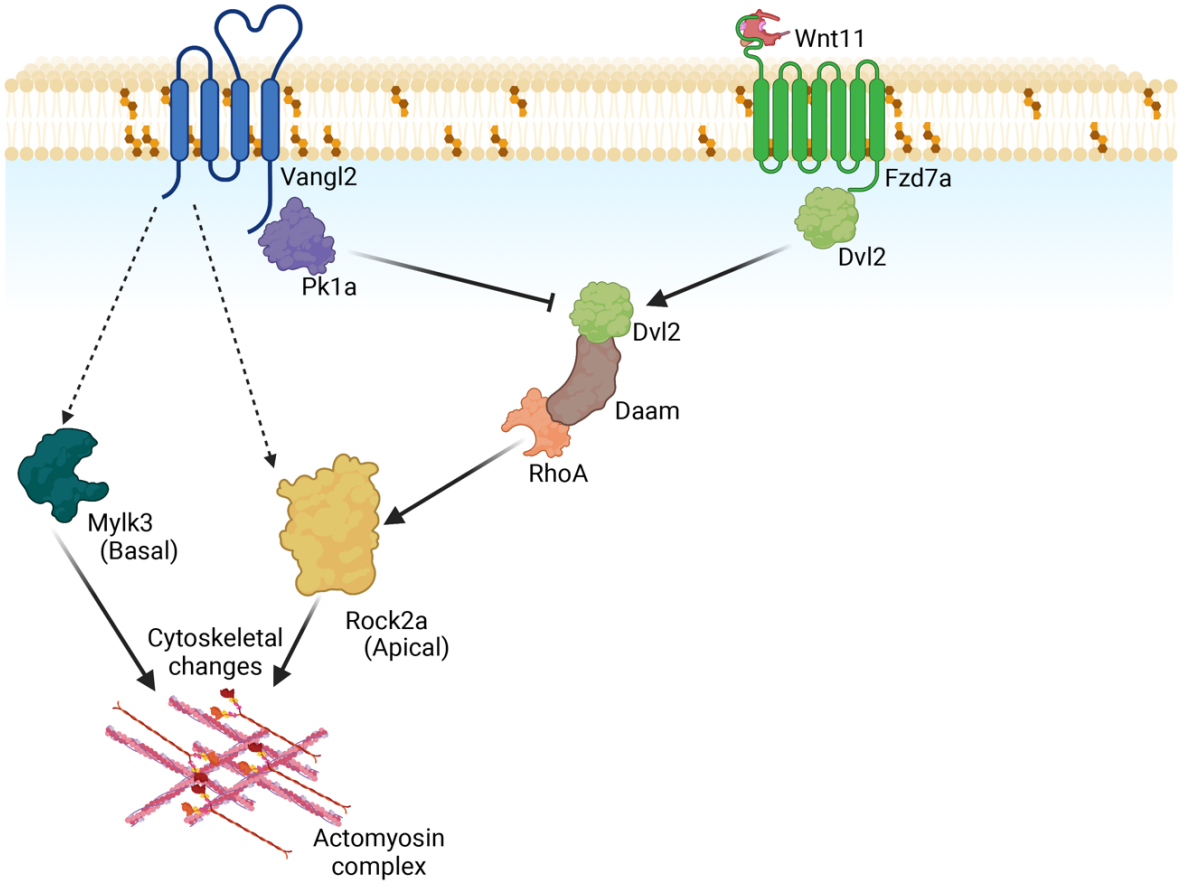

Figure 36. Proposed model of the Planar cell polarity pathway in cardiac cells. Simplified scheme of the PCP pathway including the two effector proteins described in this work: Rock2a and Mylk3. In zebrafish developing heart, the transmembrane receptor Fzd7a and the four transmembrane protein Vangl2 occupy mutually exclusive domains in the plasma membrane of the cells. Fzd7a acts as the receptor of the Wnt11 ligand, recruiting and activating the cytoplasmic protein Disheveled, which activates Daam to transduce the signal to the RhoA GTPase to activate Rock, causing phosphorylation of the non-muscle myosin II resulting in the contraction of cells. Vangl2 interacts with its cytosolic transducer Pk1a, which competes to bind Dvl2 to regulate/inhibit its downstream activity. Additionally, Vangl2 regulates the activity of the two kinases in opposite sides of the membrane: Rock2a apically and Mylk3 basally through a not yet resolved mechanism.

5. Discussion

It has been established that cardiac chamber remodeling is coordinated through tissue-scale polarization of actomyosin (Merks, 2018; Merks et al., 2018). The phosphorylated myosin accumulates apically in the outflow tract (OFT) region during heart tube remodeling; this organ scale polarization of tissue tension is required for heart tube looping. The molecular mechanisms governing the process of the heart looping and chamber expansion are not fully understood. The process itself, of how the heart is shaped, remains largely unknown. Here, I describe the cellular components involved during the looping process and chamber formation in zebrafish hearts. I found a supracellular actomyosin network required for this process forms right at the time when the heart looping process is initiated. The actomyosin-based tension is regulated mainly by two kinases, Mylk3 and Rock2a, to achieve the proper distribution of phosphorylated myosin across the ventricular myocardium. I describe the role of the pMyo distribution to generate and distribute the tension forces across the cardiac epithelium. This tension is achieved by the spatio-temporal control of the pMyo levels across the cardiac epithelium necessary to achieve a proper cardiac looping and chamber formation.
Moreover, I also identified that the Planar Cell Polarity pathway (non-canonical Wnt signaling) modulates the appropriate phosphorylation pattern in the cardiac epithelium by controlling the kinases activity in a spatio-temporal manner. My findings describe a mechano-molecular mechanism necessary for proper looping and chamber formation during cardiogenesis.

5.1 Early cardiac development: zebrafish as a reference

Danio rerio (zebrafish) has been a model organism since the 1960s (Dooley & Zon, 2000). It has grown in popularity as a model organism for studying vertebrate gene function due to many advantages it offers (Driever et al., 1996; Haffter et al., 1996): due to its external fertilization and development, it is nearly transparent during larvae stages, it develops rapidly (Jussila & Ciruna, 2017; Stainier, 2001), and it can be used for fast genetic screens and easy genetic manipulation by gene knockdown or gene overexpression (Candela & Hake, 2008; Dooley & Zon, 2000; Driever et al., 1996). Moreover, zebrafish have similar genetics to humans. Around 70% of genes are shared between both species, and 84% of genes known to be associated with human diseases have a zebrafish homolog (Howe et al., 2013).
Zebrafish has been widely used for cardiac development and disease research due to its ability to survive for several days with the impaired heart function (Arnaout et al., 2007; Bournele & Beis, 2016; Bowley et al., 2022; Giardoglou & Beis, 2019; Leong, Skinner, Shelling, & Love, 2010; Narumanchi et al., 2021; Stainier, 2001; Staudt & Stainier, 2012; Vornanen & Hassinen, 2016). This ability is possible because the oxygen supply to the cells

continues through passive diffusion at the embryonic stages. Other advantages include the zebrafish heart exhibiting similar features to the human heart in terms of physiology, including heart rate, which is closer to humans than mice (Cokkinos, 2015), contractile dynamics (Vornanen & Hassinen, 2016; F. Yu et al., 2012) and action potential (Arnaout et al., 2007; Leong et al., 2010).

For many years, the cellular and molecular events during morphogenesis have been the center of attention for cell biologists, while developmental biologists focused more on the tissue and whole organism formation (Davies, 2013a; el Azhar & Sonnen, 2021; Keller & Shook, 2011; New, 1978; Papusheva & Heisenberg, 2010b; Scott & Barresi, 2016; Shi et al., 2014; Wolpert et al., 2015; Zallen, 2007). Recently, more holistic approaches have been deployed making the study of morphogenesis a truly multidisciplinary field. And even more recently, the mechanobiology (Jansen et al., 2015), which combines different approaches to try to understand the mechanical cues involved and events necessary for morphogenesis, has entered the field. Using all these different approaches, the individual and collective cell behaviors have been studied to determine the processes underlying the organ formation (Mammoto & Ingber, 2010; Zallen & Blankenship, 2008).

For the heart is not the exception, since the genetic, molecular, and cellular levels have been described (Bakkers, 2011; Kemmler et al., 2021; Liu & Stainier, 2012; Lombardo et al., 2019; Patten, 1922; Vornanen & Hassinen, 2016), allowing us to have a better understanding of the events occurring during cardiogenesis. The morphogenetic control of heart looping has been studied in diverse context to understand the possible defects contributing to occurrence of pathological insults associated with congenital heart defects (Bakkers, 2011; Bowley et al., 2022; Kemmler et al., 2021; Lombardo et al., 2019; Olson, 2006; Phillips et al., 2007; Sinha et al., 2015; Wu et al., 2011).

Using different model organisms, it has been possible to elucidate genetic programs responsible for the differentiation of the cardiac progenitors of mesodermal origin to fully differentiated cardiomyocytes (Ahmad et al., 2004; DeRuiter et al., 1992; Devine et al., 2014; Felker et al., 2018; Harvey, 1996; Kelly et al., 2001; Kemmler et al., 2021; D. Li et al., 2016; Mosimann et al., 2015; Sinha et al., 2015; Warga & Kimmel, 1990). The transcription factors, genetic networks and protein interactions controlling or being involved have also been described during heart formation (Bussmann, Bakkers, & Schulte-Merker, 2007; J. N. Chen et al., 1997; Driever et al., 1996; Harvey, 1996; Kelly & Buckingham, 2002; Kemmler et al., 2021; Palencia-Desai et al., 2015; Ramsbottom et al., 2014; Stainier, 2001; Tessadori et al., 2021).

From the molecular perspective, just recently the attention has been focused on the cytoskeletal components, the actomyosin complex (X. Li, McLain, Samuel, Olson, & Radice, 2022; Merks et al., 2018; Risi et al., 2021). As a major component in the cardiac muscle cells, it has been shown to play an essential role for proper cardiac activity performance (Chan et

al., 2008; Ding et al., 2010; Hodatsu et al., 2019; Kamm & Stull, 2011; Massengill et al., 2016; Taniguchi et al., 2015; S. A. Warren et al., 2012). However, its role in contractility and tension generation at a cellular and tissue level, and its implication during heart formation just started to be elucidated to understand better the importance of the actomyosin complex during cardiac development (Merks et al., 2018; Priya et al., 2020).

Here, for the first time I described the pMyo patterning required during cardiac development using zebrafish as a model organism. I propose the results of my study as a starting point to understand the principles of the mechano-molecular control of cardiac morphogenesis. The importance of the actomyosin complex and its contractile properties are well known to be necessary for a myriad of cellular processes, however, its role has not been described yet in terms of the contribution for shaping of the heart as it has been shown in other body structures during development, particularly in those with no contractile capabilities (Andrew & Ewald, 2010; Navis & Nelson, 2016; Spurlin & Nelson, 2017). The pMyo patterning observed is regulated in a time-dependent manner. At 24hpf when the cardiac tissue has already formed the LHT, the distribution of the pMyo along the epithelium starts to be defined in a localized distribution. However, it is at 30hpf when the looping process occurs and a clear pattern of pMyo distribution along the myocardium is present with a characteristic switch from the apical pMyo towards a more basal pMyo localization from the distal through the proximal ventricle. Afterwards, when the looping has been completed, the patterning of the pMyo is lost, meaning that there is no such need of having a specific distribution of the contractility along the epithelium. Also, it is important to note that at this stage of the development, i.e. after the looping process is terminated, the heart muscle cells start to show sarcomere assembly and another remodeling process begins. Namely, the structure of the ventricular wall needs to be modified by adding more cell layers to the initial cardiac epithelium for the subsequent process of cardiac maturation (Jensen et al., 2016; Priya et al., 2020).

Conditions such as congenital heart defects, impair the life prognosis threatening the lifespan of the individual (Priya et al., 2020). Many signaling pathways have been identified and the regulation of different cellular processes involved have been elucidated. The heart is the first organ to be formed during development, arising from the linear heart tube as a primary structure, it undergoes a series of changes to acquire, in the case of zebrafish, the final S-shape. The changes occurring during the looping process depend on two factors, the asymmetry (left-right) and the growth of the tube itself (Desgrange et al., 2018; Le Garrec et al., 2017). Different signaling pathways have been described as having a role in the migration patterns of the cells forming the heart while shaping it as a recent example of the Bmp signaling (Chen et al., 1997; Lombardo et al., 2019; Palencia-Desai et al., 2015; Prall et al., 2007; Tran et al., 2010).

From the growth perspective, the first event to consider is the addition of new cardiomyocytes to the poles of the linear heart tube. This second wave of cellular proliferation and addition of new cardiac cells to the linear tube from the second heart field, facilitates the heart tube growth (Felker et al., 2018). In this context, Tbx5 is one of the latest regulators described controlling the rotation of cells over the LHT (Felker et al., 2018; Merks et al., 2018; Tessadori et al., 2021). All these previously described events and processes linked to cardiac morphogenesis focus mostly on genetic programs and cellular behaviors as migration, rearrangement of cell positions and cell addition. My contribution to the field is examining the mechano-molecular control of heart formation. My initial observations about the molecular dynamics of myosin phosphorylation across the time and localization served us to build a mathematical model to recapitulate the normal cardiac formation. Moreover, it also happened to be an accurate predictive model useful for probing hypothetical or real-life conditions as I discuss in the next section.

5.1.1 Models for cardiac looping

To date the modeling of heart looping has considered the cellular mechanism and the whole tissue dynamics for the tension distribution and force generation necessary for the bending of the LHT (Le Garrec et al., 2017; Shi et al., 2014; Tessadori et al., 2021). However, there is no such model considering solely mechanical forces generated by actomyosin activity as driving forces to generate the necessary tension across the cells and tissue to shape the heart. In this work, for the first time, I and my colleagues present a model based on my findings of spatio-temporal patterning of pMyo. In this model, the pMyo distribution and its levels over the cardiac epithelium in the linear heart tube is the only variable parameter. The model truly recapitulates the real-life morphology modeling the heart shape changes from the initial steps of LHT and ending in the fully formed two-chambered heart of zebrafish. The caveat of the model is that it assumes the S-looping of the heart, so it is not the model of the heart looping per se. Nevertheless, it demonstrates that the myosin is required to generate forces that are indispensable for shaping the cardiac chambers together with the atrioventricular canal formation.

Starting form experimental measurements, the model recapitulates the *in vivo* wild-type scenario, cardiac chamber expansion and ballooning and the constriction of the AVJ, generating an accurate model of the heart morphogenesis. Since the only variable considered for the model was the pMyo pattern and levels, the model was used to predict possible outcomes when the pMyo levels were reduced by half either in the apical or the basal side of the myocardium. Finally, the model was used to predict an extreme scenario where both, apical and basal, pMyo levels were abrogated to half of the values and evenly distributed. To

my surprise, the mathematical model indeed, resulted being a fairly accurate predictive tool. After the identification and characterization of Rock2a and Mylk3 as the two main kinases in the cardiomyocytes during heart formation, I could test the role of apical vs basal pMyo. My *in vivo* observations mirror the model predictions. Thus, the model recapitulates what I observed *in vivo*; first in the loss of the apical pMyo localization in the *rock2a*-deficient hearts; second in the loss of basal pMyo localization when the expression of *mylk3* was reduced; and finally, where there was a complete loss of pMyo in both sides of epithelium, apical and basal, when the expression of both kinases was decreased.

The model and the experimental observations support each other and are complementary evidence pointing out the importance of the distribution and levels of the phosphorylated myosin across the cardiac epithelium. Furthermore, the data highlights the role of pMyo as one of the main molecular players necessary for cardiac morphogenesis and the importance of its regulation in space and time.

It is interesting to consider now the possibility to combine previous models of cardiac looping and each of its variables as cell migration, rearrangements, rotation, and addition of cells with our mathematical model and the pMyo contribution, to generate the model of the cardiac looping, which will more closely model the exact conditions happening *in vivo*. The more complex and sophisticated modeling approaches would greatly contribute to a better understanding of the heart looping process from a global perspective as well as from the perspective of the molecular players, the cellular dynamics, and tissue organization. Modeling different aspects in the unified model would allow for testing various inputs in physiological contexts during heart development, and for identifying different aspects required for generation of organs in general.

5.2 Phosphorylation of myosin during cardiac development.

The non-muscle myosin II plays an essential role in cellular physiology being involved in diverse cellular processes. Phosphorylation is the main posttranslational modification that regulates its activity. There are many different amino acid residues, which are known to be subjected to phosphorylation. Among all of them, in this work I focused on the Ser18/Thr19 phosphorylation because those are the main phosphorylation sites controlling the myosin activity by increasing its affinity to bind actin (Ikebe et al., 1986; Scholey et al., 1980; Sellars et al., 1981; Umemoto et al., 1989).

It is known that the levels of pMyo are distributed across the cardiac tissue in a gradient fashion from high phosphorylation of the myosin regulatory light chain in the myocardium to lower levels in the endocardial cells (Davis et al., 2001). The importance of the cytoskeletal components in cardiac biology has been greatly demonstrated and discussed (Linask &

VanAuker, 2007). However, less attention has been focused on the actomyosin during cardiac development since most of the research has been performed on the contractility of actomyosin as sarcomere component and its role in cardiac performance and function (Bettex et al., 2014; Kamm & Stull, 2011; Massengill et al., 2016; Sheikh et al., 2015; Taniguchi et al., 2015; Tobita et al., 2017; S. A. Warren et al., 2012). Here, I described for the first time the spatio-temporal requirements of the myosin phosphorylation across the myocardium during cardiac development using zebrafish as a model organism. Previously, the importance of the pMyo at individual cellular level has been described (Lecuit et al., 2011; Lou, Diz-Muñoz, Weiner, Fletcher, & Theriot, 2015). In cells pMyo regulates the formation of diverse structures as filopodia, formation and turnover of focal adhesions, migration and polarization of cells (Heissler & Manstein, 2013; Kassianidou, Hughes, & Kumar, 2017; Kelley, Wirshing, Zaidel-Bar, & Cram, 2018; Kimura et al., 1996; Lecuit et al., 2011; Lou et al., 2015; Matsumura et al., 2001; Totsukawa et al., 2004; Vasquez et al., 2014; Vicente-Manzanares et al., 2009). In the collective cell behavior, the main contribution pMyo has been linked to, is the apical constriction or convergent extensions movements through cell intercalation induced by polarization of contractility in determined group of cells in specific locations (Andrew & Ewald, 2010; Derish et al., 2020; Ossipova, Chuykin, Chu, & Sokol, 2015; Williams et al., 2014).

At tissue level, the supracellular actin cables have been described to be an important molecular component to propagate mechanical forces across the cell layers (Keller & Shook, 2011; Mammoto & Ingber, 2010; Navis & Nelson, 2016; Poh et al., 2014) Particularly, the supracellular actin cables are important in the epithelial tissues where they are necessary for morphogenetic processes as tissue folding, branching and formation of tubes(Andrew & Ewald, 2010; Navis & Nelson, 2016; Trushko et al., 2020). In the heart, the importance of the tissue scale polarization of actomyosin has been shown for proper cardiac development (Merks et al., 2018). In our predictive model the pMyo was found to be fundamental for the proper cardiac chamber formation and ballooning and the constriction in the AVJ. Disturbances in the pMyo patterning and levels resulted in an impaired prediction of the chamber formation and AVJ constriction. Moreover, my *in vivo* results showed that the proper pMyo supracellular distribution is fundamental, since altering the expression levels of *rock2a* or *mylk3*, the main kinases responsible of the myosin phosphorylation in the cardiomyocytes, results in cardiac phenotypes with cardiac looping defects.

5.3 Protein kinases in heart development

Actin cables, distributed across the apical surfaces of cells, serve as rails for myosin to interact and generate contractile forces required in tissues for the subsequent morphogenetic processes they can be subjected to (Blankenship et al., 2006; Quinlan, Martin, & Graham,

2004). Moreover, the phosphorylation levels of the NMII are controlled and kept in equilibrium by different myosin kinases and phosphatases depending on the cell type and the tissue (Betapudi, 2014; Hong et al., 2011). In this work, I identified the two most abundant kinases in the developing cardiomyocytes of zebrafish, Rock2a and Mylk3. The expression levels differed with *mylk3* being the highest expressed; its expression levels are 3 times higher than *rock2a* in 48hpf cardiomyocytes. However, the spatial localization of the corresponding transcripts did not show any preferential localization. On the contrary, both are present across the whole cardiac tissue homogeneously. It is important to note that the kinases are expressed in the endocardial cells as well. This in accordance to the establishment of the myosin phosphorylation gradient across the three cardiac layers (Davis et al., 2001).

The Rock kinases are widely expressed in virtually every single cell type and their function as effector proteins phosphorylating a myriad of substrates including the myosin regulatory chain (Amano, Nakayama, & Kaibuchi, 2010; Hahmann & Schroeter, 2010; Loirand et al., 2006; Newell-Litwa et al., 2015). Myosin phosphorylation induces a conformational change to an open configuration, allowing it to interact with the actin filaments to generate contractility in diverse cellular processes (Conti & Adelstein, 2008; Heissler & Manstein, 2013; Hodge & Cope, 2000; Kamm & Stull, 2011; Sheikh et al., 2015; Somlyo et al., 2004; Stull, Kamm, & Vandenboom, 2011; Umemoto et al., 1989; Vicente-Manzanares et al., 2009).

In the developing organs including the heart the different Rock isoforms have been linked to multiple processes and mutations in these genes has been linked to congenital heart diseases (Hahmann & Schroeter, 2010; Loirand et al., 2006). Several morphogenetic processes have been linked to the activity of Rho-associated protein kinases, including formation of OFT (Phillips et al., 2005), adhesion and endothelial integrity during cardiac formation (Lisowska et al., 2018). Rock2a was described recently as necessary for the valve formation in zebrafish by promoting its constriction, thus controlling the tension force generation in a particular region of the cardiac tissue (Lisowska et al., 2018).

5.4 Tissue tension during heart tube remodeling

The mechanical forces required for tube bending are the main contributors to the shaping of the heart. For the buckling process to occur during organogenesis, the tension distribution along cells and tissues has been described as a main requirement to contribute to it (C. M. Nelson, 2016; Trushko et al., 2020; Van Essen, 2020). Here, I describe the tension generated by molecular forces through the phosphorylation of myosin and linked it to the tension along the linear heart tube promoting its bending and formation of cardiac chamber curvatures. This is a substantial contribution from a molecular level, complementing previous described phenomena at genetic and cellular level (Le Garrec et al., 2017; Lombardo et al., 2019; Merks

et al., 2018; Tessadori et al., 2021), since the disruption of Rock2a or Mylk3 kinases had a direct impact on the tension along the heart tube according to our measurement with the Flipper dye based on the fluorescence lifetime. No statistically significant reduction was detected when the average lifetimes were compared among the different experimental conditions and control group. However, the changes in variance between different experimental groups and control gave a clear indication that even though the tissue tension changes were not significant at the whole tissue level, the distribution of the tension across the individual cells changed when the expression of either *rock2a* or *mylk3* kinases was diminished. When the expression of both kinases was decreased at the same time, the resulting compensation of the lifetimes could be explained as lower variability of the tension forces across the cardiac tissue, i.e., not necessary resulting in the decrease of the average values but a more homogeneous tension distribution throughout the tissue.

The interlinking of the cortical cytoskeleton and the plasma membrane is important to establish and preserve the cellular form and function. Here, I showed that even without disrupting the membrane composition (i.e. lipid or transmembrane proteins) and just using pharmacological or genetic approaches to decrease the activity of two kinases, it was enough to disturb the distribution and levels of the pMyo in the cells and overall across the myocardium, thus having a direct impact on the tension distribution across the cardiac epithelium giving an indirect evidence that the cortical actomyosin was affected in specific regions of the cells supporting the evidence that the kinases act at different location within the cells and across the tissue.

The tissue tension along the heart tube seems to be tightly regulated since even if the overall mean values of the cell tension were not changed, the phenotypical assessment showed the impaired heart looping most likely because of the abnormal tension in the developing cardiac tissue.

5.5 PCP signaling pathway during cardiac development and looping

One of the main morphogenetic signaling pathways that has been shown to have a role in cardiac formation has been the PCP pathway (Desgrange et al., 2018; Foulquier et al., 2017; D. Li et al., 2016; D. Li & Wang, 2018; Merks et al., 2018; Phillips et al., 2005, 2007). My results are in line with previous reports showing that defects in different of the PCP core components of the pathway leads to heart malformations, in particular OFT defects (Table 2) (Desgrange et al., 2018; Gibbs et al., 2016; Henderson et al., 2001; Merks et al., 2018; Phillips et al., 2005; Ramsbottom et al., 2014; Sinha et al., 2015, 2012).

Here, I show the genetic interaction between the PCP components and two kinases in the context of heart formation. I corroborate the role of the already known effector protein, the Rho associated kinase (Marlow et al., 2002; Phillips et al., 2005; Unterseher et al., 2004). However,

for the cardiac cells, data showed that specifically Rock2a isoform is critical for the cardiac looping. These findings suggest a preferential role of the isoforms depending on the cell types or the tissue, with Rock2a being favored in the cardiomyocytes in contrast to Rock1 or Rock2b. Since the reduction of the *rock2a* expression was enough to cause a cardiac phenotype in the embryos. It could be interesting to explore the idea of overexpressing the other isoforms specifically in the cardiac cells to evaluate the possible rescue effect.

Another interesting finding was based on the genetic interaction experiments. Although it has been known and reported that Rock is an effector protein under the PCP control (Marlow et al., 2002; Phillips et al., 2005; Unterseher et al., 2004), here I showed that in cardiac cells Rock2a is the main isoform playing an active role during heart formation. Moreover, the genetic interaction experiment also showed that Rock2a is involved with all the PCP core components, which classically it has been attributed to the control of its activity due to the Disheveled protein via RhoA and the subsequent activation of Rock to phosphorylate myosin (Butler & Wallingford, 2017; Karner et al., 2006b; Sinha et al., 2012; Tada & Kai, 2009; Vivancos et al., 2009).

Increasingly, evidence has been shown that the regulation of Rock activity can also be regulated from the Vangl2 branch of the PCP pathway (Phillips et al., 2005; Vivancos et al., 2009), making it more complex to truly separate the pathway as two different branches due to the very likely possibility of a multi-step regulation and internal crosstalk of the different components involved in the same signaling cascade.

Here, a new genetic interaction was shown with the cardiac myosin light chain kinase and the PCP core components. Interestingly, the findings showed a strong genetic interaction with all the PCP core components but with the Dvl2 protein suggesting that the regulation of the Mylk3 activity could be through the Vangl2-Pk1a arm of the cascade. Mylk3 is the first tissue-specific effector of the PCP pathway and also independent of Dvl2. However further investigation needs to be done to test whether the same is true for the other two isoforms Dvl1 and Dvl3.

5.6 Mylk3 as a novel effector protein

In the present work, I established the link between the PCP pathway and the cardiac myosin kinase. I demonstrated that there is a strong genetic interaction between *mylk3* and the core component *vangl2*. I corroborated this data by reverting the cardiac phenotype in the *vangl2*-deficient hearts by cardiac-specific expression of Mylk3, indicating that Mylk3 is indeed downstream of Vangl2. In addition, the loss of *vangl2* did not affect the *mylk3* expression but reduced the transgenic expression of Mylk3, suggesting that Vangl2 might be regulating Mylk3 posttranslationally. Evidently, even though the absence of *vangl2* leads to the reduction in the Mylk3 levels, there is still enough Mylk3 protein available to rescue the cardiac phenotype in

vangl2 mutants. Indeed, I have observed that the homozygous Mylk3 transgene led to mild cardiac defects (data not shown) indicating that the levels of Mylk3 needs to be regulated.
Mylk3 has Ca^{2+}/CaM-independent and -dependent activity, and the phosphorylation sites to regulate its activity are not conserved with other Mylk kinases (Mylk1, Mylk2) (Chan et al., 2008; A. N. Chang et al., 2016; Seguchi et al., 2007). It would be interesting to test whether the activity of Mylk3 can be modulated with Wnt stimulation in a dose-dependent manner providing another evidence that Mylk3 is under the regulation of the PCP pathway.
Of course, the possibility of this kinase to be regulated by different proteins and/or signals cannot be discarded. The immediate candidate which could be tested is the non-canonical Wnt/Ca^{2+} signaling pathway. This also sounds feasible since Mylk3 belongs to the myosin light chain kinases, and it can be regulated through Calcium dependent mechanism that opens a door to the crosstalk of the non-canonical Wnt branches having as a result the overall control of tension generation required for the proper tissue morphogenesis to shape the heart.
The identification of a new effector protein in the PCP is an exciting finding since there is little known about the tissue specific regulation of the non-canonical Wnt signaling. Since Mylk3 is a cardiac specific kinase which is not expressed in any other tissues, my findings bring the question of whether other myosin regulatory light chain kinases can be regulated by PCP.

5.7 Vangl2 controls the pMyo patterning during cardiac development

It has been previously described that secreted Wnt ligands establish gradients and are important for the regulation of the signaling process (Beckett et al., 2013; B. Gao et al., 2011; Mehta et al., 2021; Stanganello et al., 2015). In mouse it was shown that the expression of Wn5a is spatially restricted to the pharyngeal mesoderm, suggesting a pool of cells as a source of Wnt5a (Schleiffarth et al., 2007) and its receptor Fz2 expressed specifically in cells at the OFT (Schleiffarth et al., 2007). It could be possible that a similar situation occurs for the Wnt11 secretion, spreading through the cardiac tube and establishing a gradient through the cardiac epithelium with higher concentrations in the distal ventricle close to the OFT and lower concentrations in the proximal ventricle near the AVJ, which is in agreement with the fact that wnt5a and wnt11 are required for the migration of cells in the arterial pole of the LHT, i.e. OFT region (Cohen et al., 2012).
It has been described that Wnt ligands stabilize proteins by modulating their posttranslational modifications as phosphorylation, ubiquitination and sumoylation (Kikuchi & Kishida, 2006). Wnt5a induces the formation of cross-linked actin (CLA) networks where Rock can be activated to generate contraction via pMyo and the CLA (Yuan et al., 2013)
I didn't observe any preferential expression or localization neither at transcriptional level nor at protein level of *vangl2*. However, previously it has been shown that Wnt ligands can act

through the establishment of gradients, and it has been also described that the second heart field in the arterial pole in the OFT region is a source of Wnt ligands (Schleiffarth et al., 2007). Hence, it could be plausible to hypothesize that the activity of Vangl2 as a regulator switch of the PCP pathway is dependent of the concentration of Wnt ligand. This could be also linked to the evidence that Vangl2 can interact with Wnt ligands causing its phosphorylation similarly as Frizzled receptors are activated by Wnt ligands (B. Gao et al., 2011).

A recent work has described that Vangl2 has an adjacent Pk recognition motif next to the Dvl one and the affinity is dependent on a specific tyrosine phosphorylation (Humphries, Hazelett, Molina-Pelayo, Devenport, & Mlodzik, 2022); phosphorylated state of Vangl at this specific residue results in higher affinity to Pk, while the non-phosphorylated state of Vangl favors the binding to Dvl. In this line of evidence, it is possible to think that Vangl2 acts as a regulator of the PCP signaling between the Pk or Dvl branch of the PCP cascade.

Taking into account also the previous finding of the bimodal regulation of Dvl (Seo, Habas, Chang, & Wang, 2017), it could be possible to think that the spatially restricted distribution of Dvl depends on the phosphorylation status of Vangl. In a non-phosphorylated Vangl state, Dvl is located freely in the cytosol, able to reach the Frizzled receptor on the opposite regions of the PM and interact with it, initiating the downstream signaling cascade including the Daam, RhoA and the Rock activation.

I observed that the Vangl2 is located mainly apicobasal in the cardiomyocytes. Then, it is plausible to assume the apical distribution of the frizzled receptor based on previous knowledge that both proteins localize in mutually exclusive regions of the plasma membrane (Seo et al., 2017). It has been also shown that the Rock and Mylk kinases can act preferentially in different regions of the cell (Matsui & Deguchi, 2019; Taneja, Baillargeon, & Burnette, 2021; Totsukawa et al., 2000), opening the possibility that the control of the activity of both kinases are regulated spatially by their localization but also by the downstream signals after the activation pf the PCP pathway. It is important to note that the loss of polarity can be caused due to a dysregulated expression of any of both kinases, producing a imbalanced distribution of the polarity components hence causing a disruption of the downstream signaling dependent on the proper core components distribution (Y. Yang & Mlodzik, 2015).

Also it has been described that Vangl2 can induce the phosphorylation of some kinases (Boëx et al., 2022; H. Chen, Xiao, Lui, Lee, & Cheng, 2018), which could be the case of Mylk3. Further exploration in this regard needs to be done, of either a direct or an indirect regulation of its activity by Vangl2 resulting in modulating of the actomyosin complex accordingly. All these possible scenarios need to be further addressed. Therefore, it is of critical ipmortnace to elucidate the interactive partners of the PCP core component as a starting point to be able to dissect and understand better the PCP pathway and its role in the development, not only in the heart but also in the morphogenesis and tissue formation. For that it is necessary to

address the available techniques to decipher the interactome, which I discuss in the next section.

5.8 Effector proteins of PCP pathway and techniques to study the protein components

In this work I focused on understanding and characterizing the mechano-molecular control of the heart looping, emphasizing the importance of the morphogenetic PCP signaling pathway. However, it is plausible to consider the crosstalk of other signaling pathways and the apicobasal polarity of the cardiac epithelium, which has been demonstrated to interact directly with the planar polarity components (Chuykin, Ossipova, & Sokol, 2018; Landin Malt et al., 2019). In particular, the adherent junctions where components of the PCP and the apicobasal polarity coexist and interact increase the complexity of the cell-cell interactions in the epithelia (Sebbagh & Borg, 2014).

Several techniques have been developed to study protein-protein interactions to define the molecular interactions occurring within the cell (Pires & Boxem, 2018a). The study of these interactions has been useful to better understand and dissect the molecular components involved in signaling pathways. From the classic co-immunoprecipitation experiments where the components are pulled down together with the bait to afterwards being identified using a Western blotting to newly developed techniques as proximity ligation assays and high throughput techniques as proteomics with specific aims will be discussed below. It would be insightful to dissect and define the interactors with the Mylk3 kinase under the regulation of PCP and the possible regulators at a protein level and having a better idea of the active role. Initially, the protein-protein interactions were studied using methods as affinity proximity ligation assay or affinity purification-mass spectrometry. However, the limitation of these approaches were the non-high-throughput capabilities. Since it was necessary to have a candidate as a potential interactor or a binding motif for the affinity purification. Proximity ligation assay (PLA) is a technique based on the dual proximal binding, usually antibodies with covalently oligonucleotides attached to them (Sebbagh & Borg, 2014). If the target proteins are in proximity the oligonucleotides serve as a template for a rolling circle amplification use for the detection with fluorescent-labeled complementary probes which later can be visualized directly in the microscope. Affinity purification-mass spectrometry relays on the binding activity of the protein over an activity tag used for its purification in columns hence coupled to mass spectrometry to identify the binding protein (Sebbagh & Borg, 2014). Another technique is the Foster resonance energy transfer (B. Gao et al., 2011; Matsumoto & Hammes, 1975; Pollok, 1999), in which also the principle is based in proximity and relays in fluorescent tags fused with the two interactors to interrogate its interaction due to the transference of energy between

the two fluorophores (Bajar, Wang, Zhang, Lin, & Chu, 2016; Forster, 1946).Additionally to the aforementioned approaches and with the advances in the field of proteomics, new approaches have been developed (C.-S. Chen & Zhu, 2006; Krogan et al., 2006; Lu, Beatty, & Pinthus, 2008). The main advantage of such techniques is the high-throughput properties. The proximity labeling (Branon et al., 2018; Roux, Kim, Raida, & Burke, 2012) and *in vivo* biorthogonal chemistry (Baalmann et al., 2020) are two examples of such approaches of technologies to study interactomes in a high throughput manner. The promiscuous biotin ligase acts in a similar way based on the proximity of proteins but the difference is not directed specifically to assess the interaction of pre-selected protein. Moreover, the principle relies on the non-specificity of the biotin ligase to the proteins in the vicinity. Recently, a proteome-wide interactome map of the polarity proteins was reconstructed (Pires & Boxem, 2018b) based on evidence obtained from the use of different approaches to study protein-protein interaction.

6. Conclusions

Here in the present work, I described the generation of polarized supracellular actomyosin complex (myosin phosphorylation levels and localization) across the ventricular myocardium, which contributes to the proper looping of the heart. The apicobasal localization and distribution of the pMyo through the cardiac epithelium is controlled in a spatiotemporal manner. This pMyo patterning is indispensable for the proper cardiac looping and chamber formation during development. Rock2a is the kinase acting in the apical side of the cardiomyocytes in the distal ventricle close to the OFT. Mylk3 is the kinase responsible of the basal myosin phosphorylation in the proximal ventricle near the AVJ. The two kinases are necessary for the correct cardiac development. There is a Tug-of-War relationship between Mylk3 and Rock2a activity which is necessary to achieve the proper final shape of the heart. The PCP pathway regulates the activity of the kinases to establish the pMyo pattern during cardiac looping. Mylk3 is a novel cardiac-specific effector protein under the regulation of PCP, which acts downstream of the Vangl2 branch of the pathway.

7. Outlook

Since I defined here Mylk3 as a novel effector protein under the Planar Cell Polarity (PCP) signaling pathway, which is indispensable for proper cardiac development, I discuss the possible further steps of investigation following the findings of the present work.

To identify the direct protein-protein interactions of the PCP core components using a proteomics approach; this could be based on a proximity ligation and tissue specific using zebrafish to define and map the interactome of the PCP core components and its effector in this case Mylk3.

To evaluate the role of the other Rock isoforms during cardiac development. It could be interesting to explore the idea of overexpressing the other *rock* isoforms specifically in the cardiac cells to evaluate the possible rescue effects by the means of genetic compensation.

To characterize the phospho-proteome to assess the potential regulatory mechanism and activity of the kinases based on the phosphorylated state at specific time points during cardiac development.

To investigate the role of Vangl2 and define the molecular mechanism that controls the proper pMyo distribution.

To study the Wnt control and its implications establishing gradients in *in vitro* cardiac 2D or 3D organoid models to identify the phospho-proteome and the interactome to define partners after Wnt activation.

To test the role of the PCP core components *in vitro* and/or *in vivo* using zebrafish heart as a system controlling their overexpression in the myocardium.

To elucidate the contribution of the second heart field to the pMyo patterning; if SHF induces the apical phosphorylation in the distal region of the ventricle or if the cells added possess the apical pMyo by default needs to be further addressed.

8. References

Adler, P. N., Vinson, C., Park, W. J., Conover, S., & Klein, L. (1990). *Molecular Structure*.

Agarwal, P., & Zaidel-Bar, R. (2019). Principles of Actomyosin Regulation In Vivo. *Trends in Cell Biology*, *29*(2), 150–163. https://doi.org/10.1016/j.tcb.2018.09.006

Ahmad, N., Long, S., & Rebagliati, M. (2004). A Southpaw joins the roster: The role of the zebrafish nodal-related gene Southpaw in cardiac LR asymmetry. *Trends in Cardiovascular Medicine*, *14*(2), 43–49. https://doi.org/10.1016/j.tcm.2003.11.001

Ajima, R., Bisson, J. A., Helt, J. C., Nakaya, M. A., Habas, R., Tessarollo, L., … Cohen, E. D. (2015). DAAM1 and DAAM2 are co-required for myocardial maturation and sarcomere assembly. *Developmental Biology*, *408*(1), 126–139. https://doi.org/10.1016/j.ydbio.2015.10.003

Amano, M., Nakayama, M., & Kaibuchi, K. (2010). Rho-kinase/ROCK: A key regulator of the cytoskeleton and cell polarity. *Cytoskeleton*, *67*(9), 545–554. https://doi.org/10.1002/cm.20472

Andrés-Delgado, L., & Mercader, N. (2016). Interplay between cardiac function and heart development. *Biochimica et Biophysica Acta - Molecular Cell Research*, *1863*(7), 1707–1716. https://doi.org/10.1016/j.bbamcr.2016.03.004

Andrew, D. J., & Ewald, A. J. (2010). Morphogenesis of epithelial tubes: Insights into tube formation, elongation, and elaboration. *Developmental Biology*, *341*(1), 34–55. https://doi.org/10.1016/j.ydbio.2009.09.024

Angers, S., & Moon, R. T. (2009). Proximal events in Wnt signal transduction. *Nature Reviews Molecular Cell Biology*, *10*(7), 468–477. https://doi.org/10.1038/nrm2717

Aoki, H., Sadoshima, J., & Izumo, S. (2000). Myosin light chain kinase mediates sarcomere organization during cardiac hypertrophy in vitro. *Nature Medicine*, *6*(2), 183–188. https://doi.org/10.1038/72287

Arnaout, R., Ferrer, T., Huisken, J., Spitzer, K., Stainier, D. Y. R., Tristani-Firouzi, M., & Chi, N. C. (2007). Zebrafish model for human long QT syndrome. *Proceedings of the National Academy of Sciences of the United States of America*, *104*(27), 11316–11321. https://doi.org/10.1073/pnas.0702724104

Assémat, E., Bazellières, E., Pallesi-Pocachard, E., Le Bivic, A., & Massey-Harroche, D. (2008). Polarity complex proteins. *Biochimica et Biophysica Acta - Biomembranes*, *1778*(3), 614–630. https://doi.org/10.1016/j.bbamem.2007.08.029

Aw, W. Y., Heck, B. W., Joyce, B., & Devenport, D. (2016). Transient Tissue-Scale Deformation Coordinates Alignment of Planar Cell Polarity Junctions in the Mammalian Skin. *Current Biology*, *26*(16), 2090–2100. https://doi.org/10.1016/j.cub.2016.06.030

Baalmann, M., Neises, L., Bitsch, S., Schneider, H., Deweid, L., Werther, P., … Wombacher, R. (2020). A Bioorthogonal Click Chemistry Toolbox for Targeted Synthesis of Branched and Well-Defined Protein–Protein Conjugates. *Angewandte Chemie International Edition*, *59*(31), 12885–12893. https://doi.org/10.1002/anie.201915079

Baeg, G. H., Lin, X., Khare, N., Baumgartner, S., & Perrimon, N. (2001). Heparan sulfate proteoglycans are critical for the organization of the extracellular distribution of Wingless. *Development*, *128*(1), 87–94. https://doi.org/10.1242/dev.128.1.87

Bailly, E., Walton, A., & Borg, J. P. (2018). The planar cell polarity Vangl2 protein: From genetics to cellular and molecular functions. *Seminars in Cell and Developmental Biology*, *81*, 62–70. https://doi.org/10.1016/j.semcdb.2017.10.030

Bajar, B., Wang, E., Zhang, S., Lin, M., & Chu, J. (2016). A Guide to Fluorescent Protein FRET Pairs. *Sensors*, *16*(9), 1488. https://doi.org/10.3390/s16091488

Bakkers, J. (2011). Zebrafish as a model to study cardiac development and human cardiac disease. *Cardiovascular Research*, *91*(2), 279–288. https://doi.org/10.1093/cvr/cvr098

Barber, J. C. K. (1992). Mutations of chromosome 5q21 genes in FAP and colorectal cancer patients [5]. *Journal of Medical Genetics*, *29*(1), 70.

Bastock, R., Strutt, H., & Strutt, D. (2003). Strabismus is asymmetrically localised and binds to Prickle and Dishevelled during Drosophila planar polarity patterning. *Development*, *130*(13), 3007–3014. https://doi.org/10.1242/dev.00526

Bateson, W., Mendel, G., & Leighton, A. G. (1909). *Mendel's principles of heredity, by W. Bateson*. https://doi.org/10.5962/bhl.title.1057

Beach, J. R., Shao, L., Remmert, K., Li, D., Betzig, E., & Hammer, J. A. (2014). Nonmuscle myosin II isoforms coassemble in living cells. *Current Biology*, *24*(10), 1160–1166.

https://doi.org/10.1016/j.cub.2014.03.071

Beckett, K., Monier, S., Palmer, L., Alexandre, C., Green, H., Bonneil, E., … Vincent, J. P. (2013). Drosophila S2 cells secrete wingless on exosome-like vesicles but the wingless gradient forms independently of exosomes. *Traffic*, *14*(1), 82–96. https://doi.org/10.1111/tra.12016

Betapudi, V. (2014). Life without double-headed non-muscle myosin II motor proteins. *Frontiers in Chemistry*, *2*. https://doi.org/10.3389/fchem.2014.00045

Bettex, D. A., Prêtre, R., & Chassot, P. G. (2014). Is our heart a well-designed pump? the heart along animal evolution. *European Heart Journal*, *35*(34), 2322–2332. https://doi.org/10.1093/eurheartj/ehu222

Bilder, D., Li, M., & Perrimon, N. (2000). Cooperative regulation of cell polarity and growth by Drosophila tumor suppressors. *Science*, *289*(5476), 113–116. https://doi.org/10.1126/science.289.5476.113

Bilder, D., & Perrimon, N. (2000). Localization of apical epithelial determinants by the basolateral PDZ protein Scribble. *Nature*, *403*(6770), 676–680. https://doi.org/10.1038/35001108

Blankenship, J. T., Backovic, S. T., Sanny, J. S. S. P., Weitz, O., & Zallen, J. A. (2006). Multicellular Rosette Formation Links Planar Cell Polarity to Tissue Morphogenesis. *Developmental Cell*, *11*(4), 459–470. https://doi.org/10.1016/j.devcel.2006.09.007

Boëx, M., Cottin, S., Halliez, M., Bauché, S., Buon, C., Sans, N., … Strochlic, L. (2022). The cell polarity protein Vangl2 in the muscle shapes the neuromuscular synapse by binding to and regulating the tyrosine kinase MuSK. *Science Signaling*, *15*(734). https://doi.org/10.1126/scisignal.abg4982

Bournele, D., & Beis, D. (2016). Zebrafish models of cardiovascular disease. *Heart Failure Reviews*, *21*(6), 803–813. https://doi.org/10.1007/s10741-016-9579-y

Bovellan, M., Romeo, Y., Biro, M., Boden, A., Chugh, P., Yonis, A., … Charras, G. (2014). Cellular control of cortical actin nucleation. *Current Biology*, *24*(14), 1628–1635. https://doi.org/10.1016/j.cub.2014.05.069

Bowley, G., Kugler, E., Wilkinson, R., Lawrie, A., van Eeden, F., Chico, T. J. A., … Serbanovic-

Canic, J. (2022). Zebrafish as a tractable model of human cardiovascular disease. *British Journal of Pharmacology*, *179*(5), 900–917. https://doi.org/10.1111/bph.15473

Branon, T. C., Bosch, J. A., Sanchez, A. D., Udeshi, N. D., Svinkina, T., Carr, S. A., … Ting, A. Y. (2018). Efficient proximity labeling in living cells and organisms with TurboID. *Nature Biotechnology*, *36*(9), 880–887. https://doi.org/10.1038/nbt.4201

Brennan, J. A., Chen, Q., Gams, A., Dyavanapalli, J., Mendelowitz, D., Peng, W., & Efimov, I. R. (2020). Evidence of Superior and Inferior Sinoatrial Nodes in the Mammalian Heart. *JACC: Clinical Electrophysiology*, *6*(14), 1827–1840. https://doi.org/10.1016/j.jacep.2020.09.012

Brinkman, E. K., Chen, T., Amendola, M., & Van Steensel, B. (2014). Easy quantitative assessment of genome editing by sequence trace decomposition. *Nucleic Acids Research*, *42*(22). https://doi.org/10.1093/nar/gku936

Bryant, D. M., & Mostov, K. E. (2008). From cells to organs: Building polarized tissue. *Nature Reviews Molecular Cell Biology*, *9*(11), 887–901. https://doi.org/10.1038/nrm2523

Buckberg, G. D. (2002). Basic science review: The helix and the heart. *Journal of Thoracic and Cardiovascular Surgery*, *124*(5), 863–883. https://doi.org/10.1067/mtc.2002.122439

Bulgakova, N. A., & Knust, E. (2009). The Crumbs complex: From epithelial-cell polarity to retinal degeneration. *Journal of Cell Science*, *122*(15), 2587–2596. https://doi.org/10.1242/jcs.023648

Burger, A., Lindsay, H., Felker, A., Hess, C., Anders, C., Chiavacci, E., … Mosimann, C. (2016). Maximizing mutagenesis with solubilized CRISPR-Cas9 ribonucleoprotein complexes. *Development (Cambridge)*, *143*(11), 2025–2037. https://doi.org/10.1242/dev.134809

Burkhard, S., van Eif, V., Garric, L., Christoffels, V. M., & Bakkers, J. (2017). On the evolution of the cardiac pacemaker. *Journal of Cardiovascular Development and Disease*, *4*(2), 11–13. https://doi.org/10.3390/jcdd4020004

Bussmann, J., Bakkers, J., & Schulte-Merker, S. (2007). Early endocardial morphogenesis requires Scl/Tal1. *PLoS Genetics*, *3*(8), 1425–1437. https://doi.org/10.1371/journal.pgen.0030140

Butler, M. T., & Wallingford, J. B. (2017). Planar cell polarity in development and disease. *Nature Reviews Molecular Cell Biology*, *18*(6), 375–388. https://doi.org/10.1038/nrm.2017.11

Candela, H., & Hake, S. (2008). The art and design of genetic screens: Maize. *Nature Reviews Genetics*, *9*(3), 192–203. https://doi.org/10.1038/nrg2291

Carmona-Fontaine, C., Matthews, H. K., Kuriyama, S., Moreno, M., Dunn, G. A., Parsons, M., … Mayor, R. (2008). Contact inhibition of locomotion in vivo controls neural crest directional migration. *Nature*, *456*(7224), 957–961. https://doi.org/10.1038/nature07441

Cartagena-Rivera, A. X., Logue, J. S., Waterman, C. M., & Chadwick, R. S. (2016). Actomyosin Cortical Mechanical Properties in Nonadherent Cells Determined by Atomic Force Microscopy. *Biophysical Journal*, *110*(11), 2528–2539. https://doi.org/10.1016/j.bpj.2016.04.034

Chan, J. Y., Takeda, M., Briggs, L. E., Graham, M. L., Lu, J. T., Horikoshi, N., … Kasahara, H. (2008). Identification of cardiac-specific myosin light chain kinase. *Circulation Research*, *102*(5), 571–580. https://doi.org/10.1161/CIRCRESAHA.107.161687

Chang, A. N., Mahajan, P., Knapp, S., Barton, H., Sweeney, H. L., Kamm, K. E., & Stull, J. T. (2016). Cardiac myosin light chain is phosphorylated by Ca2+/calmodulin-dependent and -independent kinase activities. *Proceedings of the National Academy of Sciences of the United States of America*, *113*(27), E3824–E3833. https://doi.org/10.1073/pnas.1600633113

Chang, C. W., & Kumar, S. (2015). Differential Contributions of Nonmuscle Myosin II Isoforms and Functional Domains to Stress Fiber Mechanics. *Scientific Reports*, *5*(March), 1–13. https://doi.org/10.1038/srep13736

Chen, C.-S., & Zhu, H. (2006). Protein Microarrays. *BioTechniques*, *40*(4), 423–429. https://doi.org/10.2144/06404TE01

Chen, H., Xiao, X., Lui, W. Y., Lee, W. M., & Cheng, C. Y. (2018). Vangl2 regulates spermatid planar cell polarity through microtubule (MT)-based cytoskeleton in the rat testis article. *Cell Death and Disease*, *9*(3). https://doi.org/10.1038/s41419-018-0339-x

Chen, J. N., Van Eeden, F. J. M., Warren, K. S., Chin, A., Nüsslein-Volhard, C., Haffter, P., & Fishman, M. C. (1997). Left-right pattern of cardiac BMP4 may drive asymmetry of the

heart in zebrafish. *Development*, *124*(21), 4373–4382. https://doi.org/10.1242/dev.124.21.4373

Chuykin, I., Ossipova, O., & Sokol, S. Y. (2018). Par3 interacts with Prickle3 to generate apical PCP complexes in the vertebrate neural plate. *ELife*, *7*. https://doi.org/10.7554/eLife.37881

Cohen, E. D., Miller, M. F., Wang, Z., Moon, R. T., & Morrisey, E. E. (2012). Wnt5a and wnt11 are essential for second heart field progenitor development. *Development*, *139*(11), 1931–1940. https://doi.org/10.1242/dev.069377

Cokkinos, D. V. (2015). Introduction to translational cardiovascular research. *Introduction to Translational Cardiovascular Research*, 1–610. https://doi.org/10.1007/978-3-319-08798-6

Colom, A., Derivery, E., Soleimanpour, S., Tomba, C., Molin, M. D., Sakai, N., … Roux, A. (2018). A fluorescent membrane tension probe. *Nature Chemistry*, *10*(11), 1118–1125. https://doi.org/10.1038/s41557-018-0127-3

Compass, C., Vladar, E. K., Antic, D., & Axelrod, J. D. (2016). *Planar Cell Polarity Signaling : The Developing*. 1–20.

Conant, D., Hsiau, T., Rossi, N., Oki, J., Maures, T., Waite, K., … Stoner, R. (2022). Inference of CRISPR Edits from Sanger Trace Data. *CRISPR Journal*, *5*(1), 123–130. https://doi.org/10.1089/crispr.2021.0113

Conti, M. A., & Adelstein, R. S. (2008). Nonmuscle myosin II moves in new directions. *Journal of Cell Science*, *121*(1), 11–18. https://doi.org/10.1242/jcs.007112

Cooley, J., Whitaker, S., Sweeney, S., Fraser, S., & Davidson, B. (2011). Cytoskeletal polarity mediates localized induction of the heart progenitor lineage. *Nature Cell Biology*, *13*(8), 952–957. https://doi.org/10.1038/ncb2291

Dann, C. E., Hsieh, J., Rattner, A., Sharma, D., Nathans, J., & Leahy, D. J. (2001). Insights into Wnt binding and signalling from the structures of two Frizzled cysteine-rich domains. *Nature*, *412*(6842), 86–90. https://doi.org/10.1038/35083601

Davies, J. A. (2013a). Key Principles of Morphogenesis. *Mechanisms of Morphogenesis*, 7–16. https://doi.org/10.1016/b978-0-12-391062-2.00002-4

Davies, J. A. (2013b). *Mechanisms of Morphogenesis*. https://doi.org/10.1016/C2010-0-66323-1

Davis, J. S., Hassanzadeh, S., Winitsky, S., Lin, H., Satorius, C., Vemuri, R., … Epstein, N. D. (2001). The overall pattern of cardiac contraction depends on a spatial gradient of myosin regulatory light chain phosphorylation. *Cell*, *107*(5), 631–641. https://doi.org/10.1016/S0092-8674(01)00586-4

Derish, I., Lee, J. K. H., Wong-King-Cheong, M., Babayeva, S., Caplan, J., Leung, V., … Torban, E. (2020). Differential role of planar cell polarity gene Vangl2 in embryonic and adult mammalian kidneys. *PLoS ONE*, *15*(3), 1–20. https://doi.org/10.1371/journal.pone.0230586

DeRuiter, M. C., Poelmann, R. E., VanderPlas-de Vries, I., Mentink, M. M. T., & Gittenberger-de Groot, A. C. (1992). The development of the myocardium and endocardium in mouse embryos - Fusion of two heart tubes? *Anatomy and Embryology*, *185*(5), 461–473. https://doi.org/10.1007/BF00174084

Desgrange, A., Garrec, J. F. Le, & Meilhac, S. M. (2018). Left-right asymmetry in heart development and disease: Forming the right loop. *Development (Cambridge)*, *145*(22). https://doi.org/10.1242/dev.162776

Devenport, D., Oristian, D., Heller, E., & Fuchs, E. (2011). Mitotic internalization of planar cell polarity proteins preserves tissue polarity. *Nature Cell Biology*, *13*(8), 893–902. https://doi.org/10.1038/ncb2284

Devine, W. P., Wythe, J. D., George, M., Koshiba-Takeuchi, K., & Bruneau, B. G. (2014). Early patterning and specification of cardiac progenitors in gastrulating mesoderm. *ELife*, *3*, 1–23. https://doi.org/10.7554/eLife.03848

Dijksterhuis, J. P., Petersen, J., & Schulte, G. (2014). WNT/Frizzled signalling: Receptor-ligand selectivity with focus on FZD-G protein signalling and its physiological relevance: IUPHAR Review 3. *British Journal of Pharmacology*, *171*(5), 1195–1209. https://doi.org/10.1111/bph.12364

Ding, P., Huang, J., Battiprolu, P. K., Hill, J. A., Kamm, K. E., & Stull, J. T. (2010). Cardiac myosin light chain kinase is necessary for myosin regulatory light chain phosphorylation and cardiac performance in vivo. *Journal of Biological Chemistry*, *285*(52), 40819–40829. https://doi.org/10.1074/jbc.M110.160499

Dominguez, R., & Holmes, K. C. (2011). Actin structure and function. *Annual Review of Biophysics*, *40*(1), 169–186. https://doi.org/10.1146/annurev-biophys-042910-155359

Dooley, K., & Zon, L. I. (2000). Zebrafish: A model system for the study of human disease. *Current Opinion in Genetics and Development*, *10*(3), 252–256. https://doi.org/10.1016/S0959-437X(00)00074-5

Dorn, G. W., & Brown, J. H. (1999). Gq signaling in cardiac adaptation and maladaptation. *Trends in Cardiovascular Medicine*, *9*(1–2), 26–34. https://doi.org/10.1016/S1050-1738(99)00004-3

Drenckhahn, D., Jons, T., Kollert-Jons, A., Koob, R., Kraemer, D., & Wagner, S. (1993). Cytoskeleton and epithelial polarity. *Renal Physiology and Biochemistry*, *16*(1–2), 6–14. https://doi.org/10.1159/000173747

Driever, W., Schier, A. F., Neuhauss, S. C. F., Malicki, J., Stemple, D. L., & Stainier, D. Y. R. (1996). A genetic screen for mutations affecting embryogenesis in zebrafish. *Development*, *123*, 37–46.

Eghiaian, F., Rigato, A., & Scheuring, S. (2015). Structural, mechanical, and dynamical variability of the actin cortex in living cells. *Biophysical Journal*, *108*(6), 1330–1340. https://doi.org/10.1016/j.bpj.2015.01.016

Ehrlich, W. (1995). [Discovery of the pacemaker and heart conduction system in mammals. Fantasy and truth]. *Zeitschrift Fur Kardiologie*, *84*(12), 963–970. Retrieved from http://www.ncbi.nlm.nih.gov/pubmed/8578792

el Azhar, Y., & Sonnen, K. F. (2021). Development in a Dish—In Vitro Models of Mammalian Embryonic Development. *Frontiers in Cell and Developmental Biology*, *9*(May), 1–8. https://doi.org/10.3389/fcell.2021.655993

Fahey, B., & Degnan, B. M. (2010). Origin of animal epithelia: Insights from the sponge genome. *Evolution and Development*, *12*(6), 601–617. https://doi.org/10.1111/j.1525-142X.2010.00445.x

Fanto, M., & McNeill, H. (2004). Planar polarity from flies to vertebrates. *Journal of Cell Science*, *117*(4), 527–533. https://doi.org/10.1242/jcs.00973

Feiguin, F., Hannus, M., Mlodzik, M., & Eaton, S. (2001). The Ankyrin Repeat Protein Diego

Mediates Frizzled-Dependent Planar Polarization. *Developmental Cell*, *1*(1), 93–101. https://doi.org/10.1016/S1534-5807(01)00010-7

Felker, A., Prummel, K. D., Merks, A. M., Mickoleit, M., Brombacher, E. C., Huisken, J., … Mosimann, C. (2018). Continuous addition of progenitors forms the cardiac ventricle in zebrafish. *Nature Communications*, *9*(1), 1–14. https://doi.org/10.1038/s41467-018-04402-6

Feng, D., Wang, J., Yang, W., Li, J., Lin, X., Zha, F., … Gao, B. (2021). Regulation of Wnt/PCP signaling through p97/VCP-KBTBD7-mediated Vangl ubiquitination and endoplasmic reticulum-associated degradation. *Science Advances*, *7*(20). https://doi.org/10.1126/sciadv.abg2099

Foord, S. M., Bonner, T. I., Neubig, R. R., Rosser, E. M., Pin, J. P., Davenport, A. P., … Harmar, A. J. (2005). International Union of Pharmacology. XLVI. G protein-coupled receptor list. *Pharmacological Reviews*, *57*(2), 279–288. https://doi.org/10.1124/pr.57.2.5

Forster, T. (1946). Energiewanderung und Fluoreszenz. *Die Naturwissenschaften*, *33*(6), 166–175. https://doi.org/10.1007/BF00585226

Foulquier, S., Daskalopoulos, E. P., Lluri, G., Hermans, K. C. M., Deb, A., & Blankesteijn, W. M. (2017). WNT Signaling in Cardiac and Vascular Disease. *Pharmacological Reviews*, *70*(1), 68–141. https://doi.org/10.1124/pr.117.013896

Franco, D., & Kelly, R. G. (2011). Contemporary cardiogenesis: new insights into heart development. *Cardiovascular Research*, *91*(2), 183–184. https://doi.org/10.1093/cvr/cvr160

Francou, A., De Bono, C., & Kelly, R. G. (2017). Epithelial tension in the second heart field promotes mouse heart tube elongation. *Nature Communications*, *8*(1), 14770. https://doi.org/10.1038/ncomms14770

Gao, B., Song, H., Bishop, K., Elliot, G., Garrett, L., English, M. A., … Yang, Y. (2011). Wnt Signaling Gradients Establish Planar Cell Polarity by Inducing Vangl2 Phosphorylation through Ror2. *Developmental Cell*, *20*(2), 163–176. https://doi.org/10.1016/j.devcel.2011.01.001

Gao, C., & Chen, Y. G. (2010). Dishevelled: The hub of Wnt signaling. *Cellular Signalling*, *22*(5), 717–727. https://doi.org/10.1016/j.cellsig.2009.11.021

Geoffrey Burns, C., & MacRae, C. A. (2006). Purification of hearts from zebrafish embryos. *BioTechniques*, *40*(3), 278–282. https://doi.org/10.2144/000112135

Giardoglou, P., & Beis, D. (2019). On zebrafish disease models and matters of the heart. *Biomedicines*, *7*(1). https://doi.org/10.3390/biomedicines7010015

Gibbs, B. C., Damerla, R. R., Vladar, E. K., Chatterjee, B., Wan, Y., Liu, X., … Lo, C. W. (2016). Prickle1 mutation causes planar cell polarity and directional cell migration defects associated with cardiac outflow tract anomalies and other structural birth defects. *Biology Open*, *5*(3), 323–335. https://doi.org/10.1242/bio.015750

Gibson, M. C., & Perrimon, N. (2003). Apicobasal polarization: Epithelial form and function. *Current Opinion in Cell Biology*, *15*(6), 747–752. https://doi.org/10.1016/j.ceb.2003.10.008

Goldstein, B., & Macara, I. G. (2007). The PAR Proteins: Fundamental Players in Animal Cell Polarization. *Developmental Cell*, *13*(5), 609–622. https://doi.org/10.1016/j.devcel.2007.10.007

Gong, Y., Allgrove, J., van den Boogaard, M. J., Baron, R., Steinmann, B., Fukai, N., … Wang, H. (2001). LDL receptor-related protein 5 (LRP5) affects bone accrual and eye development. *Cell*, *107*(4), 513–523. Retrieved from http://www.ncbi.nlm.nih.gov/pubmed/11719191%5Cnhttp://www.ncbi.nlm.nih.gov/pubmed/11719191?ordinalpos=29&itool=EntrezSystem2.PEntrez.Pubmed.Pubmed_ResultsPanel.Pubmed_DefaultReportPanel.Pubmed_RVDocSum

Gross-Thebing, Theresa;, Paksa, A., & Raz, E. (2014). Simultaneous high-resolution detection of multiple transcripts combined with localization of proteins in whole-mount embryos. *BMC Biology*, *12*(1), 55. https://doi.org/10.1186/s12915-014-0055-7

Gross, S. R. (2017). The Actomyosin Network and Cellular Motility: A Regulatory View into the Process. In *Cytoskeleton - Structure, Dynamics, Function and Disease*. https://doi.org/10.5772/66940

Gul, I. S., Hulpiau, P., Saeys, Y., & van Roy, F. (2017). Evolution and diversity of cadherins and catenins. *Experimental Cell Research*, *358*(1), 3–9. https://doi.org/10.1016/j.yexcr.2017.03.001

Guo, Y., Zanetti, G., & Schekman, R. (2013). A novel GTP-binding protein-adaptor protein

complex responsible for export of Vangl2 from the trans Golgi network. *ELife*, *2013*(2), 1–21. https://doi.org/10.7554/eLife.00160

Habas, R., Kato, Y., & He, X. (2001). Wnt/Frizzled activation of Rho regulates vertebrate gastrulation and requires a novel formin homology protein Daam1. *Cell*, *107*(7), 843–854. https://doi.org/10.1016/S0092-8674(01)00614-6

Haffter, P., Granato, M., Brand, M., Mullins, M. C., Hammerschmidt, M., Kane, D. A., … Nüsslein-Volhard, C. (1996). The identification of genes with unique and essential functions in the development of the zebrafish, Danio rerio. *Development*, *123*, 1–36. https://doi.org/10.1242/dev.123.1.1

Hahmann, C., & Schroeter, T. (2010). Rho-kinase inhibitors as therapeutics: From pan inhibition to isoform selectivity. *Cellular and Molecular Life Sciences*, *67*(2), 171–177. https://doi.org/10.1007/s00018-009-0189-x

Harvey, R. P. (1996). NK-2 homeobox genes and heart development. *Developmental Biology*, *178*(2), 203–216. https://doi.org/10.1006/dbio.1996.0212

Heisenberg, C.-P., & Bellaïche, Y. (2013). Forces in Tissue Morphogenesis and Patterning. *Cell*, *153*(5), 948–962. https://doi.org/10.1016/j.cell.2013.05.008

Heissler, S. M., & Manstein, D. J. (2013). Nonmuscle myosin-2: Mix and match. *Cellular and Molecular Life Sciences*, *70*(1), 1–21. https://doi.org/10.1007/s00018-012-1002-9

Henderson, D. J., Conway, S. J., Greene, N. D. E., Gerrelli, D., Murdoch, J. N., Anderson, R. H., & Copp, A. J. (2001). Cardiovascular defects associated with abnormalities in midline development in the Loop-tail mouse mutant. *Circulation Research*, *89*(1), 6–12. https://doi.org/10.1161/hh1301.092497

Henderson, D. J., Long, D. A., & Dean, C. H. (2018). Planar cell polarity in organ formation. *Current Opinion in Cell Biology*, *55*, 96–103. https://doi.org/10.1016/j.ceb.2018.06.011

Hodatsu, A., Fujino, N., Uyama, Y., Tsukamoto, O., Imai-Okazaki, A., Yamazaki, S., … Yamagishi, M. (2019). Impact of cardiac myosin light chain kinase gene mutation on development of dilated cardiomyopathy. *ESC Heart Failure*, *6*(2), 406–415. https://doi.org/10.1002/ehf2.12410

Hodge, T., & Cope, M. J. T. V. (2000). A myosin family tree. *Journal of Cell Science*, *113*(19),

3353–3354. https://doi.org/10.1242/jcs.113.19.3353

Hong, F., Haldeman, B. D., Jackson, D., Carter, M., Baker, J. E., & Cremo, C. R. (2011). Biochemistry of smooth muscle myosin light chain kinase. *Archives of Biochemistry and Biophysics*, *510*(2), 135–146. https://doi.org/10.1016/j.abb.2011.04.018

Howe, K., Clark, M. D., Torroja, C. F., Torrance, J., Berthelot, C., Muffato, M., … Stemple, D. L. (2013). The zebrafish reference genome sequence and its relationship to the human genome. *Nature*, *496*(7446), 498–503. https://doi.org/10.1038/nature12111

Huang, C. J., Tu, C. T., Hsiao, C. Der, Hsieh, F. J., & Tsai, H. J. (2003). Germ-line transmission of a myocardium-specific GFP transgene reveals critical regulatory elements in the cardiac myosin light chain 2 promoter of zebrafish. *Developmental Dynamics*, *228*(1), 30–40. https://doi.org/10.1002/dvdy.10356

Huang, H., & Klein, P. S. (2004). Protein family review The Frizzled family : receptors for multiple signal transduction pathways. *Protein Family Review*, *2*(Figure 1), 1–7.

Humphries, A. C., Hazelett, C. C., Molina-Pelayo, C., Devenport, D., & Mlodzik, M. (2022). *A Van Gogh/Vangl tyrosine phosphorylation switch regulates its interaction with core Planar Cell Polarity factors Prickle and Dishevelled*. 1–35.

Iden, S., & Collard, J. G. (2008). Crosstalk between small GTPases and polarity proteins in cell polarization. *Nature Reviews Molecular Cell Biology*, *9*(11), 846–859. https://doi.org/10.1038/nrm2521

Iden, S., van Riel, W. E., Schäfer, R., Song, J.-Y., Hirose, T., Ohno, S., & Collard, J. G. (2012). Tumor Type-Dependent Function of the Par3 Polarity Protein in Skin Tumorigenesis. *Cancer Cell*, *22*(3), 389–403. https://doi.org/10.1016/j.ccr.2012.08.004

Ikebe, M., Hartshorne, D. J., & Elzinga, M. (1986). Identification, phosphorylation, and dephosphorylation of a second site for myosin light chain kinase on the 20,000-dalton light chain of smooth muscle myosin. *Journal of Biological Chemistry*, *261*(1), 36–39. https://doi.org/10.1016/s0021-9258(17)42425-2

Iliescu, A., Gravel, M., Horth, C., Apuzzo, S., & Gros, P. (2011). Transmembrane topology of mammalian planar cell polarity protein vangl1. *Biochemistry*, *50*(12), 2274–2282. https://doi.org/10.1021/bi101767a

Janda, C. Y., Waghray, D., Levin, A. M., Thomas, C., & Garcia, K. C. (2012). Structural basis of Wnt recognition by frizzled. *Science*, *336*(6090), 59–64. https://doi.org/10.1126/science.1222879

Jansen, K. A., Donato, D. M., Balcioglu, H. E., Schmidt, T., Danen, E. H. J., & Koenderink, G. H. (2015). A guide to mechanobiology: Where biology and physics meet. *Biochimica et Biophysica Acta (BBA) - Molecular Cell Research*, *1853*(11), 3043–3052. https://doi.org/10.1016/j.bbamcr.2015.05.007

Jenny, A., Darken, R. S., Wilson, P. A., & Mlodzik, M. (2003). Prickle and strabismus form a functional complex to generate a correct axis during planar cell polarity signaling. *EMBO Journal*, *22*(17), 4409–4420. https://doi.org/10.1093/emboj/cdg424

Jensen, B., Agger, P., de Boer, B. A., Oostra, R. J., Pedersen, M., van der Wal, A. C., … Moorman, A. F. M. (2016). The hypertrabeculated (noncompacted) left ventricle is different from the ventricle of embryos and ectothermic vertebrates. *Biochimica et Biophysica Acta - Molecular Cell Research*, *1863*(7), 1696–1706. https://doi.org/10.1016/j.bbamcr.2015.10.018

Jessen, J. R., Topczewski, J., Bingham, S., Sepich, D. S., Marlow, F., Chandrasekhar, A., & Solnica-Krezel, L. (2002). Zebrafish trilobite identifies new roles for Strabismus in gastrulation and neuronal movements. *Nature Cell Biology*, *4*(8), 610–615. https://doi.org/10.1038/ncb828

Jiménez-Amilburu, V., Rasouli, S. J., Staudt, D. W., Nakajima, H., Chiba, A., Mochizuki, N., & Stainier, D. Y. R. (2016). In Vivo Visualization of Cardiomyocyte Apicobasal Polarity Reveals Epithelial to Mesenchymal-like Transition during Cardiac Trabeculation. *Cell Reports*, *17*(10), 2687–2699. https://doi.org/10.1016/j.celrep.2016.11.023

Jussila, M., & Ciruna, B. (2017). Zebrafish models of non-canonical Wnt/planar cell polarity signalling: fishing for valuable insight into vertebrate polarized cell behavior. *Wiley Interdisciplinary Reviews: Developmental Biology*, *6*(3). https://doi.org/10.1002/wdev.267

Kamm, K. E., & Stull, J. T. (2011). Signaling to myosin regulatory light chain in sarcomeres. *Journal of Biological Chemistry*, *286*(12), 9941–9947. https://doi.org/10.1074/jbc.R110.198697

Karner, C., Wharton, K. A., & Carroll, T. J. (2006a). Apical-basal polarity, Wnt signaling and vertebrate organogenesis. *Seminars in Cell and Developmental Biology*, *17*(2), 214–222.

https://doi.org/10.1016/j.semcdb.2006.05.007

Karner, C., Wharton, K. A., & Carroll, T. J. (2006b). Planar cell polarity and vertebrate organogenesis. *Seminars in Cell and Developmental Biology*, *17*(2), 194–203. https://doi.org/10.1016/j.semcdb.2006.05.003

Kassianidou, E., Hughes, J. H., & Kumar, S. (2017). Activation of ROCK and MLCK tunes regional stress fiber formation and mechanics via preferential myosin light chain phosphorylation. *Molecular Biology of the Cell*, *28*(26), 3832–3843. https://doi.org/10.1091/mbc.E17-06-0401

Kasza, K. E., & Zallen, J. A. (2011). Dynamics and regulation of contractile actin-myosin networks in morphogenesis. *Current Opinion in Cell Biology*, *23*(1), 30–38. https://doi.org/10.1016/j.ceb.2010.10.014

Katoh, M., & Katoh, M. (2003). Identification and characterization of human PRICKLE1 and PRICKLE2 genes as well as mouse Prickle1 and Prickle2 genes homologous to Drosophila tissue polarity gene prickle. *International Journal of Molecular Medicine*, *11*(2), 249–256. https://doi.org/10.3892/ijmm.11.2.249

Keegan, B. R., Meyer, D., & Yelon, D. (2004). Organization of cardiac chamber progenitors in the zebrafish blastula. *Development*, *131*(13), 3081–3091. https://doi.org/10.1242/dev.01185

Kelkar, M., Bohec, P., & Charras, G. (2020). Mechanics of the cellular actin cortex: From signalling to shape change. *Current Opinion in Cell Biology*, *66*, 69–78. https://doi.org/10.1016/j.ceb.2020.05.008

Keller, R., & Shook, D. (2011). The bending of cell sheets - from folding to rolling. *BMC Biology*, *9*, 2–5. https://doi.org/10.1186/1741-7007-9-90

Kelley, C. A., Wirshing, A. C. E., Zaidel-Bar, R., & Cram, E. J. (2018). The myosin light-chain kinase MLCK-1 relocalizes during Caenorhabditis elegans ovulation to promote actomyosin bundle assembly and drive contraction. *Molecular Biology of the Cell*, *29*(16), 1975–1991. https://doi.org/10.1091/mbc.E18-01-0056

Kelly, R. G., Brown, N. A., & Buckingham, M. E. (2001). The Arterial Pole of the Mouse Heart Forms from Fgf10-Expressing Cells in Pharyngeal Mesoderm. *Developmental Cell*, *1*(3), 435–440. https://doi.org/10.1016/S1534-5807(01)00040-5

Kelly, R. G., & Buckingham, M. E. (2002). The anterior heart-forming field: voyage to the arterial pole of the heart. *Trends in Genetics*, *18*(4), 210–216. https://doi.org/10.1016/S0168-9525(02)02642-2

Kelly, R. G., Buckingham, M. E., & Moorman, A. F. (2014). Heart Fields and Cardiac Morphogenesis. *Cold Spring Harbor Perspectives in Medicine*, *4*(10), a015750–a015750. https://doi.org/10.1101/cshperspect.a015750

Kelly, R. G., & Sperling, S. R. (2018). Diverging roads to the heart. *Science*, *359*(6380), 1098–1099. https://doi.org/10.1126/science.aat0230

Kemmler, C. L., Riemslagh, F. W., Moran, H. R., & Mosimann, C. (2021). From stripes to a beating heart: Early cardiac development in zebrafish. *Journal of Cardiovascular Development and Disease*, *8*(2), 1–21. https://doi.org/10.3390/JCDD8020017

Kikuchi, A., & Kishida, S. (2006). Regulation of Wnt signaling by PPI and posttranslational modifications. *EXPERIMENTAL and MOLECULAR MEDICINE*, *38*(1), 1–10.

Kimmel, C. B., Ballard, W. W., Kimmel, S. R., Ullmann, B., & Schilling, T. F. (1995). Stages of embryonic development of the zebrafish. *Developmental Dynamics*, *203*(3), 253–310. https://doi.org/10.1002/aja.1002030302

Kimura, K., Ito, M., Amano, M., Chihara, K., Fukata, Y., Nakafuku, M., … Kaibuchi, K. (1996). Regulation of myosin phosphatase by Rho and Rho-associated kinase (Rho- kinase). *Science*, *273*(5272), 245–248. https://doi.org/10.1126/science.273.5272.245

Kinzler, K. W., Nilbert, M. C., Su, L. K., Vogelstein, B., Bryan, T. M., Levy, D. B., … Nakamura, Y. (1991). Identification of FAP locus genes from chromosome 5q21. *Science*, *253*(5020), 661–665. https://doi.org/10.1126/science.1651562

Kioussi, C., Briata, P., Baek, S. H., Rose, D. W., Hamblet, N. S., Herman, T., … Rosenfeld, M. G. (2002). Identification of a WntDv-Catenin → Pitx2 Pathway.pdf. *Cell*, *111*(5), 673–685. Retrieved from http://eutils.ncbi.nlm.nih.gov/entrez/eutils/elink.fcgi?dbfrom=pubmed&id=12464179&retmode=ref&cmd=prlinks%0Apapers3://publication/uuid/809B6CD6-FB86-4A04-8644-0F3E649FB5BF

Klaus, A., & Birchmeier, W. (2008). Wnt signalling and its impact on development and cancer. *Nature Reviews Cancer*, *8*(5), 387–398. https://doi.org/10.1038/nrc2389

Klingensmith, J., Nusse, R., & Perrimon, N. (1994). The Drosophila segment polarity gene dishevelled encodes a novel protein required for response to the wingless signal. *Genes and Development*, *8*(1), 118–130. https://doi.org/10.1101/gad.8.1.118

Kosuta, C., Daniel, K., Johnstone, D. L., Mongeon, K., Ban, K., LeBlanc, S., … Pena, I. (2018). High-throughput DNA Extraction and Genotyping of 3dpf Zebrafish Larvae by Fin Clipping. *Journal of Visualized Experiments*, (136). https://doi.org/10.3791/58024

Krogan, N. J., Cagney, G., Yu, H., Zhong, G., Guo, X., Ignatchenko, A., … Greenblatt, J. F. (2006). Global landscape of protein complexes in the yeast Saccharomyces cerevisiae. *Nature*, *440*(7084), 637–643. https://doi.org/10.1038/nature04670

Kroll, F., Powell, G. T., Ghosh, M., Gestri, G., Antinucci, P., Hearn, T. J., … Rihel, J. (2021). A simple and effective F0 knockout method for rapid screening of behaviour and other complex phenotypes. *ELife*, *10*. https://doi.org/10.7554/eLife.59683

Lammi, L., Arte, S., Somer, M., Järvinen, H., Lahermo, P., Thesleff, I., … Nieminen, P. (2004). Mutations in AXIN2 Cause Familial Tooth Agenesis and Predispose to Colorectal Cancer. *American Journal of Human Genetics*, *74*(5), 1043–1050. https://doi.org/10.1086/386293

Landin Malt, A., Dailey, Z., Holbrook-Rasmussen, J., Zheng, Y., Hogan, A., Du, Q., & Lu, X. (2019). Par3 is essential for the establishment of planar cell polarity of inner ear hair cells. *Proceedings of the National Academy of Sciences*, *116*(11), 4999–5008. https://doi.org/10.1073/pnas.1816333116

Laverriere, A. C., MacNeill, C., Mueller, C., Poelmann, R. E., Burch, J. B. E., & Evans, T. (1994). GATA-4/5/6, a subfamily of three transcription factors transcribed in developing heart and gut. *Journal of Biological Chemistry*, *269*(37), 23177–23184. https://doi.org/10.1016/s0021-9258(17)31636-8

Lawrence, P. A., Struhl, G., & Casal, J. (2007). Planar cell polarity: One or two pathways? *Nature Reviews Genetics*, *8*(7), 555–563. https://doi.org/10.1038/nrg2125

Le Garrec, J. F., Domínguez, J. N., Desgrange, A., Ivanovitch, K. D., Raphaël, E., Bangham, J. A., … Meilhac, S. M. (2017). A predictive model of asymmetric morphogenesis from 3D reconstructions of mouse heart looping dynamics. *ELife*, *6*, 1–35. https://doi.org/10.7554/eLife.28951

Lecuit, T., Lenne, P. F., & Munro, E. (2011). Force generation, transmission, and integration

during cell and tissue morphogenesis. *Annual Review of Cell and Developmental Biology*, *27*, 157–184. https://doi.org/10.1146/annurev-cellbio-100109-104027

Leong, I. U. S., Skinner, J. R., Shelling, A. N., & Love, D. R. (2010). Zebrafish as a model for long QT syndrome: The evidence and the means of manipulating zebrafish gene expression. *Acta Physiologica*, *199*(3), 257–276. https://doi.org/10.1111/j.1748-1716.2010.02111.x

Levayer, R., & Lecuit, T. (2012). Biomechanical regulation of contractility: Spatial control and dynamics. *Trends in Cell Biology*, *22*(2), 61–81. https://doi.org/10.1016/j.tcb.2011.10.001

Li, D., Sinha, T., Ajima, R., Seo, H. S., Yamaguchi, T. P., & Wang, J. (2016). Spatial regulation of cell cohesion by Wnt5a during second heart field progenitor deployment. *Developmental Biology*, *412*(1), 18–31. https://doi.org/10.1016/j.ydbio.2016.02.017

Li, D., & Wang, J. (2018). Planar Cell Polarity Signaling in Mammalian Cardiac Morphogenesis. *Pediatric Cardiology*, *39*(5), 1052–1062. https://doi.org/10.1007/s00246-018-1860-5

Li, X., McLain, C., Samuel, M. S., Olson, M. F., & Radice, G. L. (2022). Actomyosin-mediated cellular tension promotes Yap nuclear translocation and myocardial proliferation through α5 integrin signaling. *BioRxiv*, 2022.06.09.495549. https://doi.org/10.1101/2022.06.09.495549

Lienkamp, S. S., Liu, K., Karner, C. M., Carroll, T. J., Ronneberger, O., Wallingford, J. B., & Walz, G. (2012). Vertebrate kidney tubules elongate using a planar cell polarity-dependent, rosette-based mechanism of convergent extension. *Nature Genetics*, *44*(12), 1382–1387. https://doi.org/10.1038/ng.2452

Lim, B. C., Matsumoto, S., Yamamoto, H., Mizuno, H., Kikuta, J., Ishii, M., & Kikuchi, A. (2016). Prickle1 promotes focal adhesion disassembly in cooperation with the CLASP-LL5β complex in migrating cells. *Journal of Cell Science*, *129*(16), 3115–3129. https://doi.org/10.1242/jcs.185439

Linask, K. K., & VanAuker, M. (2007). A role for the cytoskeleton in heart looping. *TheScientificWorldJournal*, *7*, 280–298. https://doi.org/10.1100/tsw.2007.87

Lisowska, J., Rödel, C. J., Manet, S., Miroshnikova, Y. A., Boyault, C., Planus, E., … Faurobert, E. (2018). The CCM1-CCM2 complex controls complementary functions of

ROCK1 and ROCK2 that are required for endothelial integrity. *Journal of Cell Science*, *131*(15), 1–15. https://doi.org/10.1242/jcs.216093

Liu, J., & Stainier, D. Y. R. (2012). Zebrafish in the study of early cardiac development. *Circulation Research*, *110*(6), 870–874. https://doi.org/10.1161/CIRCRESAHA.111.246504

Livak, K. J., & Schmittgen, T. D. (2001). Analysis of relative gene expression data using real-time quantitative PCR and the 2-ΔΔCT method. *Methods*, *25*(4), 402–408. https://doi.org/10.1006/meth.2001.1262

Logan, C. Y., & Nusse, R. (2004). The Wnt signaling pathway in development and disease. *Annual Review of Cell and Developmental Biology*, *20*, 781–810. https://doi.org/10.1146/annurev.cellbio.20.010403.113126

Loirand, G., Guérin, P., & Pacaud, P. (2006). Rho kinases in cardiovascular physiology and pathophysiology. *Circulation Research*, *98*(3), 322–334. https://doi.org/10.1161/01.RES.0000201960.04223.3c

Lombardo, V. A., Heise, M., Moghtadaei, M., Bornhorst, D., Männer, J., & Abdelilah-Seyfried, S. (2019). Morphogenetic control of zebrafish cardiac looping by Bmp signaling. *Development (Cambridge)*, *146*(22). https://doi.org/10.1242/dev.180091

Lombardo, V. A., Otten, C., & Abdelilah-Seyfried, S. (2015). Large-scale Zebrafish Embryonic Heart Dissection for Transcriptional Analysis. *Journal of Visualized Experiments*, (95). https://doi.org/10.3791/52087

Lou, S. S., Diz-Muñoz, A., Weiner, O. D., Fletcher, D. A., & Theriot, J. A. (2015). Myosin light chain kinase regulates cell polarization independently of membrane tension or Rho kinase. *Journal of Cell Biology*, *209*(2), 275–288. https://doi.org/10.1083/jcb.201409001

Lu, J., Beatty, L., & Pinthus, J. (2008). Dual expression recombinase based (DERB) single vector system for high throughput screening and verification of protein interactions in living cells. *Nature Precedings*. https://doi.org/10.1038/npre.2008.1550.1

Makarova, O., Roh, M. H., Liu, C. J., Laurinec, S., & Margolis, B. (2003). Mammalian Crumbs3 is a small transmembrane protein linked to protein associated with Lin-7 (Pals1). *Gene*, *302*(1–2), 21–29. https://doi.org/10.1016/S0378111902010843

Malbon, C. C. (2004). Frizzleds: New members of the superfamily of G-protein-coupled receptors. *Frontiers in Bioscience*, Vol. 9, pp. 1048–1058. https://doi.org/10.2741/1308

Mammoto, T., & Ingber, D. E. (2010). Mechanical control of tissue and organ development. *Development*, *137*(9), 1407–1420. https://doi.org/10.1242/dev.024166

Marlow, F., Topczewski, J., Sepich, D., & Solnica-Krezel, L. (2002). Zebrafish Rho kinase 2 acts downstream of Wnt11 to mediate cell polarity and effective convergence and extension movements. *Current Biology*, *12*(11), 876–884. https://doi.org/10.1016/S0960-9822(02)00864-3

Martino, F., Perestrelo, A. R., Vinarský, V., Pagliari, S., & Forte, G. (2018). Cellular mechanotransduction: From tension to function. *Frontiers in Physiology*, *9*(JUL), 1–21. https://doi.org/10.3389/fphys.2018.00824

Massengill, M. T., Ashraf, H. M., Chowdhury, R. R., Chrzanowski, S. M., Kar, J., Warren, S. A., … Kasahara, H. (2016). Acute heart failure with cardiomyocyte atrophy induced in adult mice by ablation of cardiac myosin light chain kinase. *Cardiovascular Research*, *111*(1), 34–43. https://doi.org/10.1093/cvr/cvw069

Matsui, T. S., & Deguchi, S. (2019). Spatially selective myosin regulatory light chain regulation is absent in dedifferentiated vascular smooth muscle cells but is partially induced by fibronectin and Klf4. *American Journal of Physiology - Cell Physiology*, *316*(4), C509–C521. https://doi.org/10.1152/ajpcell.00251.2017

Matsumoto, S., & Hammes, G. G. (1975). Fluorescence energy transfer between ligand binding sites on aspartate transcarbamylase. *Biochemistry*, *14*(2), 214–224. https://doi.org/10.1021/bi00673a004

Matsumura, F., Totsukawa, G., Yamakita, Y., & Yamashiro, S. (2001). Role of myosin light chain phosphorylation in the regulation of cytokinesis. *Cell Structure and Function*, *26*(6), 639–644. https://doi.org/10.1247/csf.26.639

McGreevy, E. M., Vijayraghavan, D., Davidson, L. A., & Hildebrand, J. D. (2015). Shroom3 functions downstream of planar cell polarity to regulate myosin II distribution and cellular organization during neural tube closure. *Biology Open*, *4*(2), 186–196. https://doi.org/10.1242/bio.20149589

Mehta, S., Hingole, S., & Chaudhary, V. (2021). The Emerging Mechanisms of Wnt Secretion

and Signaling in Development. *Frontiers in Cell and Developmental Biology*, *9*(August), 1–17. https://doi.org/10.3389/fcell.2021.714746

Merks, A. M. (2018). *Remodelling of the Epithelial Myocardium During Embryonic Development – Insights from Coxsackie- and Adenovirus Receptor , and Planar Cell Polarity Pathway*. Freie Universit t Berlin.

Merks, A. M., Swinarski, M., Meyer, A. M., Müller, N. V., Özcan, I., Donat, S., … Panáková, D. (2018). Planar cell polarity signalling coordinates heart tube remodelling through tissue-scale polarisation of actomyosin activity. *Nature Communications*, *9*(1). https://doi.org/10.1038/s41467-018-04566-1

Mesbah, K., Harrelson, Z., Théveniau-Ruissy, M., Papaioannou, V. E., & Kelly, R. G. (2008). Tbx3 Is Required for Outflow Tract Development. *Circulation Research*, *103*(7), 743–750. https://doi.org/10.1161/CIRCRESAHA.108.172858

Mesbah, K., Rana, M. S., Francou, A., van Duijvenboden, K., Papaioannou, V. E., Moorman, A. F., … Christoffels, V. M. (2012). Identification of a Tbx1/Tbx2/Tbx3 genetic pathway governing pharyngeal and arterial pole morphogenesis. *Human Molecular Genetics*, *21*(6), 1217–1229. https://doi.org/10.1093/hmg/ddr553

Michel, D., Arsanto, J. P., Massey-Harroche, D., Béclin, C., Wijnholds, J., & Le Bivic, A. (2005). PATJ connects and stabilizes apical and lateral components of tight junctions in human intestinal cells. *Journal of Cell Science*, *118*(17), 4049–4057. https://doi.org/10.1242/jcs.02528

Mikels, A. J., & Nusse, R. (2006). Wnts as ligands: Processing, secretion and reception. *Oncogene*, *25*(57), 7461–7468. https://doi.org/10.1038/sj.onc.1210053

Mlodzik, M. (2016). The Dishevelled Protein Family: Still Rather a Mystery After Over 20 Years of Molecular Studies. In *Current Topics in Developmental Biology* (1st ed., Vol. 117). https://doi.org/10.1016/bs.ctdb.2015.11.027

Monahan-Earley, R., Dvorak, A. M., & Aird, W. C. (2013). Evolutionary origins of the blood vascular system and endothelium. *Journal of Thrombosis and Haemostasis*, *11*(SUPPL.1), 46–66. https://doi.org/10.1111/jth.12253

Moore, R., Theveneau, E., Pozzi, S., Alexandre, P., Richardson, J., Merks, A., … Mayor, R. (2013). Par3 controls neural crest migration by promoting microtubule catastrophe during

contact inhibition of locomotion. *Development (Cambridge)*, *140*(23), 4763–4775. https://doi.org/10.1242/dev.098509

Moreno-Mateos, M. A., Vejnar, C. E., Beaudoin, J. D., Fernandez, J. P., Mis, E. K., Khokha, M. K., & Giraldez, A. J. (2015). CRISPRscan: Designing highly efficient sgRNAs for CRISPR-Cas9 targeting in vivo. *Nature Methods*, *12*(10), 982–988. https://doi.org/10.1038/nmeth.3543

Mosimann, C., Panáková, D., Werdich, A. A., Musso, G., Burger, A., Lawson, K. L., … Zon, L. I. (2015). Chamber identity programs drive early functional partitioning of the heart. *Nature Communications*, *6*. https://doi.org/10.1038/ncomms9146

Mulligan, K. A., Fuerer, C., Ching, W., Fish, M., Willert, K., & Nusse, R. (2012). Secreted Wingless-interacting molecule (Swim) promotes long-range signaling by maintaining Wingless solubility. *Proceedings of the National Academy of Sciences of the United States of America*, *109*(2), 370–377. https://doi.org/10.1073/pnas.1119197109

Munjal, A., & Lecuit, T. (2014). Actomyosin networks and tissue morphogenesis. *Development (Cambridge)*, *141*(9), 1789–1793. https://doi.org/10.1242/dev.091645

Murrell, M., Oakes, P. W., Lenz, M., & Gardel, M. L. (2015). Forcing cells into shape: The mechanics of actomyosin contractility. *Nature Reviews Molecular Cell Biology*, *16*(8), 486–498. https://doi.org/10.1038/nrm4012

Nagy, I. I., Railo, A., Rapila, R., Hast, T., Sormunen, R., Tavi, P., … Vainio, S. J. (2010). Wnt-11 signalling controls ventricular myocardium development by patterning N-cadherin and β-catenin expression. *Cardiovascular Research*, *85*(1), 100–109. https://doi.org/10.1093/cvr/cvp254

Narumanchi, S., Wang, H., Perttunen, S., Tikkanen, I., Lakkisto, P., & Paavola, J. (2021). Zebrafish Heart Failure Models. *Frontiers in Cell and Developmental Biology*, *9*(May), 1–15. https://doi.org/10.3389/fcell.2021.662583

Nasevicius, A., & Ekker, S. C. (2000). Effective targeted gene “knockdown” in zebrafish. *Nature Genetics*, *26*(2), 216–220. https://doi.org/10.1038/79951

Navis, A., & Nelson, C. M. (2016). Pulling together: Tissue-generated forces that drive lumen morphogenesis. *Seminars in Cell and Developmental Biology*, *55*, 139–147. https://doi.org/10.1016/j.semcdb.2016.01.002

Nelson, C. M. (2016). On Buckling Morphogenesis. *Journal of Biomechanical Engineering*, *138*(2). https://doi.org/10.1115/1.4032128

Nelson, W. J. (2003). *Generating polarity in single cells for mitotic division*. *422*(April). Retrieved from www.nature.com/nature

New, D. A. (1978). Whole-embryo culture and the study of mammalian embryos during organogenesis. *Biological Reviews of the Cambridge Philosophical Society*, *53*(1), 81–122. https://doi.org/10.1111/j.1469-185x.1978.tb00993.x

Newell-Litwa, K. A., Badoual, M., Asmussen, H., Patel, H., Whitmore, L., & Horwitz, A. R. (2015). ROCK 1 and 2 differentially regulate actomyosin organization to drive cell and synaptic polarity. *Journal of Cell Biology*, *210*(2), 225–242. https://doi.org/10.1083/jcb.201504046

Nichols, S. A., Dirks, W., Pearse, J. S., & King, N. (2006). Early evolution of animal cell signaling and adhesion genes. *Proceedings of the National Academy of Sciences of the United States of America*, *103*(33), 12451–12456. https://doi.org/10.1073/pnas.0604065103

Niehrs, C. (2012). The complex world of WNT receptor signalling. *Nature Reviews Molecular Cell Biology*, *13*(12), 767–779. https://doi.org/10.1038/nrm3470

Nishimura, T., Honda, H., & Takeichi, M. (2012). Planar cell polarity links axes of spatial dynamics in neural-tube closure. *Cell*, *149*(5), 1084–1097. https://doi.org/10.1016/j.cell.2012.04.021

O'Brien, L. E., Zegers, M. M. P., & Mostov, K. E. (2002). Building epithelial architecture: insights from three-dimensional culture models. *Nature Reviews Molecular Cell Biology*, *3*(7), 531–537. https://doi.org/10.1038/nrm859

Olson, E. N. (2006). Gene regulatory networks in the evolution and development of the heart. *Science*, *313*(5795), 1922–1927. https://doi.org/10.1126/science.1132292

Ossipova, O., Chuykin, I., Chu, C. W., & Sokol, S. Y. (2015). Vangl2 cooperates with Rab11 and Myosin V to regulate apical constriction during vertebrate gastrulation. *Development (Cambridge)*, *142*(1), 99–107. https://doi.org/10.1242/dev.111161

Palencia-Desai, S., Rost, M. S., Schumacher, J. A., Ton, Q. V., Craig, M. P., Baltrunaite, K.,

… Sumanas, S. (2015). Myocardium and BMP signaling are required for endocardial differentiation. *Development (Cambridge)*, *142*(13), 2304–2315. https://doi.org/10.1242/dev.118687

Panáková, D., Sprong, H., Marois, E., Thiele, C., & Eaton, S. (2005). Lipoprotein particles are required for Hedgehog and Wingless signalling. *Nature*, *435*(7038), 58–65. https://doi.org/10.1038/nature03504

Panáková, D., Werdich, A. A., & MacRae, C. A. (2010). Wnt11 patterns a myocardial electrical gradient through regulation of the L-type Ca2+ channel. *Nature*, *466*(7308), 874–878. https://doi.org/10.1038/nature09249

Pandur, P., Läsche, M., Eisenberg, L. M., & Kühl, M. (2002). Wnt-11 activation of a non-canonical Wnt signalling pathway is required for cardiogenesis. *Nature*, *418*(6898), 636–641. https://doi.org/10.1038/nature00921

Papusheva, E., & Heisenberg, C. P. (2010a). Spatial organization of adhesion: Force-dependent regulation and function in tissue morphogenesis. *EMBO Journal*, Vol. 29, pp. 2753–2768. https://doi.org/10.1038/emboj.2010.182

Papusheva, E., & Heisenberg, C. P. (2010b). Spatial organization of adhesion: Force-dependent regulation and function in tissue morphogenesis. *EMBO Journal*, *29*(16), 2753–2768. https://doi.org/10.1038/emboj.2010.182

Patten, B. M. (1922). The formation of the cardiac loop in the chick. *American Journal of Anatomy*, *30*(3), 373–397. https://doi.org/10.1002/aja.1000300304

Perl, E., & Waxman, J. S. (2020). Retinoic Acid Signaling and Heart Development. In *Sub-cellular biochemistry* (Vol. 95). https://doi.org/10.1007/978-3-030-42282-0_5

Peukes, J., & Betz, T. (2014). Direct measurement of the cortical tension during the growth of membrane blebs. *Biophysical Journal*, *107*(8), 1810–1820. https://doi.org/10.1016/j.bpj.2014.07.076

Phillips, H. M., Murdoch, J. N., Chaudhry, B., Copp, A. J., & Henderson, D. J. (2005). Vangl2 acts via RhoA signaling to regulate polarized cell movements during development of the proximal outflow tract. *Circulation Research*, *96*(3), 292–299. https://doi.org/10.1161/01.RES.0000154912.08695.88

Phillips, H. M., Rhee, H. J., Murdoch, J. N., Hildreth, V., Peat, J. D., Anderson, R. H., … Henderson, D. J. (2007). Disruption of planar cell polarity signaling results in congenital heart defects and cardiomyopathy attributable to early cardiomyocyte disorganization. *Circulation Research*, *101*(2), 137–145. https://doi.org/10.1161/CIRCRESAHA.106.142406

Pires, H. R., & Boxem, M. (2018a). Mapping the Polarity Interactome. *Journal of Molecular Biology*, *430*(19), 3521–3544. https://doi.org/10.1016/j.jmb.2017.12.017

Pires, H. R., & Boxem, M. (2018b). Mapping the Polarity Interactome. *Journal of Molecular Biology*, *430*(19), 3521–3544. https://doi.org/10.1016/j.jmb.2017.12.017

Poh, Y. C., Chen, J., Hong, Y., Yi, H., Zhang, S., Chen, J., … Wang, N. (2014). Generation of organized germ layers from a single mouse embryonic stem cell. *Nature Communications*, *5*(May). https://doi.org/10.1038/ncomms5000

Pollok, B. (1999). Using GFP in FRET-based applications. *Trends in Cell Biology*, *9*(2), 57–60. https://doi.org/10.1016/S0962-8924(98)01434-2

Prall, O. W. J., Menon, M. K., Solloway, M. J., Watanabe, Y., Zaffran, S., Bajolle, F., … Harvey, R. P. (2007). An Nkx2-5/Bmp2/Smad1 Negative Feedback Loop Controls Heart Progenitor Specification and Proliferation. *Cell*, *128*(5), 947–959. https://doi.org/10.1016/j.cell.2007.01.042

Priya, R., Allanki, S., Gentile, A., Mansingh, S., Uribe, V., Maischein, H.-M., & Stainier, D. Y. R. (2020). Tension heterogeneity directs form and fate to pattern the myocardial wall. *Nature*, *588*(7836), 130–134. https://doi.org/10.1038/s41586-020-2946-9

Quinlan, R., Martin, P., & Graham, A. (2004). The role of actin cables in directing the morphogenesis of the pharyngeal pouches. *Development*, *131*(3), 593–599. https://doi.org/10.1242/dev.00950

Raftopoulou, M., & Hall, A. (2004). Cell migration: Rho GTPases lead the way. *Developmental Biology*, *265*(1), 23–32. https://doi.org/10.1016/j.ydbio.2003.06.003

Ramsbottom, S. A., Sharma, V., Rhee, H. J., Eley, L., Phillips, H. M., Rigby, H. F., … Henderson, D. J. (2014). Vangl2-Regulated Polarisation of Second Heart Field-Derived Cells Is Required for Outflow Tract Lengthening during Cardiac Development. *PLoS Genetics*, *10*(12). https://doi.org/10.1371/journal.pgen.1004871

Rao, T. P., & Kühl, M. (2010). An updated overview on wnt signaling pathways: A prelude for more. *Circulation Research*, *106*(12), 1798–1806. https://doi.org/10.1161/CIRCRESAHA.110.219840

Riento, K., & Ridley, A. J. (2003). Rocks: Multifunctional kinases in cell behaviour. *Nature Reviews Molecular Cell Biology*, *4*(6), 446–456. https://doi.org/10.1038/nrm1128

Risi, C., Schäfer, L. U., Belknap, B., Pepper, I., White, H. D., Schröder, G. F., & Galkin, V. E. (2021). High-Resolution Cryo-EM Structure of the Cardiac Actomyosin Complex. *Structure*, *29*(1), 50-60.e4. https://doi.org/10.1016/j.str.2020.09.013

Robitaille, J., MacDonald, M. L. E., Kaykas, A., Sheldahl, L. C., Zeisler, J., Dubé, M. P., … Samuels, M. E. (2002). Mutant frizzled-4 disrupts retinal angiogenesis in familial exudative vitreoretinopathy. *Nature Genetics*, *32*(2), 326–330. https://doi.org/10.1038/ng957

Rodriguez-Boulan, E., & Macara, I. G. (2014). Organization and execution of the epithelial polarity programme. *Nature Reviews Molecular Cell Biology*, *15*(4), 225–242. https://doi.org/10.1038/nrm3775

Roh, M. H., & Margolis, B. (2003). Composition and function of PDZ protein complexes during cell polarization. *American Journal of Physiology - Renal Physiology*, *285*(3 54-3), 377–387. https://doi.org/10.1152/ajprenal.00086.2003

Roignot, J., Peng, X., & Mostov, K. (2013). Polarity in mammalian epithelial morphogenesis. *Cold Spring Harbor Perspectives in Biology*, *5*(2), 1–16. https://doi.org/10.1101/cshperspect.a013789

Roszko, I., Sepich, D. S., Jessen, J. R., Chandrasekhar, A., & Solnica-Krezel, L. (2015). A dynamic intracellular distribution of Vangl2 accompanies cell polarization during zebrafish gastrulation. *Development (Cambridge)*, *142*(14), 2508–2520. https://doi.org/10.1242/dev.119032

Roux, K. J., Kim, D. I., Raida, M., & Burke, B. (2012). A promiscuous biotin ligase fusion protein identifies proximal and interacting proteins in mammalian cells. *Journal of Cell Biology*, *196*(6), 801–810. https://doi.org/10.1083/jcb.201112098

Saito-Diaz, K., Chen, T. W., Wang, X., Thorne, C. A., Wallace, H. A., Page-Mccaw, A., & Lee, E. (2013). The way Wnt works: Components and mechanism. *Growth Factors*, *31*(1), 1–

31. https://doi.org/10.3109/08977194.2012.752737

Samsa, L. A., Fleming, N., Magness, S., Qian, L., & Liu, J. (2016). Isolation and characterization of single cells from zebrafish embryos. *Journal of Visualized Experiments*, *2016*(109), 1–10. https://doi.org/10.3791/53877

Saneyoshi, T., Kume, S., Amsaki, Y., & Mikoshiba, K. (2002). The wnt/calcium pathway activates nf-at and promotes ventral cell fate in xenopus embryos. *Nature*, *417*(6886), 295–299. https://doi.org/10.1038/417295a

Sanz-Ezquerro, J. J., Münsterberg, A. E., & Stricker, S. (2017). Editorial: Signaling pathways in embryonic development. *Frontiers in Cell and Developmental Biology*, *5*(AUG), 1–3. https://doi.org/10.3389/fcell.2017.00076

Schleiffarth, J. R., Person, A. D., Martinsen, B. J., Sukovich, D. J., Neumann, A., Baker, C. V. H., … Petryk, A. (2007). Wnt5a is required for cardiac outflow tract septation in mice. *Pediatric Research*, *61*(4), 386–391. https://doi.org/10.1203/pdr.0b013e3180323810

Scholey, J. M., Taylor, K., & Kendrick-Jones, J. (1980). Regulation of thymus myosin assembly and interaction with actin by calmodulin-dependent light chain kinase. *Cell Biology International Reports*, *4*(8), 763. https://doi.org/10.1016/0309-1651(80)90116-2

Schulte, G. (2010). International Union of Basic and Clinical. *Pharmacological Reviews*, *62*(4), 632–667. https://doi.org/10.1124/pr.110.002931.632

Schulte, G., & Bryja, V. (2007). The Frizzled family of unconventional G-protein-coupled receptors. *Trends in Pharmacological Sciences*, *28*(10), 518–525. https://doi.org/10.1016/j.tips.2007.09.001

Scott, G. F., & Barresi, M. J. F. (2016). *Developmental Biology* (11th ed.). Sunderland, Massachusetts.: Sinauer Associates, Inc.

Sebbagh, M., & Borg, J.-P. (2014). Insight into planar cell polarity. *Experimental Cell Research*, *328*(2), 284–295. https://doi.org/10.1016/j.yexcr.2014.09.005

Seguchi, O., Takashima, S., Yamazaki, S., Asakura, M., Asano, Y., Shintani, Y., … Kitakaze, M. (2007). A cardiac myosin light chain kinase regulates sarcomere assembly in the vertebrate heart. *Journal of Clinical Investigation*, *117*(10), 2812–2824. https://doi.org/10.1172/JCI30804

Sellars, J. R., Pato, M. D., & Adelstein, R. S. (1981). Reversible phosphorylation of smooth muscle myosin, heavy meromyosin, and platelet myosin. *Journal of Biological Chemistry*, *256*(24), 13137–13142. https://doi.org/10.1016/s0021-9258(18)43018-9

Sellers, J. R. (2000). Myosins: A diverse superfamily. *Biochimica et Biophysica Acta - Molecular Cell Research*, *1496*(1), 3–22. https://doi.org/10.1016/S0167-4889(00)00005-7

Sens, P., & Plastino, J. (2015). Membrane tension and cytoskeleton organization in cell motility. *Journal of Physics Condensed Matter*, *27*(27), 273103. https://doi.org/10.1088/0953-8984/27/27/273103

Seo, H. S., Habas, R., Chang, C., & Wang, J. (2017). Bimodal regulation of Dishevelled function by Vangl2 during morphogenesis. *Human Molecular Genetics*, *26*(11), 2053–2061. https://doi.org/10.1093/hmg/ddx095

Sharma, M., Castro-Piedras, I., Simmons, G. E., & Pruitt, K. (2018). Dishevelled: A masterful conductor of complex Wnt signals. *Cellular Signalling*, *47*(2017), 52–64. https://doi.org/10.1016/j.cellsig.2018.03.004

Sheikh, F., Lyon, R. C., & Chen, J. (2015). Functions of myosin light chain-2 (MYL2) in cardiac muscle and disease. *Gene*, *569*(1), 14–20. https://doi.org/10.1016/j.gene.2015.06.027

Shi, Y., Yao, J., Xu, G., & Taber, L. A. (2014). Bending of the looping heart: Differential growth revisited. *Journal of Biomechanical Engineering*, *136*(8). https://doi.org/10.1115/1.4026645

Shin, K., Fogg, V. C., & Margolis, B. (2006). Tight junctions and cell polarity. *Annual Review of Cell and Developmental Biology*, *22*, 207–235. https://doi.org/10.1146/annurev.cellbio.22.010305.104219

Shindo, A., & Wallingford, J. B. (2014). PCP and septins compartmentalize cortical actomyosin to direct collective cell movement. *Science*, *343*(6171), 649–652. https://doi.org/10.1126/science.1243126

Sinha, T., Li, D., Théveniau-Ruissy, M., Hutson, M. R., Kelly, R. G., & Wang, J. (2015). Loss of Wnt5a disrupts second heart field cell deployment and may contribute to OFT malformations in DiGeorge syndrome. *Human Molecular Genetics*, *24*(6), 1704–1716. https://doi.org/10.1093/hmg/ddu584

Sinha, T., Wang, B., Evans, S., Wynshaw-Boris, A., & Wang, J. (2012). Disheveled mediated planar cell polarity signaling is required in the second heart field lineage for outflow tract morphogenesis. *Developmental Biology*, *370*(1), 135–144. https://doi.org/10.1016/j.ydbio.2012.07.023

Sitarska, E., & Diz-Muñoz, A. (2020). Pay attention to membrane tension: Mechanobiology of the cell surface. *Current Opinion in Cell Biology*, *66*, 11–18. https://doi.org/10.1016/j.ceb.2020.04.001

Slusarski, D. C., Corces, V. G., & Moon, R. T. (1997). Interaction of Wnt and a Frizzled homologue triggers G-protein-linked phosphatidylinositol signalling. *Nature*, *390*(6658), 410–413. https://doi.org/10.1038/37138

Slusarski, D. C., Yang-Snyder, J., Busa, W. B., & Moon, R. T. (1997). Modulation of Embryonic Intracellular Ca2+Signaling byWnt-5A. *Developmental Biology*, *182*(1), 114–120. https://doi.org/10.1006/dbio.1996.8463

Somlyo, A. V., Khromov, A. S., Webb, M. R., Ferenczi, M. A., Trentham, D. R., He, Z. H., … Somlyo, A. P. (2004). Smooth muscle myosin: Regulation and properties. *Philosophical Transactions of the Royal Society B: Biological Sciences*, *359*(1452), 1921–1930. https://doi.org/10.1098/rstb.2004.1562

Spurlin, J. W., & Nelson, C. M. (2017). Building branched tissue structures: From single cell guidance to coordinated construction. *Philosophical Transactions of the Royal Society B: Biological Sciences*, *372*(1720). https://doi.org/10.1098/rstb.2015.0527

Stahley, S. N., Basta, L. P., Sharan, R., & Devenport, D. (2021). Celsr1 adhesive interactions mediate the asymmetric organization of planar polarity complexes. *ELife*, *10*, 1–26. https://doi.org/10.7554/eLife.62097

Stainier, D. Y. R. (2001). Zebrafish genetics and vertebrate heart development. *Nature Reviews Genetics*, *2*(January 2001), 39–48.

Stainier, D. Y. R., Lee, R. K., & Fishman, M. C. (1993). Cardiovascular development in the zebrafish: I. Myocardial fate map and heart tube formation. *Development*, *119*(1), 31–40.

Stanganello, E., Hagemann, A. I. H., Mattes, B., Sinner, C., Meyen, D., Weber, S., … Scholpp, S. (2015). Filopodia-based Wnt transport during vertebrate tissue patterning. *Nature Communications*, *6*. https://doi.org/10.1038/ncomms6846

Staudt, D., & Stainier, D. (2012). Uncovering the molecular and cellular mechanisms of heart development using the zebrafish. *Annual Review of Genetics*, *46*, 397–418. https://doi.org/10.1146/annurev-genet-110711-155646

Stephenson, A., Adams, J. W., & Vaccarezza, M. (2017). The vertebrate heart: an evolutionary perspective. *Journal of Anatomy*, *231*(6), 787–797. https://doi.org/10.1111/joa.12687

Stooke-Vaughan, G. A., & Campàs, O. (2018). Physical control of tissue morphogenesis across scales. *Current Opinion in Genetics and Development*, *51*, 111–119. https://doi.org/10.1016/j.gde.2018.09.002

Stull, J. T., Kamm, K. E., & Vandenboom, R. (2011). Myosin light chain kinase and the role of myosin light chain phosphorylation in skeletal muscle. *Archives of Biochemistry and Biophysics*, *510*(2), 120–128. https://doi.org/10.1016/j.abb.2011.01.017

Summerton, J. (1999). Morpholino antisense oligomers: the case for an RNase H-independent structural type. *Biochimica et Biophysica Acta (BBA) - Gene Structure and Expression*, *1489*(1), 141–158. https://doi.org/10.1016/S0167-4781(99)00150-5

Summerton, J., & Weller, D. (1997). Morpholino Antisense Oligomers: Design, Preparation, and Properties. *Antisense and Nucleic Acid Drug Development*, *7*(3), 187–195. https://doi.org/10.1089/oli.1.1997.7.187

Svitkina, T. (2018). The actin cytoskeleton and actin-based motility. *Cold Spring Harbor Perspectives in Biology*, *10*(1). https://doi.org/10.1101/cshperspect.a018267

Tada, M., & Kai, M. (2009). Noncanonical Wnt/PCP signaling during vertebrate gastrulation. *Zebrafish*, *6*(1), 29–40. https://doi.org/10.1089/zeb.2008.0566

Taneja, N., Baillargeon, S. M., & Burnette, D. T. (2021). Myosin light chain kinase-driven myosin II turnover regulates actin cortex contractility during mitosis. *Molecular Biology of the Cell*, *32*(20), 1–11. https://doi.org/10.1091/mbc.E20-09-0608

Taniguchi, M., Okamoto, R., Ito, M., Goto, I., Fujita, S., Konishi, K., … Itoh, T. (2015). New isoform of cardiac myosin light chain kinase and the role of cardiac myosin phosphorylation in α1-adrenoceptor mediated inotropic response. *PLoS ONE*, *10*(10), 1–17. https://doi.org/10.1371/journal.pone.0141130

Taylor, J., Abramova, N., Charlton, J., & Adler, P. N. (1998). Van Gogh: A new Drosophila

tissue polarity gene. *Genetics*, *150*(1), 199–210. https://doi.org/10.1093/genetics/150.1.199

ten Berge, D., Brugmann, S. A., Helms, J. A., & Nusse, R. (2008). Wnt and FGF signals interact to coordinate growth with cell fate specification during limb development. *Development*, *135*(19), 3247–3257. https://doi.org/10.1242/dev.023176

Tepass, U., Tanentzapf, G., Ward, R., & Fehon, R. (2001). Epithelial Cell Polarity and Cell Junctions in Drosophila. *Annual Review of Genetics*, *35*(1), 747–784. https://doi.org/10.1146/annurev.genet.35.102401.091415

Tessadori, F., Tsingos, E., Colizzi, E. S., Kruse, F., Van Den Brink, S. C., Van Den Boogaard, M., … Bakkers, J. (2021). Twisting of the zebrafish heart tube during cardiac looping is a tbx5-dependent and tissue-intrinsic process. *ELife*, *10*, 1–34. https://doi.org/10.7554/eLife.61733

Tessadori, F., van Weerd, J. H., Burkhard, S. B., Verkerk, A. O., de Pater, E., Boukens, B. J., … Bakkers, J. (2012). Identification and Functional Characterization of Cardiac Pacemaker Cells in Zebrafish. *PLoS ONE*, *7*(10), 1–9. https://doi.org/10.1371/journal.pone.0047644

Theisen, H., Purcell, J., Bennett, M., Kansagara, D., Syed, A., & Marsh, J. L. (1994). Dishevelled is required during wingless signaling to establish both cell polarity and cell identity. *Development*, *120*(2), 347–360. https://doi.org/10.1242/dev.120.2.347

Tobita, T., Nomura, S., Morita, H., Ko, T., Fujita, T., Toko, H., … Komuro, I. (2017). Identification of MYLK3 mutations in familial dilated cardiomyopathy. *Scientific Reports*, *7*(1), 1–9. https://doi.org/10.1038/s41598-017-17769-1

Topczewski, J., Sepich, D. S., Myers, D. C., Walker, C., Amores, A., Lele, Z., … Solnica-Krezel, L. (2001). The Zebrafish Glypican Knypek Controls Cell Polarity during Gastrulation Movements of Convergent Extension. *Developmental Cell*, *1*(2), 251–264. https://doi.org/10.1016/S1534-5807(01)00005-3

Tota, B., & Gattuso, A. (1996). Heart ventricle pumps in teleosts and elasmobranchs: A morphodynamic approach. *Journal of Experimental Zoology*, *275*(2–3), 162–171. https://doi.org/10.1002/(sici)1097-010x(19960601/15)275:2/3<162::aid-jez8>3.0.co;2-b

Totsukawa, G., Wu, Y., Sasaki, Y., Hartshorne, D. J., Yamakita, Y., Yamashiro, S., &

Matsumura, F. (2004). Distinct roles of MLCK and ROCK in the regulation of membrane protrusions and focal adhesion dynamics during cell migration of fibroblasts. *Journal of Cell Biology*, *164*(3), 427–439. https://doi.org/10.1083/jcb.200306172

Totsukawa, G., Yamakita, Y., Yamashiro, S., Hartshorne, D. J., Sasaki, Y., & Matsumura, F. (2000). Distinct roles of ROCK (Rho-kinase) and MLCK in spatial regulation of MLC phosphorylation for assembly of stress fibers and focal adhesions in 3T3 fibroblasts. *Journal of Cell Biology*, *150*(4), 797–806. https://doi.org/10.1083/jcb.150.4.797

Tran, H. T., Sekkali, B., Van Imschoot, G., Janssens, S., & Vleminckx, K. (2010). Wnt/β-catenin signaling is involved in the induction and maintenance of primitive hematopoiesis in the vertebrate embryo. *Proceedings of the National Academy of Sciences of the United States of America*, *107*(37), 16160–16165. https://doi.org/10.1073/pnas.1007725107

Trinkaus, J. P. (1984). *Cells into organs : the forces that shape the embryo* (2nd ed.). Englewood Cliffs, N.J.: Prentice-Hall.

Trushko, A., Di Meglio, I., Merzouki, A., Blanch-Mercader, C., Abuhattum, S., Guck, J., … Roux, A. (2020). Buckling of an Epithelium Growing under Spherical Confinement. *Developmental Cell*, *54*(5), 655-668.e6. https://doi.org/10.1016/j.devcel.2020.07.019

Umemoto, S., Bengur, A. R., & Sellers, J. R. (1989). Effect of multiple phosphorylations of smooth muscle and cytoplasmic myosins on movement in an in vitro motility assay. *Journal of Biological Chemistry*, *264*(3), 1431–1436. https://doi.org/10.1016/s0021-9258(18)94205-5

Unterseher, F., Hefele, J. A., Giehl, K., De Robertis, E. M., Wedlich, D., & Schambony, A. (2004). Paraxial protocadherin coordinates cell polarity during convergent extension via Rho A and JNK. *EMBO Journal*, *23*(16), 3259–3269. https://doi.org/10.1038/sj.emboj.7600332

Van Essen, D. C. (2020). A 2020 view of tension-based cortical morphogenesis. *Proceedings of the National Academy of Sciences*, *117*(52), 32868–32879. https://doi.org/10.1073/pnas.2016830117

Vasquez, C. G., Tworoger, M., & Martin, A. C. (2014). Dynamic myosin phosphorylation regulates contractile pulses and tissue integrity during epithelial morphogenesis. *Journal of Cell Biology*, *206*(3), 435–450. https://doi.org/10.1083/jcb.201402004

Veeman, M. T., Slusarski, D. C., Kaykas, A., Louie, S. H., & Moon, R. T. (2003). Zebrafish Prickle, a Modulator of Noncanonical Wnt/Fz Signaling, Regulates Gastrulation Movements. *Current Biology*, *13*(8), 680–685. https://doi.org/10.1016/S0960-9822(03)00240-9

Vicente-Manzanares, M., Ma, X., Adelstein, R. S., & Horwitz, A. R. (2009). Non-muscle myosin II takes centre stage in cell adhesion and migration. *Nature Reviews Molecular Cell Biology*, *10*(11), 778–790. https://doi.org/10.1038/nrm2786

Vinson, C. R., Conover, S., & Adler, P. N. (1989). A Drosophila tissue polarity locus encodes a protein containing seven potential transmembrane domains A Pseudomonas thrives in high concentrations of toluene Akira Inoue & Koki Horikoshi *. *Nature*, *338*(March), 263–264.

Vivancos, V., Chen, P., Spassky, N., Qian, D., Dabdoub, A., Kelley, M., … Guthrie, S. (2009). Wnt activity guides facial branchiomotor neuron migration, and involves the PCP pathway and JNK and ROCK kinases. *Neural Development*, *4*(1), 1–16. https://doi.org/10.1186/1749-8104-4-7

Vornanen, M., & Hassinen, M. (2016). Zebrafish heart as a model for human cardiac electrophysiology. *Channels*, *10*(2), 101–110. https://doi.org/10.1080/19336950.2015.1121335

Wang, Y., Chang, H., Rattner, A., & Nathans, J. (2016). Frizzled Receptors in Development and Disease. In *Current Topics in Developmental Biology* (1st ed., Vol. 117). https://doi.org/10.1016/bs.ctdb.2015.11.028

Warga, R. M., & Kimmel, C. B. (1990). Cell movements during epiboly and gastrulation in zebrafish. *Development*, *108*(4), 569–580. https://doi.org/10.1242/dev.108.4.569

Warren, S. A., Briggs, L. E., Zeng, H., Chuang, J., Chang, E. I., Terada, R., … Kasahara, H. (2012). Myosin light chain phosphorylation is critical for adaptation to cardiac stress. *Circulation*, *126*(22), 2575–2588. https://doi.org/10.1161/CIRCULATIONAHA.112.116202

Warren, S. C., Margineanu, A., Alibhai, D., Kelly, D. J., Talbot, C., Alexandrov, Y., … French, P. M. W. (2013). Rapid Global Fitting of Large Fluorescence Lifetime Imaging Microscopy Datasets. *PLoS ONE*, *8*(8). https://doi.org/10.1371/journal.pone.0070687

Wharton, K. A. (2003). Runnin' with the Dvl: Proteins that associate with Dsh/Dvl and their significance to Wnt signal transduction. *Developmental Biology*, *253*(1), 1–17. https://doi.org/10.1006/dbio.2002.0869

Wilkinson, R. N., Elworthy, S., Ingham, P. W., & van Eeden, F. J. M. (2013). A method for high-throughput PCR-based genotyping of larval zebrafish tail biopsies. *BioTechniques*, *55*(6), 314–316. https://doi.org/10.2144/000114116

Williams, M., Yen, W., Lu, X., & Sutherland, A. (2014). Distinct apical and basolateral mechanisms drive planar cell polarity-dependent convergent extension of the mouse neural plate. *Developmental Cell*, *29*(1), 34–46. https://doi.org/10.1016/j.devcel.2014.02.007

Winter, C. G., Wang, B., Ballew, A., Royou, A., Karess, R., Axelrod, J. D., & Luo, L. (2001). Drosophila Rho-associated kinase (Drok) links Frizzled-mediated planar cell polarity signaling to the actin cytoskeleton. *Cell*, *105*(1), 81–91. https://doi.org/10.1016/S0092-8674(01)00298-7

Wolff, T., & Rubin, G. M. (1998). strabismus, a novel gene that regulates tissue polarity and cell fate decisions in Drosophila. *Development*, *125*(6), 1149–1159. https://doi.org/10.1242/dev.125.6.1149

Wolpert, L., Tickle, C., & Martinez Arias, A. (2015). *Principles of Development*. Oxford University Press.

Wu, G., Ge, J., Huang, X., Hua, Y., & Mu, D. (2011). Planar Cell Polarity Signaling Pathway in Congenital Heart Diseases. *Journal of Biomedicine and Biotechnology*, *2011*, 1–8. https://doi.org/10.1155/2011/589414

Yang, S., Wu, Y., Xu, T. H., de Waal, P. W., He, Y., Pu, M., … Xu, F. (2018). Crystal structure of the Frizzled 4 receptor in a ligand-free state. *Nature*, *560*(7720), 666–670. https://doi.org/10.1038/s41586-018-0447-x

Yang, Y., & Mlodzik, M. (2015). Wnt-Frizzled/Planar Cell Polarity Signaling: Cellular Orientation by Facing the Wind (Wnt). *Annual Review of Cell and Developmental Biology*, *31*(1), 623–646. https://doi.org/10.1146/annurev-cellbio-100814-125315

Yogurtcu, O. N., Kim, J. S., & Sun, S. X. (2012). A mechanochemical model of actin filaments. *Biophysical Journal*, *103*(4), 719–727. https://doi.org/10.1016/j.bpj.2012.07.020

Yu, F., Zhao, Y., Gu, J., Quigley, K. L., Chi, N. C., Tai, Y. C., & Hsiai, T. K. (2012). Flexible microelectrode arrays to interface epicardial electrical signals with intracardial calcium transients in zebrafish hearts. *Biomedical Microdevices*, *14*(2), 357–366. https://doi.org/10.1007/s10544-011-9612-9

Yu, Q., Li, J., Murrell, M. P., & Kim, T. (2018). Balance between Force Generation and Relaxation Leads to Pulsed Contraction of Actomyosin Networks. *Biophysical Journal*, *115*(10), 2003–2013. https://doi.org/10.1016/j.bpj.2018.10.008

Yuan, Y., Call, M. K., Yuan, Y., Zhang, Y., Fischesser, K., Liu, C. Y., & Kao, W. W. Y. (2013). Dexamethasone induces cross-linked actin networks in trabecular meshwork cells through noncanonical Wnt signaling. *Investigative Ophthalmology and Visual Science*, *54*(10), 6502–6509. https://doi.org/10.1167/iovs.13-12447

Zaidel-Bar, R., Zhenhuan, G., & Luxenburg, C. (2015). The contractome - A systems view of actomyosin contractility in non-muscle cells. *Journal of Cell Science*, *128*(12), 2209–2217. https://doi.org/10.1242/jcs.170068

Zallen, J. A. (2007). Planar Polarity and Tissue Morphogenesis. *Cell*, *129*(6), 1051–1063. https://doi.org/10.1016/j.cell.2007.05.050

Zallen, J. A., & Blankenship, J. T. (2008). Multicellular dynamics during epithelial elongation. *Seminars in Cell and Developmental Biology*, *19*(3), 263–270. https://doi.org/10.1016/j.semcdb.2008.01.005

Zhang, L., Luga, V., Armitage, S. K., Musiol, M., Won, A., Yip, C. M., … Wrana, J. L. (2016). A lateral signalling pathway coordinates shape volatility during cell migration. *Nature Communications*, *7*(1), 11714. https://doi.org/10.1038/ncomms11714

Zhang, L., & Wrana, J. L. (2018). Regulation of Rho GTPases from the lateral sides of migrating cells. *Small GTPases*, *9*(4), 345–348. https://doi.org/10.1080/21541248.2016.1234430

Zhang, X., Zhu, J., Yang, G.-Y., Wang, Q.-J., Qian, L., Chen, Y.-M., … Luo, Z.-G. (2007). Dishevelled promotes axon differentiation by regulating atypical protein kinase C. *Nature Cell Biology*, *9*(7), 743–754. https://doi.org/10.1038/ncb1603

Zhou, W., Lin, L., Majumdar, A., Li, X., Zhang, X., Liu, W., … Evans, S. M. (2007). Modulation of morphogenesis by noncanonical Wnt signaling requires ATF/CREB family-mediated

transcriptional activation of TGFβ2. *Nature Genetics*, *39*(10), 1225–1234. https://doi.org/10.1038/ng2112

9. Appendix

9.1 Abbreviations

ALPM	Anterior lateral plate mesoderm
AVJ	Atrioventricular canal/junction
aPKC	Atypical protein kinase C
APC	Axin and adenomatosis polyposis coli
bmp	beats per minute
BS	Blocking Solution
BSA	Bovine serum Albumin)
CaMK	Calcium/calmodulin-dependent kinase
CKIα	Casein kinase Iα
Celsr	Cadherin EGF LAG seven-pass G-type receptor
CHD	Congenital heart diseases
CRD	cysteine-rich domain (CRD)
DAAM	Disheveled-associated activator of morphogenesis
DEP	Disheveled, Egl-10, Pleckstrin
Dgo	Diego
DLG	Discs large
Dvl	Disheveled
DIX	Disheveled-Auxin domain
EGFP	Enhanced Green fluorescent Protein
EMT	epithelial to mesenchymal transition
MET	epithelial transition
FLIM	Fluorescence ifetime imaging
FACS	Fluorescent-Activated Cell Sorting
Fz	Frizzled
SFRP	Secreted Frizzled-related proteins
GSK3	glycogen synthase kinase 3
HBSS	Hank's Balanced Salt Solution
hpf	hours post-fertilization
ICE	Inference of CRISPR Edits
IFT	inflow tract
JNK	JUN-N-terminal kinase
LEF	Lymphoid enhancer-binding factor
LGL	Lethal giant larvae

ZIPK	leucine zipper interacting kinase
LHT	linear heart tube
MO	Morpholino oligonucleotide
MYLK	myosin light chain kinase
Mylk3	Myosin Light Chain Kinase 3
MYTP	myosin phosphatase
MRLC	Myosin Regulatory Light Chain
MRCK	myotonic dystrophy kinase-related Cdc42-binding kinase
NFAT	nuclear factor of activated T cells
NMII	non-muscle myosin
NE	nuclear export
NLS	nuclear localization signal
OFT	outflow tract
PARD	partitioning defective
PALS1	Protein associated with LIN-7 1
PATJ	PALS1-associated tight junction protein
PDZ	Post synaptic density-95/Discs large/Zonula-occludens-1
PBM	PDZ binding motif
PLC	phospholipase C
pMyo	phosphorylated myosin
PCP	Planar cell polarity
PM	plasma membrane
PTM	post-translational modification
Pk	Prickle
PKC	protein kinase C
ROI	region of interest
RLC	regulatory light chains
ROCK	Rho-associated kinase
SD	Standard deviation
SEM	Standard error
TCF	T cell factor
TCSPC	Time correlated single photon counting
Vang	Van Gogh
VIM	p97/VCP interacting motif

9.2 List of figures

9.3 List of tables